Dissertation zur Erlangung des Doktorgrades
der Fakultät für Chemie und Pharmazie
der Ludwig-Maximilians-Universität München

Anti-angiogenic effects of cytotoxic, microbial derived compounds – Evaluation of the tubulin inhibitor pretubulysin and its derivatives and characterization of the v-ATPase inhibitor concanamycin A

Sebastian Rath
aus Rüdersdorf/Fürstenwalde, Deutschland
2012

Erklärung

Diese Dissertation wurde im Sinne von § 7 der Promotionsordnung vom 28. November 2011 von Herrn Prof. Dr. Stefan Zahler betreut.

Eidesstattliche Versicherung

Diese Dissertation wurde eigenständig und ohne unerlaubte Hilfe erarbeitet.

München, den 24.09.2012

.....

Unterschrift des Autors, Sebastian Rath

Dissertation eingereicht am:	24.09.2012
1. Gutachter:	Prof. Dr. Stefan Zahler
2. Gutachter:	Prof. Dr. Angelika M. Vollmar
Mündliche Prüfung am:	25.10.2012

To my Mum and Dad

Content

1 Introduction

1.1 Background and purpose

Background: Tumor growth strongly depends on oxygen and nutrient supply [1, 2]. Thus, inhibition of tumor induced blood vessel recruitment, i.e. tumor angiogenesis, is a highly rational concept to treat cancer [2]. The vast majority of approved drugs that have been designed for this purpose selectively interfere with one or few pro-angiogenic signaling cascades, predominantly with the VEGF pathway [3]. The benefits of these agents were lower than expected. This is mainly due to complex intertwining signaling networks in tumor angiogenesis, which can compensate inhibition [4-7].

Conventionally used anti-cancer drugs, like tubulin antagonists exhibit desirable anti-angiogenic 'side effects' with reduced toxicity, when used at low and frequently applied doses [8]. Numerous of such 'metronomic dosing' combinations show synergistic benefits [8-10]. Tubulysins, a novel class of tubulin antagonists from unusual microbes, called myxobacteria [11] exhibit quite impressive anti-cancer and anti-angiogenic potential far beyond the level of the clinically established agents paclitaxel and vinblastine [12, 13]. However, their supply is an issue, as for many natural compounds, which hampers clinical development [14]. This problem was tried to be solved by total synthesis attempts, which are inefficient due to challenging structural features [15]. But total synthesis strategies of simplified analogues have been successful and efficient [15-17]. The most promising of these synthesized analogues, pretubulysin, was identified as direct precursor to tubulysins [18] and is almost similarly active in cancer cells compared to its more complex relatives [19].

First part of the work: Since no information about the anti-angiogenic profile of pretubulysin was available, we tested its potential in angiogenesis assays *in vitro* in comparison to an established relative, tubulysin A [13]. Furthermore, we compared seven modified pretubulysinerivatives [15, 16]. Finally, the most promising pretubulysin-like compound from the *in vitro* evaluations, pretubulysin itself, was assessed in an *in vivo* tumor model [20].

Second part of the work: Besides tubulin, other central cellular structures might be promising targets for the anti-angiogenic approach in tumor therapy. The vacuolar H^+-ATPase (v-ATPase) could be such a target, since it is closely associated with migration and invasion of cancer [21-23] and endothelial cells [24, 25]. Moreover, v-ATPases are known to influence intracellular membrane trafficking [23, 26, 27].

Based on this, we decided to study the impact of a specific v-ATPase inhibitor on cellular angiogenesis assays *in vitro*, with emphasis on the analysis of function and distribution of the most important angiogenesis receptor: VEGFR2 [6, 28]. We hypothesized to find a possible mechanism for anti-angiogenic effects of v-ATPase inhibition via disturbance of VEGFR2 traffic.

1.2 Tumor angiogenesis

Angiogenesis is defined as the formation of new blood vessels from the pre-existing vasculature. In healthy adults angiogenesis induction and termination is tightly regulated by pro- and anti-angiogenic factors. This facilitates controlled physiological processes like wound healing, female reproductive cycling and the general maintenance of tissue homeostasis [29, 30]. In contrast to that, cancer, inflammatory diseases, or age related macular degeneration, represent uncontrolled scenarios with sustained, pathological angiogenesis[29, 31]. One reason for the permanent induction of angiogenesis in the tumor context is an imbalanced ratio between enormous tumor growth and metabolic rate on the one hand, and insufficient supply with oxygen and nutrients on the other.

To cope with the resulting hypoxia, tumors start an expression program, called 'angiogenic switch'. By continuous activation of transcription factors like the hypoxia inducible factor (HIF) [31] and of oncogenes, such as *ras, myc* or *c-kit* [3], pro-angiogenic growth factors (e.g. vascular endothelial growth factor, VEGF) and other factors such as proteases (e.g. matrix metalloprotease 9, MMP-9) are continuously secreted, and stimulate the neovascularization process, which drives tumor growth and metastasis [3, 31] (Fig.1.1).

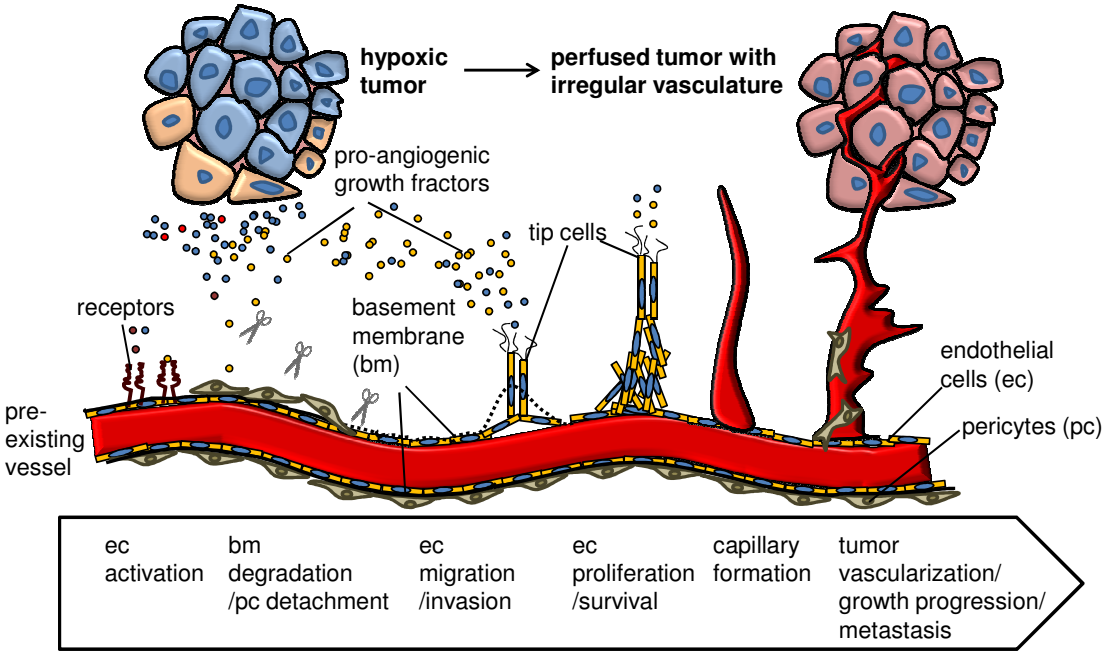

Fig. 1.1 Simplified model of tumor angiogenesis. In quiescent state, endothelial cells (ec) are enveloped by a basement membrane (bm) and pericytes (pc), thus keeping the vascular shape [29, 32]. This structure is destroyed by tumor derived proteases (e.g. MMP-9, depicted as scissors) [29, 33, 34]. Pro-angiogenic growth factors are simultaneously secreted to activate endothelial cells and to serve as orientation cues for sprouting tip cells [31, 32]. These endothelial cells break through the porous basement membrane. By amplification of proliferation and survival signaling, the number of endothelial cells is increased and maintained. Finally, new capillaries are formed and provide ongoing tumor growth and metastasis [29, 31, 32]. Similarly, other strategies of vessel formation, like the recruitment of endothelial progenitors are used, as reviewed by Jain and Carmeliet [30].

1.2.1 Tumor angiogenesis – signaling and ways to interfere

VEGF-A, often simply referred to as VEGF, belongs to a family of growth factors with five members in mammalians (VEGF A-D and placental growth factor (PlGF)).

VEGF plays a dominant role in physiological and pathological angiogenesis, including tumor angiogenesis. It transduces its pro-angiogenic effects mainly via VEGFR2, a receptor tyrosine kinase (RTK) [28, 35]. The central cellular functions, that are regulated via this axis are endothelial cell survival, proliferation and migration [36] (Fig. 1.2). A characteristic feature, which discriminates this growth factor system from others, is the induction of vascular permeability. This also explains the high leakiness of tumor vessels due to VEGF over-expression [29, 36, 37].

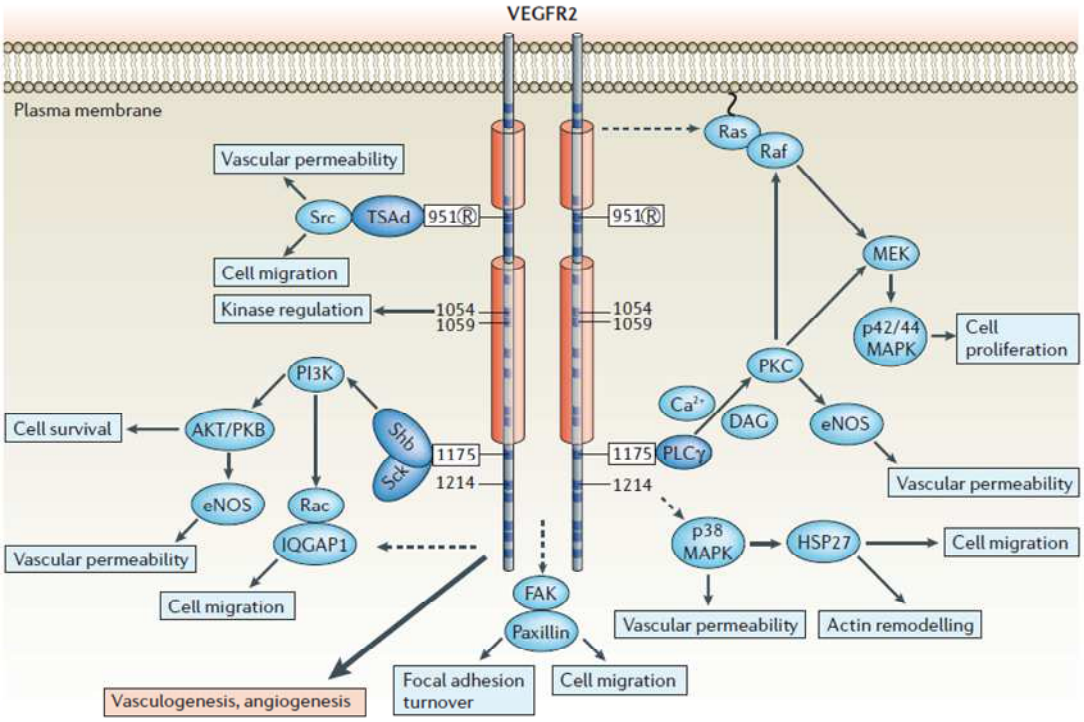

Fig. 1.2 The VEGF/VEGFR2 axis in control of angiogenesis functions. VEGFR2 is a receptor tyrosine kinase (RTK), that in response to its ligand VEGF dimerizes and autophosphorylates specific intracellular tyrosine residues (indicated by numbers). In the following, various signaling cascades like the PI3K/Akt pathway, and corresponding cellular functions, e.g. cell survival are activated. Image from Olsson et al. [36]

The list of selective anti-angiogenic drugs is headed by the anti-VEGF antibody bevacizumab, which is approved for the treatment of a variety of solid tumors in combination with chemotherapy or immune-therapy [30, 38-40]. Other approved anti-VEGF drugs belong to the class of receptor tyrosine kinase inhibitors (RTKIs) and affect multiple pro-angiogenic (e.g. VEGFR2 and Tie2) and oncogenic RTKs (e.g. c-Kit and Raf). However, tumors develop various evasion mechanisms like the over-expression of alternative pro-angiogenic molecules, which limits clinical success [3, 4, 41].

One of the intertwining pro-angiogenic pathways, which provide an escape mechanism to anti-VEGF therapy, is the Notch system. Tie2 and FGF among others extend the complexity of the image [4, 5].

In addition to 'specific' anti-angiogenic agents, conventional cytotoxic anti-cancer drugs have recently been recognized for their 'unspecific' anti-angiogenic potential, when frequently applied at low concentrations [8]. In preclinical models it was even shown that tumors, which were *per se* resistant to the chemotherapeutic, could be effectively treated with this 'metronomic chemotherapy' schedule [42, 43]. The combination with specific anti-angiogenic drugs, such as bevacizumab, often resulted in a further improved outcome of this approach [8, 9, 42, 43].

Hence, for the improvement of antitumor therapy it takes both: development of novel 'specific' anti-angiogenic drugs [44], and of multi-talented chemotherapeutics, that are evaluated for their anti-cancer activity but also for their anti-angiogenic potential [45, 46].

1.2.2 Microbial derived anti-cancer drugs

Microorganisms are considered as significant contributors to the discovery of innovative and potent anti-cancer drugs [47]. Particularly the recent reinforcement of myxobacteria research by the groups of Reichenbach and Höfle further extended the pharmacological repertoire [48]. To date at least 100 novel core structures with highly diverse bioactivities, many of them cancer relevant, [49] have been identified in myxobacteria.

The compounds applied in the present work, all have direct or indirect microbial origin, either from *myxobacteria* or from *streptomyces* species. See Material and Methods chapter for chemical structures, Fig. 2.1 and 2.2.

Tubulysin A (TubA) is a microtubule destabilizing agent [12], which is isolated from the myxobacterial strains *Archangium gephyra* and *Angiococcus disciformis*, though at very low yield (0.3 mg/ l) [50]. Recently, TubA has shown to have very promising anti-cancer and anti-angiogenic activities *in vitro* and *in vivo* [13, 51], but the step into clinical use was hampered by its poor supply [17, 19], also due to complicated total synthesis [15]. An alternative to tubulysin might be pretubulysin (Prt), a direct biosynthesis precursor to tubulysins [18]. Prt can be efficiently produced by total synthesis. In addition, its anti-cancer activities are fairly close to its complex tubulysin relatives [18, 19]. Based on the pretubulysin structure, various derivatives were synthesized [15, 16]. In the first part, we tested Prt and seven Prt derivatives for their anti-angiogenic potential in comparison to tubulysin A.

In the second part, we applied a specific v-ATPase inhibitor, concanamycin A (ConcmA), Fig. 2.2 [52, 53]. This compound is produced by *Streptomyces diastatochromogenes* [54]. We used ConcmA to study anti-angiogenic effects of

v-ATPase inhibition on a cell functional and mechanistic level, thereby focusing on VEGFR2 function.

1.3 Targets in focus – Microtubules and v-ATPases

1.3.1 Microtubules

Together with microfilaments and intermediate filaments, microtubules form the eukaryotic cytoskeleton, which provides cellular shape, stability and polarization, 'highway function' for the transport of various cargo, cell division and migration [45, 55-57].

Microtubules are highly dynamic tube-shaped polymers with a polar assembly: One end, which is called (-) end, finishes with α-tubulin. This side is embedded at the origin of microtubule growth, the microtubule organization centre (MTOC)[58], Fig. 1.3. The other end finishes with β-tubulin and is called (+) end. At this side, α- and β-tubulin heterodimers are constantly integrated, and again separated from the polymer, a behavior called 'dynamic instability' [45]. Tubulin inhibitors can either subtly modulate this process at small concentration, or completely destabilize, respectively stabilize the polymer at higher concentration (see Fig. 1.3). Tubulysin A binds to a specific region within the *Vinca* domain (peptide binding site) and destabilizes the polymer [12, 59]. Pretubulysin is assumed to similarly bind to this site [19, 60].

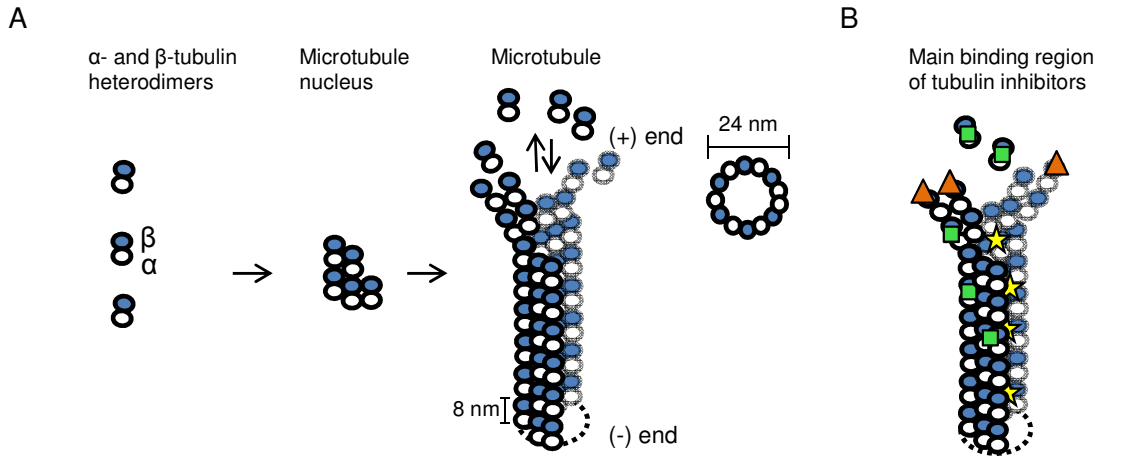

Fig. 1.3 A) Assembly of microtubules. Soluble heterodimers of α- and β-tubulin align together to a short microtubule nucleus, which is elongated into a polymeric cylinder, with β-tubulin at one end, called (+) end, and α-tubulin at the other, (-) end. At the (+) end, dimers are constantly added or released, leading to phases of growth or shrinkage, respectively.
B) Main drug binding domains. Microtubule destabilizing drugs usually bind either to the *Vinca domain*, at the (+) end of microtubules (orange triangles, e.g. vinca alkaloids, dolastatins or tubulysins) or to the *Colchicine domain*, situated within α- and β-tubulin of soluble subunits, that get incorporated and destabilize the polymer (green squares, e.g. colchicines, combretastatins). Stabilizing agents such as taxanes (paclitaxel, shown as yellow stars) bind at the inner surface of the polymer on β-tubulin (*Taxane domain*). Myxobacteria derived epothilones bind close nearby at a distinct site and thus can be used in cases of taxane resistance[61]. Images and binding sites adapted from Dumontet and Jordan [45].

1.3.1.1 Microtubules – relevant functions in cancer and tumor angiogenesis

The importance of microtubules in both anti-cancer [45, 62] and anti-angiogenic strategies[8, 46, 63] is not coincidental. In proliferating cells (Fig. 1.4 A), the highly dynamic mitotic spindle apparatus is particularly vulnerable to tubulin inhibition. This leads to a certain specificity of tubulin antagonists to fast dividing cells[45].

Interphase microtubule dynamics are strongly required during processes of migration [56, 64] and differentiation, i.e. capillary formation, of endothelial cells [55, 65]. Here, microtubule dynamics provide transport function[56], which leads to a polarized distribution of signaling molecules, such as small Rho-GTPases, and cytoskeletal elements (actin, intermediary filaments), which themselves generate a polarized actin cytoskeleton, that drives migration [64, 66] (see Fig. 1.4 B). Interestingly, tubulin antagonists have been shown to exert anti-angiogenic effects at very low, non-toxic concentrations, which do not affect cell cycling [46, 67, 68]. Thus, it can be discriminated between anti-mitotic and non-mitotic effects.

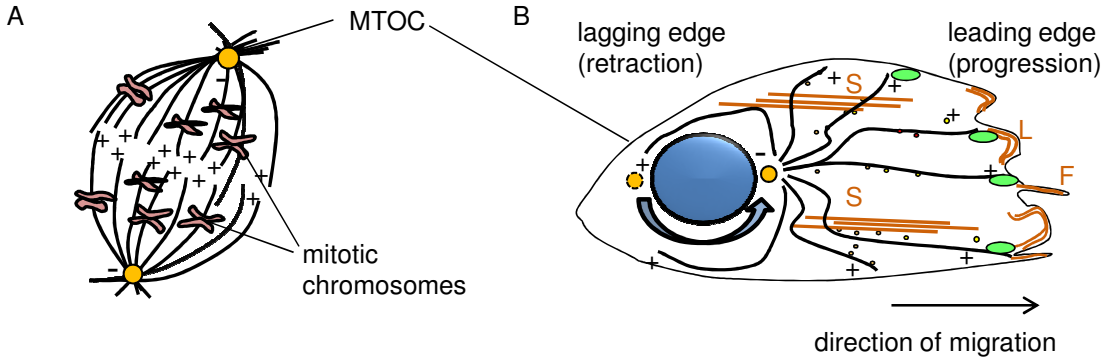

Fig. 1.4 Microtubule functions in A) dividing and in B) interphase cells A) Assembly of the mitotic spindle. B) Cell migration and polarization depend on microtubules. Interphase microtubules lead to asymmetric distribution of signaling molecules, such as small Rho-GTPases, e.g. Rac-1 and Cdc42 (green ovals), which lead to the formation of a polarized actin network, with membrane protrusion (L: lammelipodia and F: filopodia) at the progressing leading edge and stress fibers (S) across the whole cell which generate membrane retraction at the lagging edge [64, 66]. Note, that the microtubule origin, the microtubule organizing centre (MTOC), is similarly re-orientated towards the direction of migration[69]. Image in B adapted from Watanabe et al. [64]

1.3.2 V-ATPases

Vacuolar H^+-ATPases (v-ATPases) are heteromultimeric ATP-driven proton pumps, that are ubiquitously expressed in membranes of eukaryotic cells in order to regulate pH in vesicular compartments, the cytoplasm and the extracellular space [70]. Tight control of pH is essential to a plethora of physiological processes [70], as for instance receptor mediated endocytosis [71, 72], membrane trafficking [27], homeostasis of bone tissue, or renal acid secretion [70]. Hence, malfunction of these enzymes can cause

diseases such as osteopetrosis [73] or renal acidosis [70]. The other way around, over-expression of v-ATPases is evidently associated with other severe diseases such as osteoporosis and cancer [70, 72]. This has evoked great interest of biomedical research [22, 70] in terms of inhibiting v-ATPases as anti-osteoporosis and anti-cancer approach [74].

The assembly of v-ATPases appears complex (see Fig. 1.5), but the functional principle is simple: Two major domains, one situated in the cytoplasm (V_1), and the other one largely integrated in membranes (V_0), build the holoenzyme. V_1 provides ATP hydrolysis. Released energy is transduced into rotation of the membrane embedded proteolipid ring in the V_0 domain, whereby protons get translocated (see Fig. 1.5). The enzyme activity is regulated by reversible association and dissociation [72].

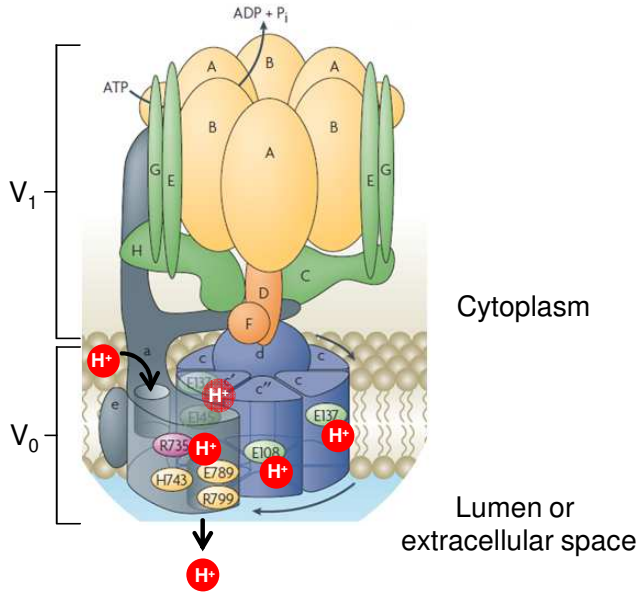

Fig. 1.5 Assembly of v-ATPases and principle of proton transprt. The cytoplasmic part (V_1) consists of eight different proteins with the putative stoichiometry $A_3B_3CDE_2FG_2H$, whereas the membrane integrated part (V_0) contains six different proteins (a_1, $c_{4\text{-}5}$, c'_1, c''_1, d_1 and e_1) [74]. When the holoenzyme is assembled, ATP is hydrolyzed in the V_1 part (via A and B), energy is translated by the circulating rotor (D, F, d) into rotation of the membrane integrated proteolipid ring (built of c,c' and c''). Protons pass the membrane via two hemi-channels (located in subunit a) by intermediate binding to glutamate (in c, c', c'' and a) and arginine residues (in subunit a). Peripheral stalks (G, E, H, C, and the N-terminal domain of a) are used to stabilize the connection between V_1 and V_0. The horizontal stalk of subunit a is likely to prevent passive rotation and thus uncontrolled proton translocation [72]. Image from Forgac [72].

The first specific inhibitors of v-ATPases, the plecomacrolides bafilomycin and concanamycin (ConcmA) were discovered in 1984 in *Streptomyces* strains [53, 54, 75]. By screenings in further natural sources (e.g. marine sponges [76] or myxobacteria [77, 78]) new potent classes of v-ATPase antagonists, e.g. benzolactone enamides (salicylamide [76] and apicularen [77]) and macrolactones (archazolid [78]), were identified. Indolyls were the first synthetic inhibitors, inspired by the bafilomycin structure [74, 79]. Astonishingly, it seems that most v-ATPase inhibitors, including concanamycin A, block v-ATPase function via binding to the subunit c proteolipid ring or nearby to the subunit a, though with clear differences concerning their exact binding site [52, 74, 80-83].

With respect to their high inhibition potency on isolated enzyme (EC_{50} in low nanomolar range[74]), interference with proteolipid ring rotation or proton association seems to be the most efficient inhibitory strategy [74, 80].

1.3.2.1 V-ATPases – relevant functions in cancer and tumor angiogenesis

Cancer cells and cancer associated endothelial cells (Fig 1.6 A) are exposed to a highly acidic environment, caused by the upregulated metabolic rate and poor oxygen supply within the tumor tissue [31, 84]. To cope with these hostile living conditions, tumors evolve strategies for acid elimination [84]. One of these strategies is the increased expression of v-ATPases at the plasma membrane (pm v-ATPases) [22, 25], since this creates a slight alkaline intracellular pH, which is favorable for cell proliferation and tumor cell survival [84]. Furthermore, acidification of the tumor environment is detrimental to most chemotherapeutics, which often are weak bases and cannot reach intracellular targets in protonated status [84].

In terms of cell migration and matrix invasion, it was reported, that highly invasive tumor cells and endothelial cells, over-express pm v-ATPases at the leading edge, which creates an intracellular pH gradient (Fig 1.6) [21, 24, 25]. Similarly to the function of a polarized microtubule cytoskeleton, [64] it was proposed that intracellular pH asymmetry determines asymmetric actin polymerization, which generates cell migration [21, 64] (Fig.1.4 and Fig.1.6). Moreover, low extracellular pH is reported to activate proteases which degrade and remodel the extracellular matrix (ECM), and thus facilitate cell invasion and migration into the underlying tissues[21, 34]. Relevant for tumor angiogenesis is also the finding, that pm v-ATPases may differentially activate certain isoforms of these proteases (e.g. MMP 9) [34], which are described to release sequestered growth factors, particularly VEGF, from the ECM [33], and thus further sustain the angiogenic switch (Fig. 1.6).

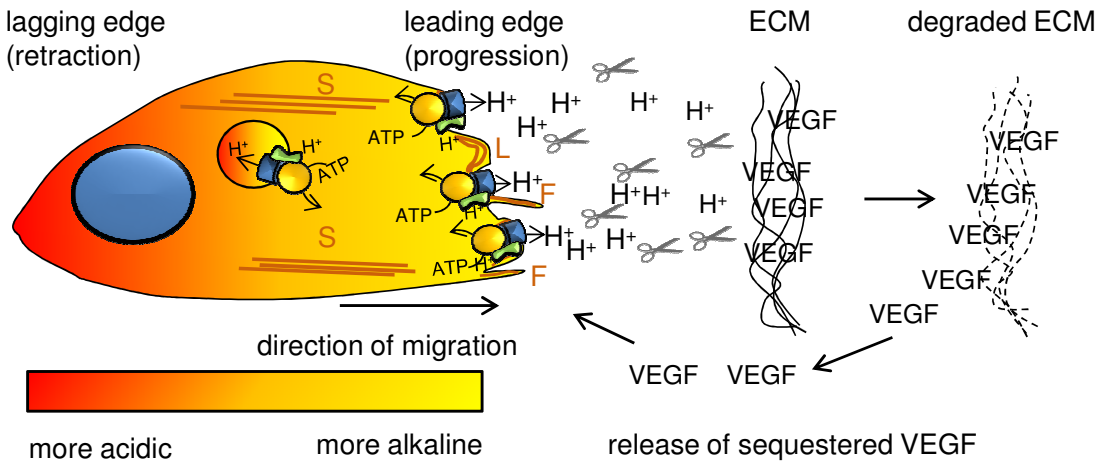

Fig. 1.6 Functions of plasma membranous v-ATPases with relevance to cancer and angiogenesis. Enhanced expression of plasmalemmal (pm) v-ATPases at the leading edge of migrating cells (endothelial cells or cancer cells) provides a polarized intracellular pH, which might favor the formation of an asymmetric actin network (S: Stress fibers, L: Lammelipodia, F: Filopodia). Acidification of extracellular space activates proteolytic enzymes (Matrix metalloproteinases, scissors) to degrade matrix proteins and release pro-angiogenic growth factors [33], which in turn promote tumor angiogenesis. Proposed mechanism adapted from Perez-Sayans et al. [21] and Bergers et al. [33].

V-ATPases are distributed along the whole endo- and exocytic pathway (Fig. 1.7) and known to control crucial functions such as membrane trafficking [27, 70, 85]. Therefore, besides pm v-ATPases, intracellular v-ATPases display a further potential 'target', whose functional inhibition might contribute to anti-cancer or anti-angiogenic effects.

Recently, Wiedmann and colleagues could demonstrate, that the application of low nanomolar doses of a v-ATPase inhibitor disturbs intracellular membrane traffic in highly invasive cancer cells, and thus potently inhibits cancer cell migration and matrix invasion.
The treatment induced a delay in endocytosis of EGFR. Furthermore, v-ATPase inhibition disorganized the spatial distribution of EGFR and Rac-1, and consequently the activation of Rac-1 [23, 86].

1.3.3 VEGFR2 trafficking as target of v-ATPase inhibition

The intracellular trafficking of VEGFR2 could be similarly affected by v-ATPase inhibition. But it has to be considered that its trafficking behavior is unique among RTKs, Fig 1.7. One characteristic feature is the steady state cycling between cell surface and intracellular compartments under non-stimulated conditions with approx. 40 % of VEGFR2 being resident in an intracellular sorting compartment [87]. The receptor recycling rate is increased under stimulation with VEGF [28, 87, 88]. In contrast to that, the vast majority of EGFR resides at the cell surface in non stimulated condition, and gets largely internalized upon stimulation with EGF [89].

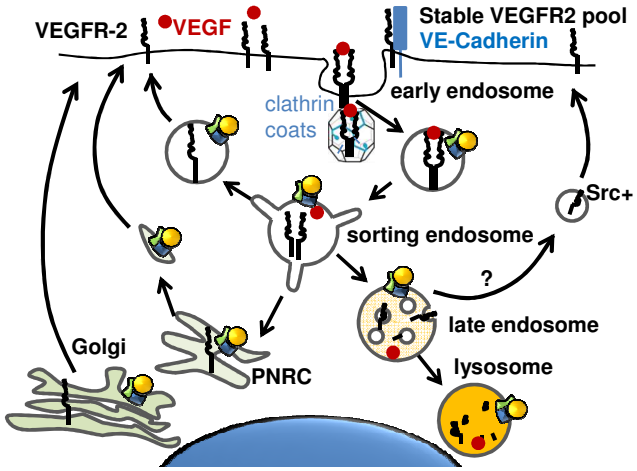

Fig. 1.7 Distribution of intracellular v-ATPases [70] and regular VEGFR2 trafficking [28].

Intracellular v-ATPases provide constant pH levels, specific for each membrane compartment along the endocytic pathway [70].
VEGFR2 undergoes a unique way of receptor trafficking. Characteristic are for instance two VEGFR2 fractions at the cell surface. One is constantly internalized via clathrin dependent endocytosis, the other one is stabilized by VE-cadherin. Internalized VEGFR2 traffics via early endosomes and sorting endosomes back to the surface (short loop). Another recycling pathway goes via the perinuclear recycling compartment (PNRC, long loop), and a third putative loop goes via a src containing (src+) compartment [28, 87]. Minor portions of VEGFR2 get lost in lysosomes. Stimulation with VEGF does not increase receptor uptake, as for EGFR [89], but accelerates intracellular trafficking and slightly increases lysosomal degradation [28]. Image adapted from Scott et al.[28] and Hinton et al.[70]

1.4 Aims

In the first part, we wanted to evaluate the anti-angiogenic potential of a chemically accessible tubulysin precursor, pretubulysin, and seven of its derivatives in comparison with the anti-angiogenic established but poorly accessible tubulysin A. Further, we wanted to assess the most active candidate of *in vitro* tests in an *in vivo* tumor model for inhibition of tumor growth and tumor vascularization.

In the second part, we wanted to characterize the influence of v-ATPase inhibition on VEGFR2 trafficking, by measuring key parameters on function and distribution of the receptor in endothelial cells. We wanted to test, if these parameters could be connected to angiogenesis related cell functional changes after v-ATPase inhibition.

2 Materials and Methods

2.1 Materials

2.1.1 Test compounds

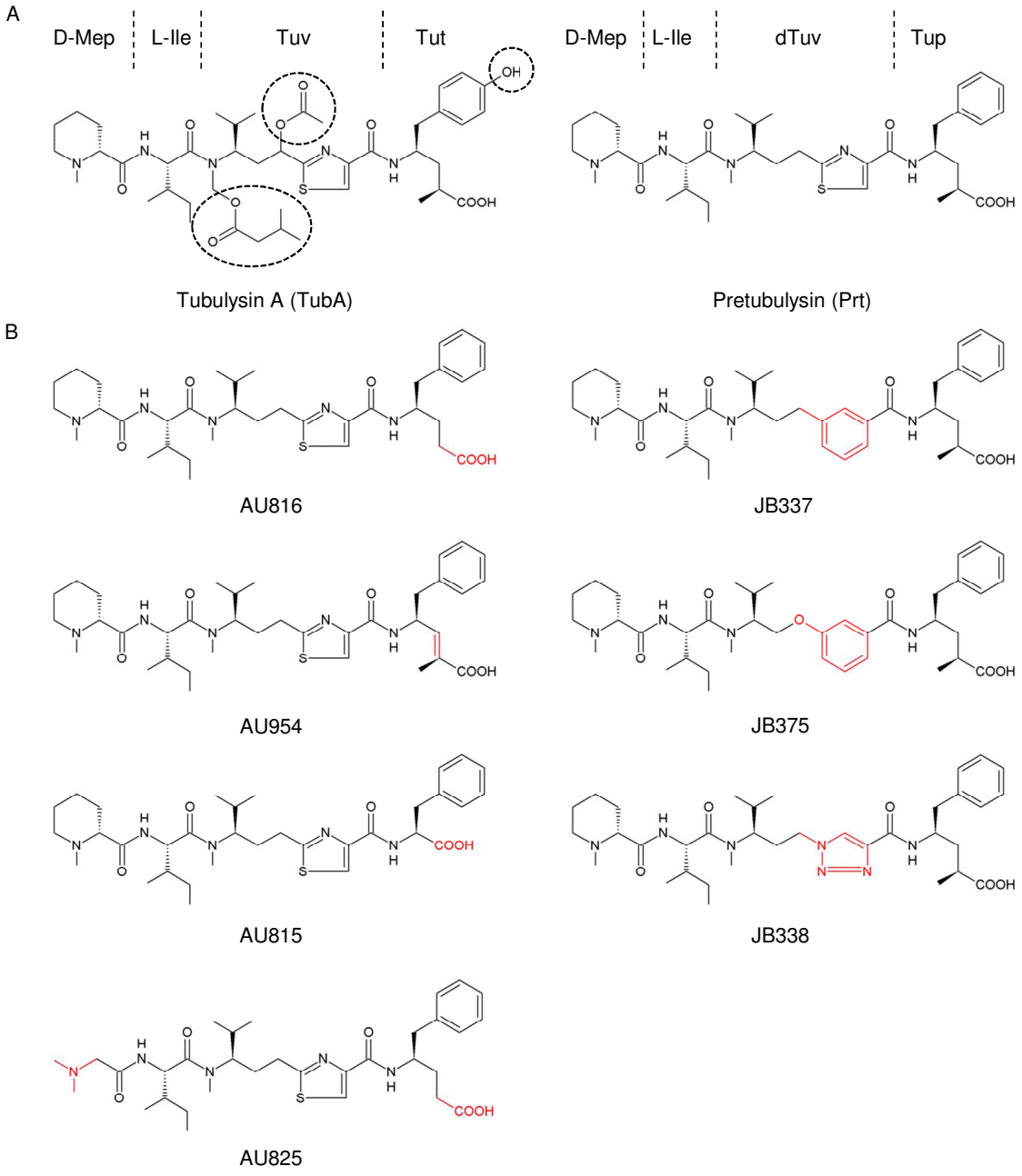

Fig. 2.1 A) Chemical structures of tubulysin A (TubA) and pretubulysin (Prt); TubA and Prt each contain four different amino acids. Prt lacks the acyloxy-side moieties, which are introduced after assembly of the tetrapeptidic core. In addition, Prt has a different C-terminal amino-acid than TubA (Tup instead of Tut)[18]. **B) Prt-analogues** were either modified at N/C terminal position or at central position[15, 16]. Abbreviations: D-Mep (N-Methylated D-pipecolic acid), L-Ile (L-Isoleucine), Tuv (Tubuvaline with C-acetoxy and N,O-acetal moeities), dTuv (C-desacetoxy-tubuvaline), Tut (Tubutyrosine), Tup (Tubuphenylalanine). Structural differences from Prt are indicated by dotted circles (A) or by red color (B). Structures adapted from Ullrich et al., Burkhart et al. [15, 16] and from A.Ullrich and J.Burkhart, personal communication.

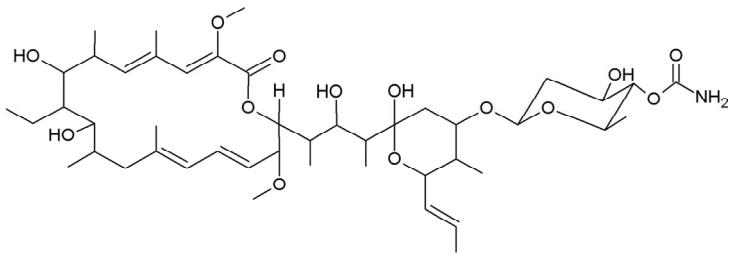

Concanamycin A (ConcmA)

Fig. 2.2 Chemical structure of Concanamycin A (ConcmA). ConcmA is a specific v-ATPase inhibitor with plecomacrolide structure. Structure adapted from Huss et al.[74]

2.1.1.1 Tubulin inhibitors

Pretubulysin (Prt) and derivatives thereof (Fig. 2.1) were kindly provided from Dr. Angelika Ullrich and Dr. Jens Burkhart from the Institute of Organic Chemistry, Saarland University, Chair Prof. Uli Kazmaier[15, 16]. Tubulysin A (TubA), Fig. 2.1 A, was purchased from Merck Calbiochem (Darmstadt, Germany). 10 mM stock solutions of the compounds were prepared in DMSO. The final DMSO concentration did not exceed 0.3 %, a concentration verified not to affect respective experimental parameters.

2.1.1.2 V-ATPase inhibitors

Concanamycin A (ConcmA), Fig.2.2, was purchased from Alexis Biochemicals (Enzo Life Sciences Inc., Lörrach, Germany). DMSO stock solutions of 0.5 mM were kept in 1 µl aliquots at – 80 °C and were used once to avoid repeated freeze-thaw cycles. The highest final DMSO concentration in the experiments with ConcmA did not exceed 60 ppm.

2.1.2 Technical equipment

Table 2.1 Technical Equipment

Name	Device	Producer
AB7300 RT-PCR	Real-time PCR system	Applied Biosystems, Foster City, CA, USA
Axioskop	Upright microscope	Zeiss, Jena, Germany
Axiovert 200	Inverted microscope	Zeiss, Jena, Germany
'The Brick'	Heat and CO_2-flow rate controlling device	Life imaging services, Basel, Switzerland

Name	Device	Producer
Culture flasks, plates, dishes, cell scrapers	Disposable cell culture material	TPP, Trasadingen, Switzerland
Custom made climate chamber	Life cell observation on Axiovert 200	Ibidi GmbH, Munich, Germany
Curix 60	Tabletop film processor	Agfa, Cologne, Germany
E835, EV202	Electrophoresis power supplies	Consort, Turnhout, Belgium
FACScalibur	Flow cytometer	Becton Dickinson, Heidelberg, Germany
Heating block	Heating block	Peqlab, Erlangen, Germany
HT 50	Climate controlling device	Ibidi GmbH, Munich, Germany
Imago-QE camera and appending software	Life cell observation on Axiovert 200	Till Phototonics Gräfelfing, Germany
LSM 510 Meta	Confocal laser scanning microscope	Zeiss, Jena, Germany
Mikro 220R	Table centrifuge	Hettich, Tuttlingen, Germany
Nanodrop® ND-1000	Spectrophotometer	Peqlab, Wilmington, DE, USA
AMAXA Nucleofector II	Electroporation device	Lonza GmbH, Cologne, Germany
Odyssey 2.1	Infrared Imaging System	LI-COR Biosciences, Lincoln, NE, USA
Olympus BX41	Clinical microscope	Olympus, Hamburg, Germany
SpectraFluor Plus™	Microplate multifunction reader	Tecan, Männedorf, Austria
Spectrophotometer DU 7500	Diode array photometer	Beckmann Coulter, Krefeld, Germany
Sunrise™	Microplate absorbance reader	Tecan, Männedorf, Austria
Vi-Cell™ XR	Cell viability analyzer	Beckman Coulter, Krefeld, Germany

Name	Device	Producer
µ-slide Chemotaxis; Angiogenesis; 8 well	µ - slides for microscopy	Ibidi GmbH, Munich, Germany

2.1.3 Biochemicals, inhibitors, dyes and cell culture reagents

Table 2.2 Biochemicals, inhibitors, dyes and cell culture reagents

Reagent	Provider
Accustain® paraformaldehyde	Sigma-Aldrich, Taufkirchen, Germany
Amphotericin B	PAA Laboratories, Pasching, Austria
BC Assay reagent	Interchim, Montlucon, France
Bovine Serum Albumin (BSA)	Sigma-Aldrich, Taufkirchen, Germany
Collagen G	Biochrom AG, Berlin, Germany
Collagenase A	Biochrom AG, Berlin, Germany
Complete® mini EDTA free	Roche diagnostics, Penzberg, Germany
Coomassie brilliant blue G250	Carl Roth, Karlsruhe, Germany
DMEM	PAA Laboratories, Pasching, Austria
DMSO	AppliChem, Darmstadt, Germany
EGTA-K	AppliChem, Darmstadt, Germany
Endothelial Cell Growth Medium (ECGM)	PromoCell, Heidelberg, Germany
FCS gold	PAA Laboratories, Pasching, Austria
Fibronectin	BD Biosciences, Heidelberg, Germany
FluorSave™ Reagent mounting medium	Merck, Darmstadt, Germany
GTP	Sigma Aldrich, Taufkirchen, Germany
Leibowitz Medium L15	Biochrom AG, Berlin, Germany
M199 Medium	PAA Laboratories, Pasching, Austria
MAP - rich tubulin from porcine brain	Cytoskeleton Inc., Denver, CO, USA
Matrigel™	BD Biosciences, Heidelberg, Germany
$MgSO_4$	Merck, Darmstadt, Germany
NaF	Merck, Darmstadt, Germany
Na_3VO_4	ICN Biomedicals, Aurora, OH, USA
Page Ruler™ Prestained Protein Ladder	Fermentas, St. Leon-Rot, Germany
Penicillin, Streptomycin	PAA Laboratories, Pasching, Austria

Reagent	Provider
PIPES	AppliChem, Darmstadt, Germany
PMSF	Sigma-Aldrich, Taufkirchen, Germany
Streptavidin-agarose beads	Millipore, Temecula, CA, USA
Sulfo-NHS-lc-biotin	Interchim, Montluçon, France
Tris HCl	Sigma Aldrich Taufkirchen, Germany
Triton X-100	Merck, Darmstadt, Germany
Tween®20	BDH/Prolabo®, Ismaning, Germany
VEGF 165, human recombinant	PeproTech GmbH, Hamburg, Germany

2.1.4 Cell culture media and buffers

The following cell culture media and buffers were used as indicated.

2.1.4.1 Cell culture media

Table 2.3 Cell growth media

Endothelial Cell Growth medium	
ECGM PromoCell	500 ml
Supplement Mix #C-39215	23.5 ml
FCS gold	50 ml
Penicillin/Streptomycin	5 ml
Amphothericin B	5 ml

HuH7 Cell Growth Medium	
DMEM	500 ml
FCS	50 ml

Before use, FCS gold and FCS were heat inactivated at 56°C for 30 min. FCS aliquots were kept at -20°C for storage. Regularly, cell media were tested for mycoplasma contamination with the Venor®GeM PCR detection kit (Minerva Biolabs, Berlin, Germany).

Table 2.4 Starvation media

Starvation Medium		pH buffered starvation Medium	
M199	500 ml	Leibowitz Medium L15	500 ml

Table 2.5 Freezing medium

Freezing medium	
FCS gold	10%
DMSO	10%
ECGM or HuH7 growth medium	

2.1.4.2 Coating matrices

If not other stated, Collagen G was used for coating cell culture plastic surfaces

Table 2.6 Coating solution

Collagen G	
Collagen G	0.001%
PBS	

2.1.4.3 Cell detachment and isolation media

Table 2.7 Cell detachment media

Trypsin/EDTA (T/E)		Collagenase A for HUVEC isolation	
Trypsin	0.05%	Collagenase A	0.01%
EDTA	0.20%	PBS+ Mg^{2+}/Ca^{2+}	
PBS			

Table 2.8 Stopping medium

Stopping medium	
M199	500ml
FCS	

2.1.4.4 Commonly used buffers

Table 2.9 Commonly used buffers

PBS (pH 7.4)	
NaCl	132.2 mM
Na_2HPO_4	10.4 mM
KH_2PO_4	3.2 mM
H_2O	

PBS + Mg^{2+}/Ca^{2+}	
NaCl	137 mM
KCl	2.68 mM
Na_2HPO_4	8.10 mM
KH_2PO_4	1.47 mM
$MgCl_2$	0.25 mM
H_2O	

2.2 Methods

2.2.1 Cell culture

2.2.1.1 Cell lines

2.2.1.1.1 Human Microvascular Endothelial Cells (HMEC-1)

Human Microvascular Endothelial Cells (HMEC-1) were obtained from the Centre for Disease Control and Prevention (CDC, Atlanta, GA, USA) and were used until twelfth passage maximum. This immortalized cell line was originally created by transfection of human dermal microvascular endothelial cells with a SV40 large T-antigen containing plasmid. Still, HMEC-1 are known to retain characteristics of primary endothelial cells in shape and function [90]. We used HMEC-1 for experiments on endothelial cell proliferation, cell cycle distribution, DNA fragmentation, tube formation and in assays using immune-cytochemistry. Furthermore, HMEC-1 were assessed for changes on lysosomal pH, cell morphology, endothelial wound repair, cell to matrix adhesion, ruffle formation, VEGF induced signaling and for the biochemical analysis of VEGFR2 surface levels.

2.2.1.1.2 Primary human umbilical vein endothelial cells (HUVEC)

Primary human umbilical vein endothelial cells (HUVEC) were freshly isolated by Collagenase A treatment, as previously described [91]. The human umbilical cords therefore were kindly provided from Munich hospitals and from the Munich

surroundings: Klinikum München Pasing, Frauenklinik München West/Krüsmannklinik, Rotkreuzklinikum München, and Wolfart Klinik Gräfelfing and were kept at 4°C in PBS+Ca^{2+}/Mg^{2+} containing penicillin (100 U/ml) and streptomycin (100 µg/ml) until isolation procedure. HUVEC were used at passage #3 for the following assays: endothelial wound repair, chemotaxis, cell matrix adhesion, DNA fragmentation, Rac-1 activation, tube formation, immune-cytochemistry assays, siRNA transfection combined with scratch migration, cell morphology assays and for the biochemical analysis of VEGFR2 surface levels.

2.2.1.1.3 HuH7- human hepatocellular carcinoma cell line

HuH7 cells were obtained from the Japan Health Science Research Bank (JCR B0403) and cultivated in DMEM medium containing 10% FCS. They were used between passage #10 and #14 for a subcutaneous xenograft tumor model in SCID mice (2.2.7). Furthermore, HuH7 cells were tested in an *in vitro* proliferation assay (2.2.5).

2.2.1.2 Cell passaging and cultivation

For passaging and seeding, confluent cells were washed twice with pre-warmed PBS to remove serum and growth factors, the cells were detached by incubation with 1-2 ml Trypsin/EDTA (T/E) for a few minutes at 37 °C (HUVEC: 1-2 min, HMEC-1: 3 min, HuH7: 5 min). To saturate trypsin and EDTA with a surplus of substrate, 10 ml stopping medium were added. Cells were poured into 50 ml falcons and centrifuged for 5 min at 180 rcf. The supernatant was discarded and cells were resuspended in the referred growth medium. Subsequently, cells were either split at a ratio of 1:3 into new flasks or used for experiments. In the latter case, cell numbers are indicated for the respective experiment. For a better adhesion and cell function, surface materials were precoated with 0.001% collagen G (Hersteller Biochrom, Berlin) or with another coating matrix, when indicated. Cell concentration and viability were determined using ViCELL™ cell viability analyzer (Beckman Coulter, Krefeld, Germany). All cell lines were cultured under constant humidity at 37°C with 5% CO_2 in a cell incubator (Heraeus, Hanau, Germany).

2.2.1.3 Cell freezing and thawing

For long term cell storage, cells were kept in liquid nitrogen. Before freezing, confluent cells from a 150 cm^2 flask were trypsinized, centrifuged in stopping medium (180 rcf, 5 min) and resuspended to 2 x 10^6 cells/ml in ice-cold freezing medium. Then, aliquots of 1.5 ml were distributed in cryovials and kept at -80 °C for 24 h. Finally, cells were transferred into liquid nitrogen tanks for long term storage. For thawing, an aliquot in a cryovial was warmed to 37 °C. The contained cell suspension was then immediately

dissolved in pre-warmed stopping medium, centrifuged (180 rcf, 5 min) in order to remove residual DMSO and finally resuspended in the respective growth medium and cultivated in a precoated 75 cm^2 culture flask.

2.2.2 Confocal microscopy

By use of immune-cytochemistry or chemical fluorescence labeling, sub-cellular structures were analyzed with a confocal microscope (Zeiss LSM 510 META, Zeiss, Oberkochen, Germany). The staining procedures are described below.

2.2.2.1 Microtubule staining

30.000 HMEC-1 were seeded into 0,001% collagen G coated 8-well µ-slides (Ibidi, Martinsried, Germany) and stimulated with Tubulysin A (TubA); Pretubulysin (Prt) or the Prt-derivatives for 16 h. Cell extraction buffer (80 mM PIPES pH 6,8; 1 mM $MgCl_2$, 5 mM EGTA-K and 0.5%Triton X-100) was used in order to remove monomeric and dimeric tubulin subunits to reduce background staining. After 30 sec of extraction, cells were fixed for 10 min by adding glutaraldehyde to final 0.5%. Excess glutaraldehyde was removed and quenched with 0.1% $NaBH_4$ in PBS for 7 min. Cells were washed thoroughly with PBS again, blocked with PBS 0.2% BSA and stained for α-tubulin and nuclei (see 2.2.2.2. for immune-staining procedure and table for antibodies, reagents and dilutions).

2.2.2.2 v-ATPase subunit c staining in migrating human endothelial cells

100.000 HMEC-1 and HUVEC were seeded into 8-well µ-slides from Ibidi and left untreated to grow to confluent level. Cell monolayers were scratched using a yellow pipette tip. Detached cells were removed by washing twice with pre-warmed PBS+. Endothelial cells were allowed to migrate for 8 h, to establish a migration leading edge. All further incubation steps were performed under gentle agitation at RT. Cells were fixed with 4% paraformaldehyde for 10 min. For permeabilization, cells were incubated for 2 min with 0.2% Triton/PBS. As blocking solution 1% BSA/PBS was added and incubated for 10 min. Antibodies were diluted in 0.1% Triton/1% BSA/PBS. Samples were generally incubated with the primary antibodies for 1 h at RT, followed by three washing steps with PBS+ and the 1 h incubation with the secondary antibodies and staining reagent rhodamine phalloidin for f-actin for 1 h. Hoechst 33342 was added for 5 min at a concentration of 0.05 µg/ml, if nucleus staining was required. Cells were then washed further three times with PBS+ and finally covered with 1 drop FluorSave mounting medium and a glass coverslip (custom made by Helmut Saur Laborbedarf, Reutlingen, Germany). Thus, samples could be stored at 4 °C until analysis at the confocal microscope.

Besides by immune-cytochemistry, subunit c protein in untreated HMEC-1 and HUVEC monolayers were determined by Western blot analysis, see 2.2.10.

2.2.2.3 pH dependent detection of lysosomes

Lysosomes in ConcmA treated HMEC-1 were labeled by 2 h incubation with 75 nM LysoTracker® Red. Nuclei were stained by addition of 0.1µg/ml Hoechst 33342, 5 min. Here, no washing steps, fixation or coverslips were used prior to confocal microscopy. Lysosomal pH dependent staining was analyzed 2 h and 24 h after ConcmA addition.

2.2.2.4 Immune-staining of VEGFR2

In HMEC-1, VEGFR2 was either stained alone (after 2 and 24 h ConcmA treatment) or together with markers for the endocytic pathway (after 24 h ConcmA treatment) using appropriate primary antibodies and fluorophore-labeled secondary antibodies (see table). In addition, nuclei were stained with Hoechst 33342, as described (2.2.2.3.).

Table 2.10 Primary antibodies used for immune-cytochemistry

Antigen	Source	Dilution	Provider
α-tubulin	rabbit	1:100	Abcam
subunit c (ATP6L)	rabbit	1:100	Millipore
VEGFR2	mouse	1:400	Abcam
VEGFR2	rabbit	1:200	Cell Signaling
Lamp 1	mouse	1:400	Hybridoma Bank, Univ. of IOWA, USA
Caveolin 1	rabbit	1:100	Novus Biologicals
Rab 5a	rabbit	1:100	Santa Cruz
Clathrin HC	rabbit	1:500	Abcam

Table 2.11 Secondary antibodies used for immune-cytochemistry

Antibody	Dilution	Provider
Alexa Fluor® 488 goat anti-mouse IgG (H+L)	1:600	Molecular Probes
Alexa Fluor® 647 chicken anti-rabbit IgG (H+L)	1:600	Molecular Probes

Table 2.12 Staining reagents used for immune-cytochemistry

Staining reagent	Dilution	Provider
Rhodamin-phalloidin	1:400	Molecular Probes
Hoechst 33342 (Bisbenzimide)	1:1000	Sigma-Aldrich

2.2.3 Tubulin polymerization assay

Porcine brain tubulin, enriched with Microtubule-associated proteins (MAP) was obtained from Cytoskeleton Inc. (Cat.# ML116 Denver, CO, USA). Tubulin polymerization was monitored by use of turbidometry as described by Gaskin et al. [92]. Samples (200 µl, 10 µM tubulin) dissolved in polymerisation buffer (0.1 molar PIPES, pH 6.6, 1 mM EGTA, 1 mM $MgSO_4$, and 1 mM GTP) were rapidly warmed to 37 °C in a water-jacketed cuvette holder of a diode array photometer (Spectrophotometer DU 7500, Beckmann Coulter, Krefeld, Germany). Absorbance at 350 nm was monitored in absence and presence of TubA, Prt or Prt-derivatives at indicated concentrations. This experiment was kindly performed by Jennifer Herrmann from the Helmholtz Centre for Pharmaceutical Research, University of Saarland, Saarbrücken, Germany.

2.2.4 Flow cytometry

2.2.4.1 Quantification of nuclear fragmentation and cell cycle

In order to determine, the extent of cytotoxicity contribution to the overall inhibition of functional parameters important for angiogenic morphogenesis (Rac-1 activation, ruffle formation, migration, chemotaxis, tube formation), HMEC-1 or HUVEC, respectively, were incubated with the compounds in 24 well plates at the same density, drug:cell ratio and within appropriate time frames as in the respective functional assays (24 h or 48 h). As one late indicator for cell death, the nuclear fragmentation was determined according to Nicoletti et al [93]. In brief, after treatment, cells were harvested on ice and incubated in a hypotonic buffer (0.1% sodium citrate, 0.1% Triton X-100 and 50 µg/ml propidium iodide (PI)) overnight at 4°C, and then analyzed by flow cytometry on a FACScalibur (Becton Dickinson, Heidelberg, Germany) using Cell Quest Pro Software (Becton Dickinson, Heidelberg, Germany). Nuclei to the left of the G_1-peak containing hypodiploid DNA were considered as fragmented. In the same set of experiments the percentage of cells in G_2/M phase was evaluated using the Flow Jo software (Tree Star Inc. Ashland, OR, USA).

2.2.4.2 Determination of membrane integrity

As an independent marker for cytotoxicity, membrane integrity was tested by examining the uptake of PI in non-permeabilized cells *in situ* subsequently to the functional assay (e.g. in the scratch assay, 24 well format). Cells were incubated with 10 µg/ml PI, not containing any detergent, for 30 min. Under these conditions, PI only can enter cells with a damaged cell membrane (i.e. dead cells). Cells were harvested on ice and analyzed by flow cytometry or for PI fluorescence. PI-positive cells were gated and analyzed using Cell Quest Pro Software. Alternatively, tubes generated on Matrigel™, or HUVEC from scratch assays in a 96 well format, were incubated with propidium iodide to detect dead cells *in situ* by fluorescence microscopy.

2.2.5 Proliferation assay

The Proliferation assay was performed according to NCI protocols for angiogenesis. Briefly, 1.500 HMEC-1 per well were seeded into 96 well plates in 100 µl of media. After 24 h, one plate of control cells was fixed and stained with crystal violet solution. The other plates were incubated with increasing concentrations of the compounds to be tested for 72 h. After this time, cells were fixed and stained as well with crystal violet solution (0.5% crystal violet in 20% methanol) for 10 min. Unbound crystal violet was removed by rinsing with distilled water and cells were subsequently air dried. Crystal violet, which mainly binds to DNA, was eluted from cells with 0.1 M sodium citrate in 50% ethanol. The absorbance of crystal violet is proportional to the cell number and was determined at 540nm with Magellan 6 (TECAN, Männedorf, Switzerland). By comparing the staining intensity at day 3 of treatment with staining intensity of untreated cells at day 0, the relative proliferation was calculated. Proliferation of untreated cells was set as 100%. For the investigation of effects of Tubulysin A and Pretubulysin on the proliferation of the HuH7 tumor cells, used in the *in vivo* assay (2.2.7), the same protocol was used.

2.2.6 Angiogenic morphogenesis assays

For assays connected to endothelial migration and differentiation (scratch assay, chemotaxis assay, Rac-1 activation), primary endothelial cells (HUVEC) were used instead of HMEC-1, since they yielded more stable effects. Nevertheless, scratch migration and tube formation experiments with ConcmA were performed by comparing both cell lines HUVEC and HMEC-1, since it was reported, that microvascular endothelial cells exhibit higher migratory potential than macrovascular endothelial cells due to different pm v-ATPase expression [25].

2.2.6.1 Migration scratch assay

In preparation of the scratch assay, cells were seeded into 24 well plates at densities of 0.75 x 10^5 per well and were grown to confluency. A wound of approx. 1 mm was inflicted into the monolayers by scratching with a yellow pipette tip. Detached cells were removed by washing with PBS+. Remaining cells were incubated for 16 h either in starvation medium (free of growth factors and serum, 0% migration), culture medium (100% migration) or culture medium containing increasing concentrations of the test compounds. When ConcmA was applied, confluent cells had been pre-incubated for 24 h prior to scratch infliction additionally to the presence of compound for the duration of the migration assay. Then, cells were washed with PBS+ and fixed with 4% formaldehyde for 10 min at RT. One image was taken of each well (centre position) on an inverted light microscope (Axiovert 200; Zeiss, Jena Germany) with a 5x lens using an Imago-QE camera system and the appending software (Till Photonics, Graefelfing, Germany). For quantification, these images were analyzed with WimScratch Wound Healing Module (WIMASIS, Munich, Germany). This online software tool is able to distinguish the cell-covered from the wounded area by using an algorithm based on brightness and contrast values. The increase of cell covered area correlates with the ability of the HUVEC to migrate into the wound. Relative migration was calculated related to control and to starvation control.

2.2.6.2 Migration scratch assay with siRNA transfected HUVEC

For siRNA transfected HUVEC (2.2.11), the scratch assay protocol was slightly alterated. Transfected cells were seeded into precoated 96 well plates at a concentration of 80.000 and 100.000/100 µl to quickly reach confluent levels overnight. 24 h after transfection, monolayers were scratched, using a multi scratch device (custom made LMU Munich), resulting in an equal wound size of approx. 0.7 mm. For evaluation, the initial wound size was compared to the final wound size after 16 h of incubation using the same optical devices as described above.

2.2.6.3 Chemotaxis assay

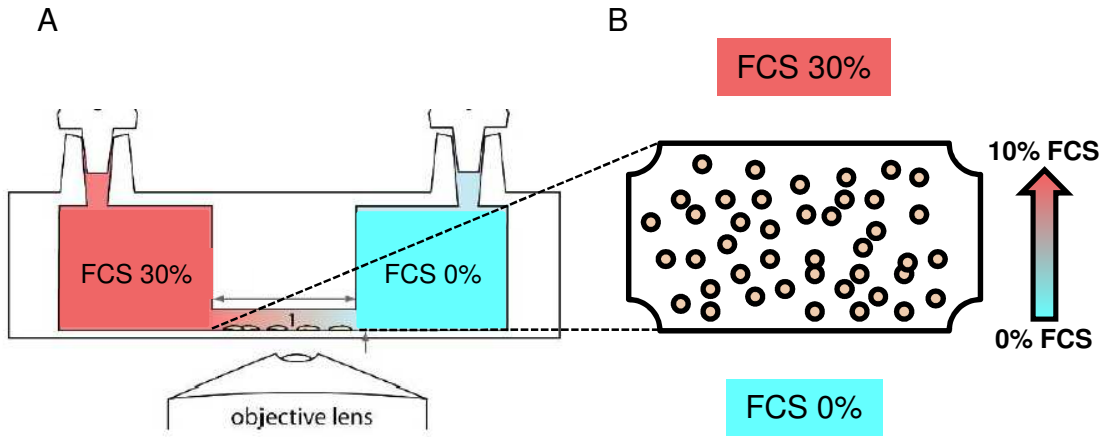

Fig. 2.3 Chemotaxis assay, gradient assembly. (A) Cross section of a chemotaxis slide and (B) bird perspective on the observation area bearing adhered HUVEC. (B) Two reservoirs, above and below the observation field, contain either 30% FCS or starvation medium (M199 or L15). Thus, a serum gradient of 0% to 10% FCS is established in the middle of these reservoirs, where the HUVEC are seeded. HUVEC movement is observed for 20 h. Finally, their orientation ability for the higher serum concentration is evaluated. Image (A) adapted from Ibidi GmbH, chemotaxis application note 14.

Prior to the chemotaxis assay, 10 µl of 5 x 10^6 HUVEC (suspended in ECGM) were seeded into 'µ-slides chemotaxis' chambers coated with collagen IV (Ibidi, Martinsried, Germany) and incubated for 1 h at 37°C. In order to remove growth factors and unattached cells, HUVEC were cautiously flushed twice with M199 (used in the case of external CO_2 supply) or L15 (used when no CO_2 supply was available). Then, a FCS gradient from 0% FCS to 10% FCS inside of the cell observation chamber (Fig. 2.3) was created either with M199 or with L15, according to the manufacturer's application note. Life cell imaging was performed with the setup described under 'Migration scratch assay', either using a device able to follow one single experiment, or alternatively using a motorized stage combined with autofocus (x,y,z), which allows the observation of three experiments in parallel (appending software LA Tillvision). Climate was kept at 37° C, 5% CO_2 or buffered pH (L15), and 80% relative humidity. Images of cell migration were obtained every 10 min for 20 h. For analysis, Image J plugins 'Manual Tracking' and 'Chemotaxis Analysis' (National Institutes of Health, USA) were used. These tracking modules allow assessment of both, overall migration parameters, such as the total path, a cell has covered (accumulative distance) and directional parameters such as the 'air-line distance' (Euclidean distance) and the tendency of forward migration to the higher serum concentration (y-forward index). For Prt evaluation, HUVEC were directly treated with Prt or TubA for the duration of the chemotaxis experiment (20 h). For experiments with ConcmA, HUVEC were treated as described in 2.2.6.1. Only vital cells were taken into account for the chemotaxis evaluation.

2.2.6.4 Cell adhesion and ruffle formation

HMEC-1 were pre-treated for 24 h with ConcmA and then seeded at densities of 0.75 x 10^5 cells per well inro 24 well plates. Adhesion surfaces had been precoated with various matrix solutions (0.001% collagen G, 25µg/ml fibronectin, 10% Matrigel™) for 30 min at RT. Alternatively, plates were left uncoated to test cell plastic adhesion. After an incubation of 30 min at 37°C, supernatants were discarded and unbound cells were removed by once washing with pre-warmed PBS+. Remaining adhered cells were fixed using 4% formaldehyde. For analysis, two central images were taken per well, 10 x magnification (Axiovert 200, Zeiss, QE Imago camera). Cells were counted and number of cells with clear ruffle formation was calculated in % of total adhered cells.

2.2.6.5 Rac-1 pulldown assay

Confluent HUVEC monolayers were either treated for 24 h with 10 nM of ConcmA or left untreated. Rac-1 activation was then induced by seeding each 4 Mio cells on collagen precoated 100 cm dishes, as previously described (2.2.6.4). After 30 min, cells were harvested on ice and the Rac-1 pulldown was performed with a biochemical kit (Product # 16118, Pierce, Thermo Scientific Inc., Rockford, IL USA) according to the manufacturer's instructions. Thereby, the binding domain of a downstream substrate of Rac-1, called PAK, was used to extract the active GTP-bound Rac-1 from the total cell lysate. After the pulldown, probes were mixed with 2 x Laemmli sample buffer (see table 2.15 for content), and stored at -20 °C until separation in a SDS-PAGE (2.2.10.3) and Western Blot analysis (2.2.10).

2.2.6.6 Tube formation assay

Growth Factor reduced Matrigel™ (BD Discovery Labware, Bedford MA, USA) was placed into the lower chambers of µ-slide angiogenesis wells (Ibidi), and hardened for 30 min at 37 °C. For the evaluation of Prt and derivatives, test compounds (500 µl of 2x the final concentration) were each mixed with 500 µl of HMEC-1 (4 x 10^5/ml). 50 µl of this suspension was placed into µ-slides angiogenesis wells, containing hardened Matrigel. Cells were incubated for 16 h. For the characterization of v-ATPase inhibitor ConcmA, confluent HMEC-1 and HUVEC monolayers in 6 well plates were pretreated for 24 h, prior to the protocol as described for Prt evalution. For evaluation, one Image per well was taken on the Axiovert 200 microscope as described in 2.2.6.1. The images were processed with the tube formation module of WIMASIS Image Analysis (Munich, Germany). This online software module identifies cellular tubes on a multiparametric basis (depending on brightness and contrast differences, length and width of the structure) and interprets tubes and non-tube complexes using an

automated mathematic algorithm. Drug effects were assessed, analyzing total tube length and number of tube connecting nodes. *In situ* cytotoxicity tests were performed as described in 2.2.4.2.

2.2.7 Subcutaneous murine tumor xenograft model

HuH7 liver tumor cells (5 million per mouse) were subcutaneously injected into 6-8 week old female SCID (severe combined immune deficiency) mice (CB17/lcr-PrkdcSCID/lcrlcocrl from Charles River; Wilmington, MA, USA). Six days after tumor cell application, when tumors had reached a detectable volume of approximately 10-15 mm^3, mice were treated intravenously every second day either with 0.1 mg/kg Prt dissolved in PBS or with PBS alone for a total of 5 treatments.

Tumor volume was determined continuously with a caliper for the duration of the treatment. Mouse weight and general health status were observed throughout the experiment to exclude severe side effects caused by treatment.

At day 16 after tumor cell application mice were sacrificed, tumors were excised and tumor mass was determined. Tumors were formalin fixed, paraffin embedded and cut into 5 µm slices. Immunostaining for microvessels and nuclei was performed according the manufacturer's protocol of VECTASTAIN Elite ABC kit (Vector Laboratories Inc., Burlingame, CA, USA) using a CD31 antibody (BD Biosciences 553370) and hematoxylin (Sigma-Aldrich), respectively. From every tumor four images were obtained with a 10 x lense. Within each of the overview fields, four high power (40 x) images were obtained (image area 0.0355 mm^2). These 40x pictures were used for vessel counting. Data for tumor volume, tumor weight, microvessel density, and mice weight are expressed as means ± SEM. Five and six mice were used in the control group and in the Prt group respectively. All *in vivo* experiments were performed according to the legal terms for animal experiments of the local administration (Government of Upper Bavaria).

This *in vivo* experiment was kindly performed by Laura Schreiner, Dr. Johanna Liebl and Dr. Michael Guenther, Department of Pharmacy, Ludwig-Maximilians-University Munich.

2.2.8 VEGF induced signaling in HMEC-1

HMEC-1 were seeded into 6 well plates at 0.4 10^6 per 2 ml per well and were allowed to reach confluent state. Then, cells were treated either for 2 h or for 20 h with 1, 3 or 10 nmolar ConcmA. In order, to decrease signaling background, HMEC-1 were washed twice with PBS and incubated for 4 h in serum free medium (M199, PAA, Laboratories, Pasching, Austria). ConcmA was also present during this serum deprivation period. 50ng/ml VEGF-A (rh VEGF165, Peprotech, Hamburg Germany) was added to the

medium for 10 min in order to stimulate Akt (S473) and ERK1/2 (T202/Y204) phosphorylation. Most adequate VEGFR2 (Y1775) phosphorylation was achieved after 2 min of incubation with VEGF. One positive and two negative controls were used: (VEGF/ConcmA +/-; VEGF/ConcmA -/- and VEGF/ConcmA -/10 nM, respectively). After VEGF stimulation, cells were further processed as described in 2.2.10.

2.2.9 Biochemical quantification of extracellular VEGFR2 levels

HMEC-1 and HUVEC were seeded at concentrations of 0.5 x 10^6 into 60 cm dishes. Confluent endothelial monolayers were treated for 22 h with ConcmA in ECGM and 2 h under serum deprivation, in order to assess the VEGFR2 surface levels after ConcmA treatment in serum deprived condition. Cell surface proteins were covalently labeled with a membrane impermeant biotinylation reagent (sulfo-NHS-lc-biotin, Uptima, France), as schematically described in Fig. 2.4.

All steps were performed on ice. At start, cell monolayers were washed twice with ice-cold PBS, PBS was completely removed. Ice-cold sulfo-NHS-lc-biotin (0.2 mg/ml in PBS, 10ml per dish) was added, 30 min gentle rocking on ice. Unreacted biotin was saturated by washing three times with 100 mM glycine PBS solution, third time for 15 min, gentle rocking on ice. Endothelial monolayers were washed three times with PBS. PBS was completely removed. 500 µl of cell lysis buffer was added per well and kept on for 15 min (see table 2.13 for lysis buffer content, enough for four treatment groups). Meanwhile, streptavidin agarose beads (Uptima, France) were washed once with lysis buffer for equilibration. Cell lysates were centrifuged at 14.000 rcf for 10 min at 4° C and one sample (20 µl) was taken to represent the total cellular VEGFR2. Remaining lysate was incubated with equilibrated streptavidin agarose beads (200µl 50% beads slurry per 500 µl lysate) by gentle shaking for 1 h at 4°C. Beads were collected by centrifugation at 14.000 rcf for 10 min. Supernatant, representing the intracellular VEGFR2 pool, was removed. Beads were cautiously washed three times with lysis buffer, using a syringe. Protein was extracted from the beads by mixture with 2x SDS sample buffer (see table 2.15 for content) and heating at 95°C for 5 min. This protein fraction represents the surface VEGFR2 pool. As negative control, HMEC-1 and HUVEC were treated with PBS instead of surface biotinylation reagent and were tested for VEGFR2 levels in the beads fraction. Probes were mixed with 2 x SDS buffer, boiled for 5 min at 95°C and kept at -20°C until separation with SDS-PAGE and western blot analysis (2.2.10).

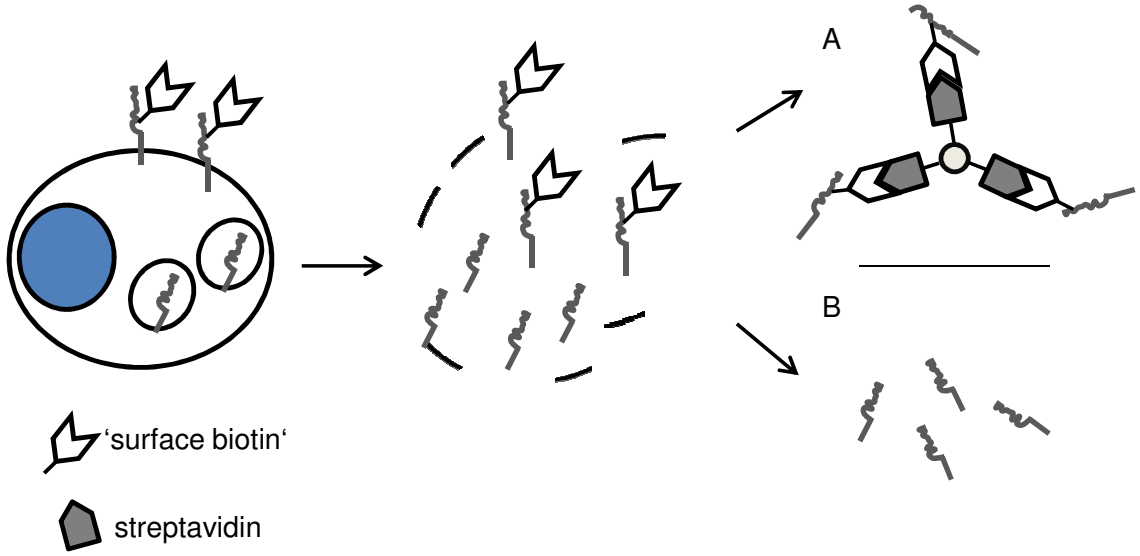

Fig. 2.4 Biochemical quantification of surface receptor levels. Only receptors located at the cell surface get biotinylated by the membrane impermeant 'surface biotin' (left part of the image). After cell lysis (middle part of the image), this receptor fraction can be separated from the non-biotinylated receptors (B) by precipitation with streptavidin, bound to agarose beads (A).

Table 2.13 Lysis buffer used for surface biotinylation assay

Lysis buffer for surface biotinylation, 40 ml	
Tris, pH 7.5	75 mM
NaCl	200 mM
TX-100	1.5 %
NP-40	0.75 %
NaF	15 mM
Na_3VO_4	1.5 mM
EDTA	1 mM
Complete® mini EDTA free	1 tablet per 40 ml

2.2.10 Western blot analysis

2.2.10.1 Protein sample preparation

For protein harvest, confluent HMEC-1 or HUVEC in 6 well plates were put on ice and washed once with ice-cold PBS, which was completely removed with a Pasteur pipette. RIPA-lysis buffer (used for the verification of subunit c protein expression in HMEC-1 and HUVEC) or lysis buffer for phosphorylated proteins (used for VEGF-signaling experiments 2.2.8) was added, 130 µl per well, see Table 2.14. Then, cell plates were immediately put into -80°C. Earliest one h later, frozen cell samples were put onto ice.

Lysate was scraped off using cell scrapers (TPP, Trasadingen, Switzerland) and transferred to pre-cooled Eppendorf tubes (Peske, Aindling-Arnhofen, Germany) to incubate on ice for 5 min. Then, cell lysates were centrifuged (14.000 rcf, 10 min, 4°C) and supernatant was transferred into new pre-cooled Eppendorf tubes. One sample of the supernatant (5 µl) was diluted 1:10 in H_2O for protein quantification with the Bradford method (2.2.10.2). The remaining cell lysate was mixed with 5x SDS sample buffer, heated at 95°C for 5 min and was kept frozen at -20°C until SDS PAGE (see 2.2.10.3). Protein concentrations were adjusted according to the values of the Bradford experiment by mixing the samples with adequate volumes of 1x SDS sample buffer, before SDS PAGE.

Table 2.14 Commonly used cell lysis buffers for Western Blot analysis

RIPA buffer	
Tris/HCl (pH 7.4)	50 mM
NaCl	150 mM
Nonidet NP 40	1%
Deoxycholic acid	0.25%
SDS	0.10%
H_2O	
Complete®mini EDTAfree	4.0 mM
PMSF	1.0 mM
Na_3VO_4	1.0 mM
NaF	1.0 mM

Lysis buffer for phosphoproteins	
Tris/HCl (pH 7.4)	50 mM
NaCl	150 mM
Nonidet NP 40	1%
Deoxycholic acid	0.25%
SDS	0.10%
Na_3VO_4	0.3 mM
NaF	1.0 mM
β-Glycerophosphate	3.0 mM
Pyrophosphate	10 mM
H_2O	
Complete®mini EDTAfree	4.0 mM
PMSF	1.0 mM
H_2O_2	600 µM

Table 2.15 Protein sample buffers

5x SDS-sample buffer	
Tris/HCl (pH 6.8)	3.125 M
Glycerol	10 ml
SDS	5%
DTT	2%
Pryonin Y	0.025%
H_2O	

3x Laemmli buffer	
Tris/HCl (pH 6.8)	187.5 mM
SDS	6%
Glycerol	30%
Bromphenol blue	0.025%
H_2O	
β-Mercaptoethanol	12.5%

2.2.10.2 Protein quantification

Total protein amount in cell lysate was determined according to Bradford et al. [94]. A defined BSA dilution series (from 500 µg/ml to 0 µg/ml (H_2O)) was used for standard calibration. Protein samples were diluted 1:10 in H_2O. 10 µl aliquots of protein sample dilutions and BSA standard respectively, were added to a 96 well flat bottom plate. 190 µl of the Bradford reagent (Coomassie brilliant blue G 250 concentrate was diluted 1:5 in H_2O) were added per sample. Probes were incubated for 5 min and absorbances were finally analyzed with the SpectraFluor Plus™ (Tecan, Männedorf, Austria).

2.2.10.3 SDS-PAGE

Protein samples were boiled for 5 min at 95°C and briefly centrifuged before equal amounts of protein were loaded onto the SDS-gel. For identification of protein, PageRuler™ pre-stained 10-170 kDa or Spectra Multicolor™ high range protein 10-260 kDa, both from Fermentas, St. Leon-Rot, Germany were used (1x 1µl per approx. 40µl 1x SDS sample buffer per gel). As described by Laemmli et al. [95], proteins were separated in a discontinuous SDS - PAGE, using first a stacking gel, pH 6.8 to focus proteins at a common starting line (Electrophoresis conditions 100 V, 20 min), and then a separation gel, pH 8.8 (Electrophoresis conditions 200 V, 45 min) with adequate polyacrylamid concentrations depending on the weight of the protein of interest (see table 2.16). The apparatus for SDS-PAGE performance was the Mini Protean III system from Bio-Rad (Munich, Germany). Power supplies E835 were from Consort, Belgium.

Table 2.16 Preparation of SDS-PAGE

Separation gel 7.5%/10%/12%		**Stacking gel**	
Rotiphorese™ Gel 30	25% /33.3% /40%	Rotiphorese™ Gel 30	17%
Tris (pH 8.8)	375 mM	Tris (pH 6.8)	125 mM
SDS	0.1%	SDS	0.1%
TEMED	0.1%	TEMED	0.2%
APS	0.05%	APS	0.1%
H_2O		H_2O	

Table 2.17 Electrophoresis buffer for SDS-PAGE

Electrophoresis buffer	
Tris	4.9 mM
Glycine	38 mM
SDS	0.1%
H_2O	

2.2.10.4 Tank blotting

Table 2.18 Tank buffer

5x Tank buffer		1x Tank buffer	
Tris base	240 mM	5x Tank buffer	20 %
Glycine	195 mM	Methanol	20 %
SDS	0.05%	SDS	0.01%
H_2O		H_2O	

After SDS-PAGE, the separation gel was transferred into a blotting sandwich soaked in 1 x pre-cooled Tank buffer. Assembly of the sandwich: cathode-pad, blotting paper, separation gel, nitrocellulose membrane (Hybond-ECL™, Amersham Bioscience, Freiburg, Germany), blotting paper, anode-pad. All parts of the sandwich, except for the separation gel, were soaked in 1 x pre-cooled Tank buffer for 15 min. The assembled sandwich was kept for further 5 min in the cool 1xTank buffer before running the tank blot. For Tank blot electrophoresis, the sandwich was pushed into the Mini Trans Blot® system (Bio-Rad, Munich, Germany), 1x Tank Buffer was poured into the tank. For cooling, a cassette filled with ice was pushed into the tank as well. Transfer was either carried out at 4°C at 23 V overnight or at 4°C for 90 min at 100 V under stirring conditions.

2.2.10.5 Protein detection

In order to get an impression about the homogeneity of gel loading, polyacrylamid gels were stained after Tank Blotting with Coomassie-blue for 30 min, and de-stained with Coomassie-destaining solution for 20 min and washed with water overnight.

Table 2.19 Coomassie staining and de-staining solutions

Coomassie staining solution		Coomassie de-staining solution	
Coomassie blue	3.0 g	Glacial acetic acid	100 ml
Glacial acetic acid	100 ml	Ethanol	333 ml
Ethanol	450 ml		
H_2O	ad 1 l	H_2O	ad 1 l

2.2.10.5.1 Enhanced Chemiluminescence (ECL)

Membranes that were incubated with HRP-labeled secondary antibodies, were washed with PBS-T, (4 x 5 min, RT). For ECL reaction, luminol (5-Amino-2,3-dihydro-1,4-phthalazinedione) was used as a substrate. The membrane was incubated with ECL solution for 1 minute, excluded from light. The resulting luminescence was detected by exposure of the membrane to a X-ray film (Super RX, Fuji, Düsseldorf, Germany). This film was developed with a Curix 60 system (Agfa-Gevaert AG, Cologne, Germany) for adequate durations.

Table 2.20 ECL solution

ECL solution	
Tris (pH 8.5)	100 mM
luminol	2.5 mM
p-Coumaric acid	1 mM
H_2O_2	17 µM
H_2O	

2.2.10.5.2 LI-COR detection method

When incubated with secondary antibodies coupled to IR(infrared)Dye™ 800 or Alexa Fluor® 680 (emission at 800 and 700 nm, respectively), membranes were washed as described in 2.2.10.5.1, and then analyzed with the Odyssey imaging system (Li-COR Biosciences, Lincoln, NE, USA), allowing the quantification of each band's intensity.

Table 2.21 Primary antibodies used for Western Blot analysis

Antigen	Source	Dilution	In	Provider
β-actin	mouse	1:2000	5% Blotto-T	Millipore
β-tubulin	mouse	1:1000	1% Blotto-T	Santa Cruz

ATP6V0C (subunit c)	rabbit	1:1000	5% BSA-T	Novus Biolog.
Akt	rabbit	1:1000	5% BSA-T	Cell Signaling
p-Akt (S473)	mouse	1:1000	5% Blotto-T	Cell Signaling
Erk 1/2	rabbit	1:1000	1% Blotto-T	Cell Signaling
p-Erk1/2 (T202/Y204)	mouse	1:1000	1% Blotto-T	Cell Signaling
VEGFR2	rabbit	1:1000	5% BSA-T	Cell Signaling
p-VEGFR2 (Y1175)	rabbit	1:1000	5% BSA-T	Cell Signaling
Rac-1	mouse	1:1000	3 %BSA-T	Pierce

Table 2.22 Secondary antibodies used for Western Blot analysis

Source, Antigen, Label	Dilution	In	Provider
Goat anti-mouse IgG1 HRP	1:1000	1% Blotto-T	Biozol
Goat anti mouse $IgG2_{2b}$ HRP	1:2000	1% Blotto-T	Biozol
Goat anti-mouse IgG HRP	1:2000	1% Blotto-T	Santa Cruz
Goat anti-rabbit IgG HRP	1:2000	1% Blotto-T	Dianova
Goat anti-mouse IgG Alexa Fluor® 680	1:20.000	1% Blotto-T	Molecular Probes
Goat anti-rabbit IgG Alexa Fluor® 680	1:20.000	1% Blotto-T	Molecular Probes
Goat anti-rabbit IgG H+L IRDyeTM 800CW	1:20.000	1% Blotto-T	LI-COR Biosciences

2.2.10.6 Quantification of band intensity

Developed x-ray films were photographed using an illuminated table, and a LuCam system (Lumenera, Ottawa, ON, CA). Intensity of bands was densitometrically quantified with ImageJ Gel analyzer (Version 1.43q; NIH, Bethesda, MD, USA). When the Li-COR system was used, band intensities were quantified with the appending Odyssey software (v 1.2, Li-COR Biosciences, Lincoln, NE, USA). Band intensities were normalized to loading controls (β-actin, β-tubulin).

2.2.11 siRNA transfection

In order to downregulate gene expression of the subunit c, HUVEC were transfected with a mix of four siRNAs on human ATP6V0C (ON-TARGET plus® SMART pool, Cat #

L-017620-01-0005, Thermo Scientific Dharmacon®). In brief, HUVEC were trypsinized and adjusted to a cell number of 2 x 10^6. This suspension was centrifuged, supernatant was removed and cells were re-suspended in 90 µl of HUVEC Nucleofactor Solution (AMAXA). This suspension was mixed with 10 µl (3 µg or 200 pmol) of target siRNA or control siRNA (ON-TARGET plus® control siRNA; Cat #: D-001810-01-05, Dharmacon). Cells were transfected in cuvettes using the AMAXA electroporation apparatus (program A – 034), then immediately pre-warmed ECGM was added for cell recovery. For a scratch assay on 96 well format (2.2.6.2), 0.8 to 1 x 10^5 of transfected cells were seeded per well. Additionally, cell aliquots of 0.4 x 10^6 were seeded into one well of a 12 well plate. 24 h after transfection, efficiency of mRNA downregulation was assessed by real time PCR within the 12-well probe and in parallel, scratch assay was started.

Table 2.23 Target sequences of ON-TARGET plus® SMART pool on human ATP6V0C

siRNA name	Target Sequence
J-017620-12, ATP6V0C	CCAGCUAUCUAUAACCUUA
J-017620-11, ATP6V0C	CCCGACUAUUCGUGGGCAU
J-017620-10, ATP6V0C	GCUCUGUGUAUGCGGAUGA
J-017620-09, ATP6V0C	GGCACAGCCAAGAGCGGUA

2.2.12 Quantification of mRNA

2.2.12.1 mRNA isolation

Total mRNA was isolated with the RNeasy Kit from Qiagen (Hilden, Germany) according to the producer's protocol. RNA was eluted in RNAse free water and RNA concentrations were determined using the NanoDrop spectrophotometer (Peqlab, Wilmington, DE, USA).

2.2.12.2 Reverse Transcriptase reaction

With the high capacity cDNA Reverse Transcription Kit (Applied Biosystems, Foster City, CA, USA) which includes random primers, the isolated mRNA (0.9 µg used per reaction) was written into cDNA. The reaction was run at 37°C for 2 h. cDNA aliquots were stored at 4°C until performing quantitative RT-PCR.

2.2.12.3 Quantificative Real-Time PCR

For the quantitative RT-PCR the ABI 7300 Real Time PCR system with the TaqMan® Universal PCR Mastermix (Life Technologies Corporation, Carlsbad , CA, USA) with the program described below was used. Probes and primers for the v-ATPase subunit c (ATP6L) were also from Life Technologies, supplied as a mix. As control gene, GAPDH (glycerinaldehyd-3-phosphat-dehydrogenase, forward/reverse primer and probe sequence mix were supplied from Biomers, Ulm, Germany) was used. Fluorescence development was analyzed with the ABI 7300 appending software. For evaluation, relative quantification according to the Pfaffl [96] was used.

Table 2.24 RT-PCR thermal program

RT PCR thermal program	
95°C	5 min
(40 cycles)	
95°C	30 sec
55°C	30 sec
72°C	30 sec
72°C	5 min
4°C	∞

2.2.13 Statistical analysis

Graph Pad Prism (Graph Pad Software, La Jolla, CA, USA) was used for statistical calculations. For comparison of two groups, Student's unpaired t-test was performed. Three or more groups were compared by one way analysis of variance (ANOVA), followed by Bonferroni's or Dunnett's multiple comparisons versus control. EC_{50} values were calculated with nonlinear curve fitting, variable slope. All experiments were, if not differently indicated, performed at least three times in duplicates/triplicates/sextuplicates. Results are expressed as means ± SEM. P values < 0.05 were considered as significant.

3 Results – part 1: Anti-angiogenic potential of pretubulysin and its derivatives

3.1 Depolymerization of the microtubule cytoskeleton in HMEC-1 endothelial cells

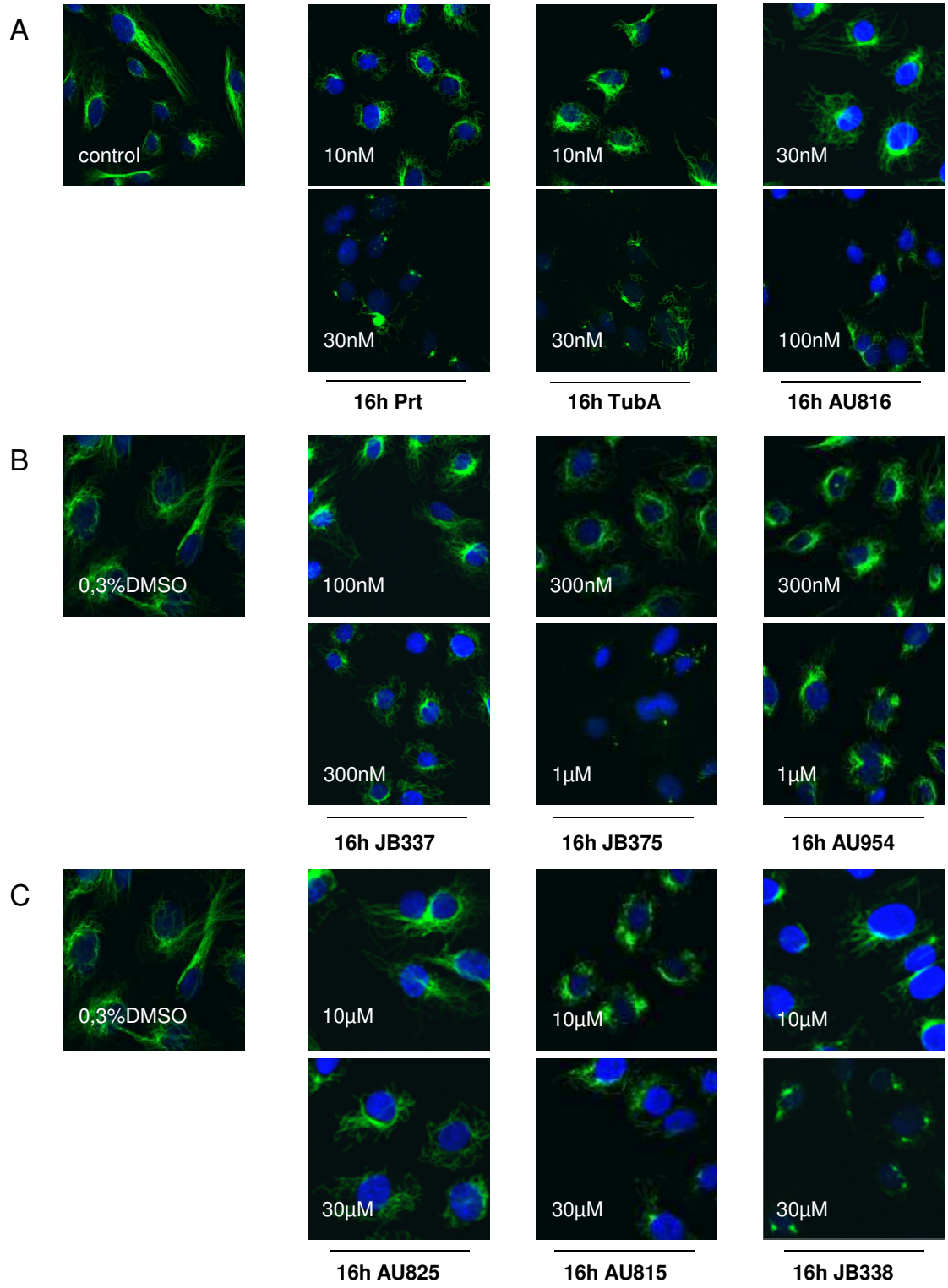

Fig. 3.1 MT depolymerization in proliferating HMEC-1. Representative immune-fluorescence stainings of microtubules (green) after 16 h of treatment with TubA, Prt, (Fig. A middle and left panels) or the Prt-derivatives (A: right panel and all panels in B - C). Blue: nuclear staining.

We initially tested whether, and at which concentrations pretubulysin (Prt) and its derivatives act destructive on the microtubule cytoskeleton in intact proliferating endothelial cells, using tubulysin A (TubA) as reference compound.

Therefore, we performed an immunefluorescence-staining in HMEC-1 treated with the indicated compound for 16 h. The concentrations were chosen in order to achieve complete microtubule depolymerization. Control cells show intact, long and polarized microtubules (Fig. 3.1 A, B, C, the very left panel), whereas addition of Prt or TubA decreased both microtubule (MT) polarization and MT total mass at 10 and 30 nmolar, with Prt (Fig. 3.1 A left panels and middle panels). To achieve the same level of MT breakdown with AU816, 100 nmolar were necessary (Fig. 3.1 A right panels). The intermediately potent derivatives JB337, JB375 and AU954 had to be dosed either at 300 nmolar, or 1 µmolar, respectively, for similar effects (Fig. 3.1 B left to right panels). The substances with the lowest potency, AU825, AU815 and JB338 had to be used at concentrations of at least 30 µmolar (Fig 3.1 C from the left to the right panels), i.e. about three orders of magnitude higher than those of TubA and Prt which clearly indicates a loss of activity due to chemical variation of Prt.

3.2 Effects of pretubulysin (Prt) on endothelial cell growth and survival

3.2.1 Prt inhibits proliferation of HMEC-1 similarly to TubA

Using a three day incubation of sparse HMEC-1 with final crystal violet staining, the growth inhibitory potential for every compound and a potency ranking were established. The most potent anti-proliferative agents (Fig. 3.2 left panel) were TubA (EC_{50} 1.2 nmolar), Prt (EC_{50} 2.3 nmolar) and AU816 (EC_{50} 4.4 nmolar). The phenyl- and phenoxypretubulysins JB337 and JB375 still exhibited EC_{50} values at low nanomolar levels (13.2 nmolar and 55 nmolar, respectively), followed by the 2,3-didehydropretubulysin AU954 with 60 nmolar (Fig. 3.2 middle panel). The remaining Prt-derivatives were three orders of magnitude less potent than TubA and Prt. AU825 and AU815, both Prt-derivatives with N- and C-terminal alterations (Fig. 2.1) had EC_{50} values of 1.3 µmolar and 1.6 µmolar. The central substitution of a triazole ring showed a further loss of function (EC_{50} 2.1 µmolar, Fig 3.2 right panel). EC_{50} values with 95% confidence intervals are summarized in table 3.1.

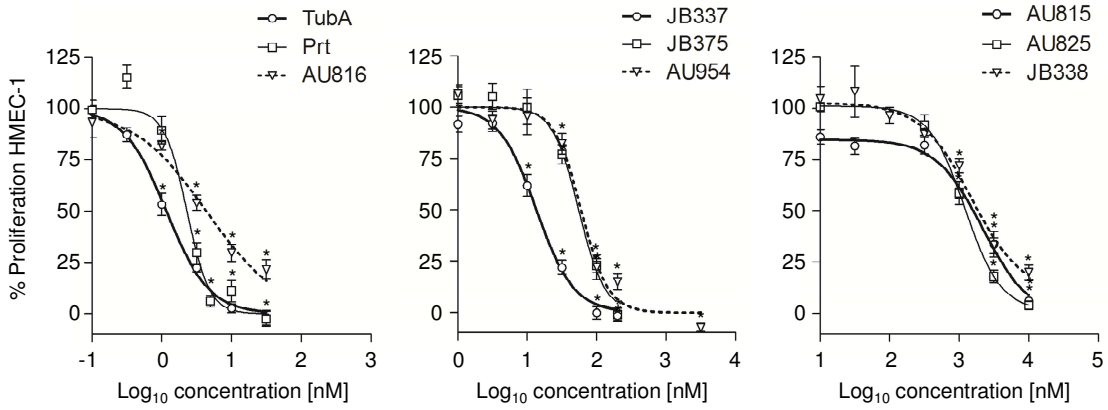

Fig. 3.2 TubA, Prt and Prt-derivatives inhibit endothelial cell proliferation. Compounds were classified into three groups of different potencies (left, middle and right panels), whereby Prt had a growth inhibitory potency comparable to TubA. Data are means ± SEM of three independent experiments. * significantly different from control $p < 0.05$, 1-way ANOVA, Bonferroni's multiple comparison test

3.2.2 Prt causes anti-mitotic effects similarly to TubA

Tubulin inhibitors induce cell cycle arrest in the G_2/M phase and consequently apoptosis by interfering with the assembly of the mitotic spindle apparatus [97]. In order to test these anti-mitotic effects with Prt and its derivatives, HMEC-1 were treated for 24 h and 48 h using the same set of concentrations as in the proliferation assay at sub-confluent status.

After 24 h, nuclear fragmentation in HMEC-1 occurred at negligible levels (Fig. 3.3 B), whereas a dose dependent G_2/M arrest was clearly detectable at this time (Fig. 3.3 A).

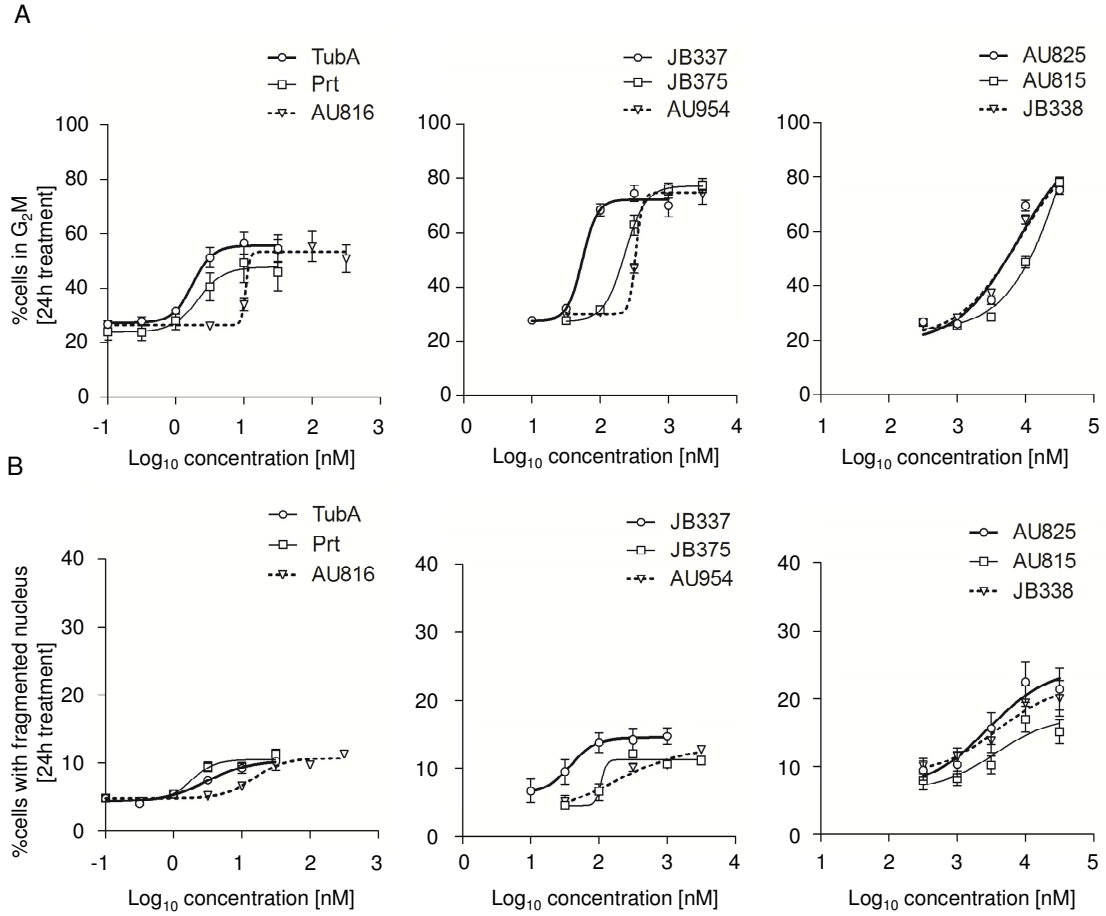

Fig. 3.3 (A) G_2/M arrest and (B) nuclear fragmentation in HMEC-1 after 24 h of treatment with TubA, Prt and Prt-derivatives. Data are means ± SEM of three different independent experiments for each compound.

After 48 h, a clear dose-dependent induction of G_2/M arrest (Fig. 3.4 A) and nuclear fragmentation (Fig. 3.4 B) in HMEC-1 was detectable for all derivatives, whereby the order of ranking in this assay totally matched with that in the proliferation assay, with TubA and Prt being the most potent candidates (Fig. 3.4 left panel).

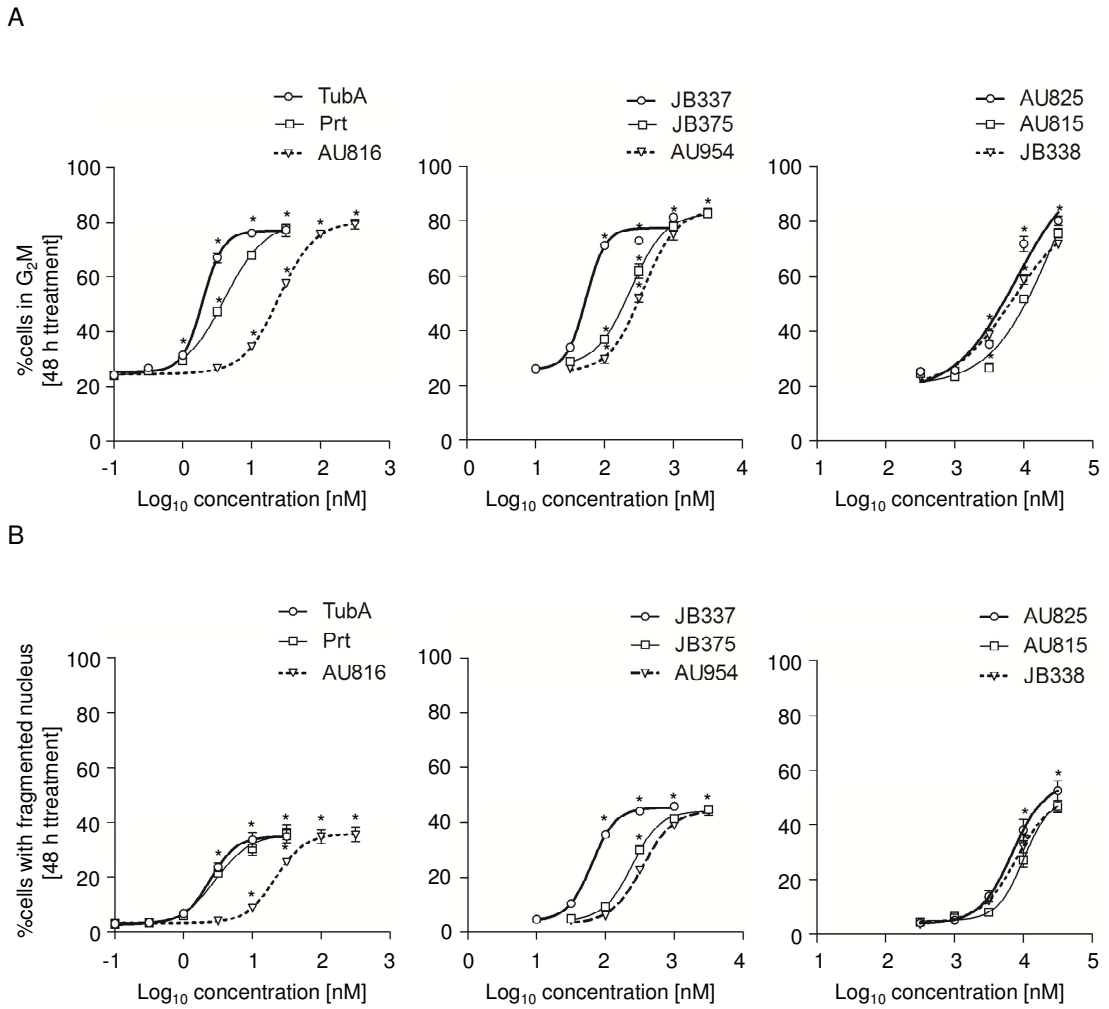

Fig. 3.4 Analysis of G_2/M arrest and nuclear fragmentation in HMEC-1 after 48 h of treatment with TubA, Prt and Prt-derivatives. Similar to the proliferation assay, compounds were classified into three groups of different potencies (left, middle and right panels). Prt induces G_2M/arrest and nucleic fragmentation at a similar degree as TubA (Fig A and B left panels). Data are means ± SEM of three independent experiments. * $p < 0.05$ vs. untreated controls, 1-way ANOVA, Bonferroni's multiple comparison

3.3 Effects of pretubulysin (Prt) on endothelial cell (EC) migration

Migration of endothelial cells (EC) is a hallmark of angiogenesis. Therefore the compounds were evaluated both in tests on migration into a wounded HUVEC monolayer (scratch assay) and on chemotactic migration towards a serum gradient.

3.3.1 Prt inhibits EC wound healing similarly to TubA

Prt, TubA and AU816 efficiently inhibited wound closure in an endothelial cell monolayer in a dose dependent manner with EC_{50} values of 5.3 nmolar, 3.4 nmolar

and 11 nmolar, respectively, whereas JB337, JB375 and AU954 exhibited EC_{50} of 26 nmolar, 260 nmolar and 200 nmolar. Chemical variations as done for the three remaining compounds led to a drastic decrease of anti-migratory potential (Fig. 3.5, right panel). All EC_{50} values are summarized in table 3.1. Figure 3.5 B depicts representative images of scratch assays. Importantly, Prt was only slightly less potent than TubA itself, once more indicating Prt to be a potent alternative.

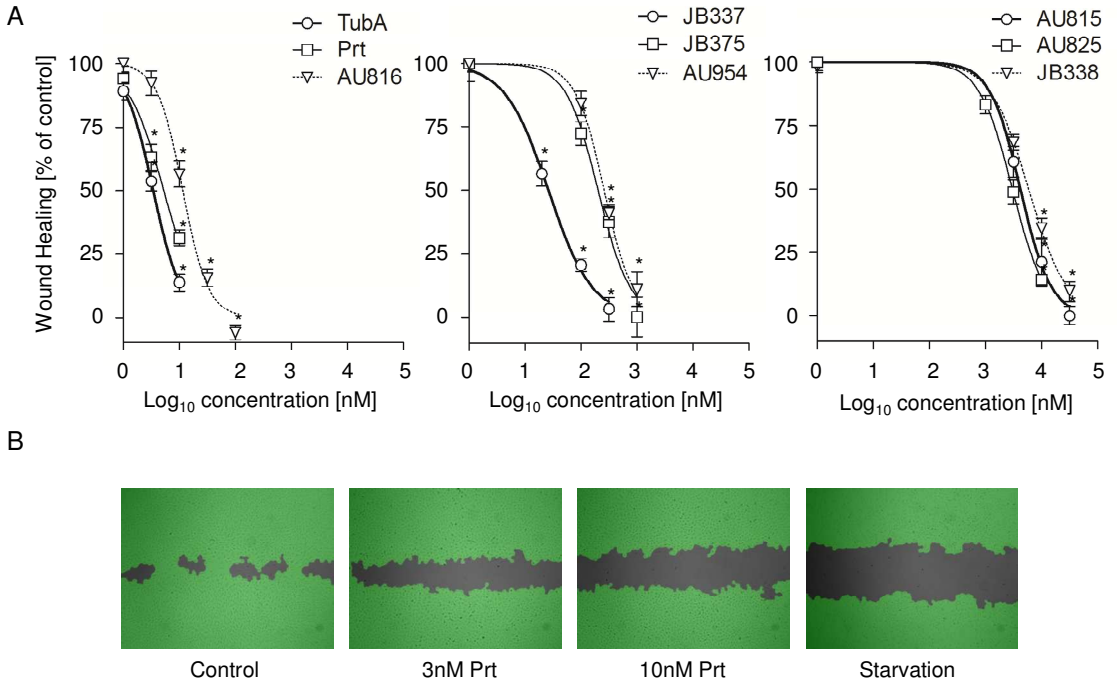

Fig. 3.5 A) TubA, Prt and Prt-derivatives concentration dependently inhibit endothelial cell migration. Data are means ± SEM for three independent experiments, $^{*}p<0.05$ vs. untreated controls, 1-way ANOVA, Bonferroni's multiple comparison. B) Representative images of the wound closure in an HUVEC monolayer in absence or presence of Pretubulysin or in the absence of growth factors ('starvation'). The cell free area is gray, the area covered with cells as detected by the imaging software is depicted in green.

3.3.2 Prt impairs EC chemotaxis similarly to TubA

To analyze, whether both TubA and Prt inhibit cellular motility *per se* or only the ability to orientate, a two-dimensional chemotaxis assay was performed. Fig. 3.6 A shows three representative trackings of HUVEC in a 0 to 10% FCS gradient. The directional components of migration (y-forward index and mean Euclidean distance) were significantly inhibited by either 3 nmolar of Prt or TubA (Fig 3.6 B1). The non-directional aspect with the accumulative distance was not significantly affected by the same treatment indicating that at this concentration the cells were still able to move. However, as velocity of movement was significantly reduced (Fig. 3.6 B1), it can be assumed, that overall motility at least begins to be hampered by the concentrations in the investigated time frame. Furthermore, the mean number of tracked cells per experiment is not significantly affected (Fig. 3.6 B2), suggesting a non-toxic effect.

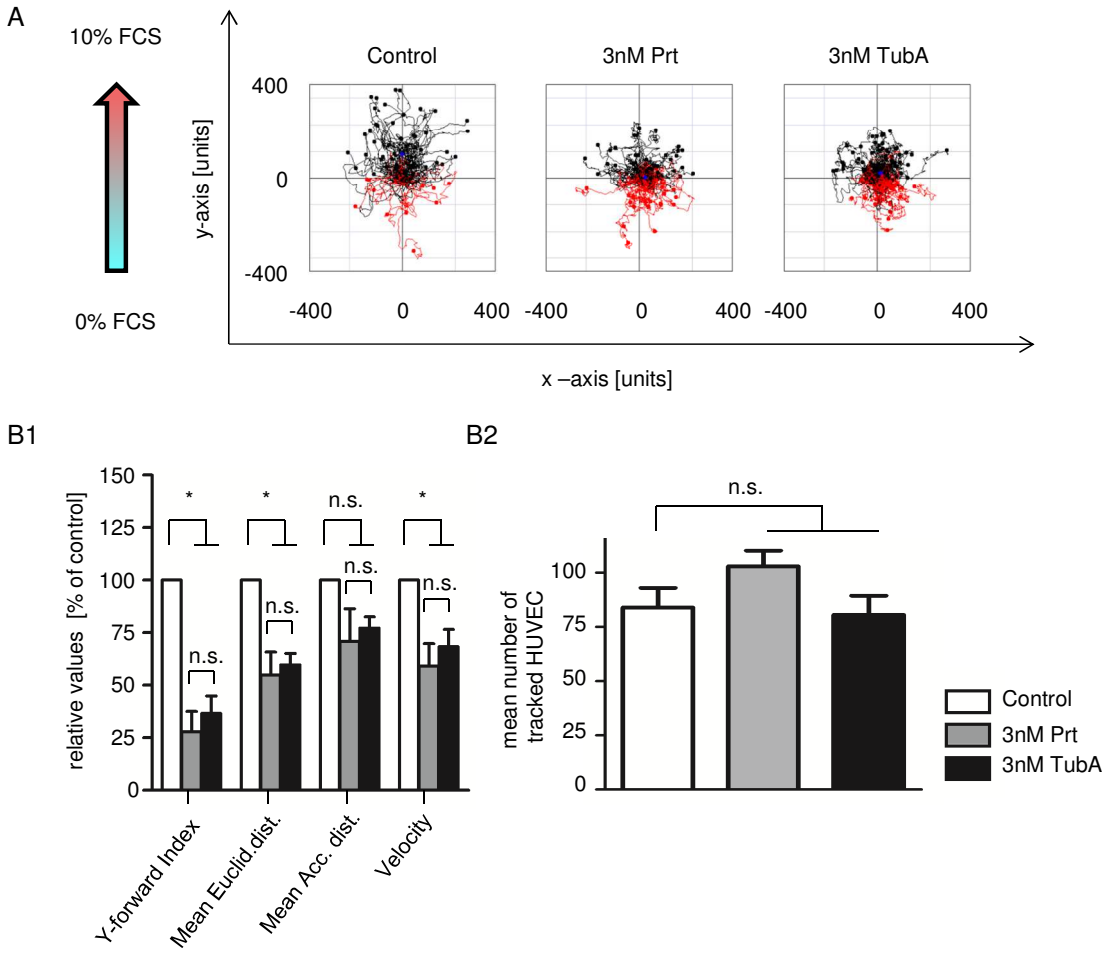

Fig. 3.6 Prt inhibits serum directed chemotaxis in HUVEC at similar level as TubA
A) Representative trackings of the chemotactic movement of endothelial cells in a serum gradient. The starting point of each single cell is placed in the centre of the diagrams. Red tracks: cells migrating against the gradient, black tracks: cells migrating along the gradient. In the control most cells migrated directionally, while in the presence of Prt or TubA, cells lost their sense for orientation.
B) Quantitative analysis of the chemotaxis experiments. B1) shows reduced parameters of directionality (Y-forward and Euclidean distance), while motility as such (accumulative distance) is not significantly inhibited and velocity only starts to be hampered. B2) Mean number of tracked cells per experiment is not significantly reduced. Data are means ± SEM of three independent experiments. * Significantly different from controls, $p < 0.05$, n.s.: not significant, 1-way ANOVA, Bonferroni's multiple comparison

3.3.3 Cytotoxic side effects of Prt during migration inhibition

Measurement of nuclear fragmentation with TubA or Prt in time matched experiments, showed no dramatic increase in HUVEC at concentrations up to 30 nmolar, indicating that effects on migration are not primarily due to cytotoxity (Fig. 3.7). This is in line with the HMEC-1 experiments, where relevant nucleic fragmentation occurred after 48 h, but not after 24 h (Fig 3.4 and Fig 3.3).

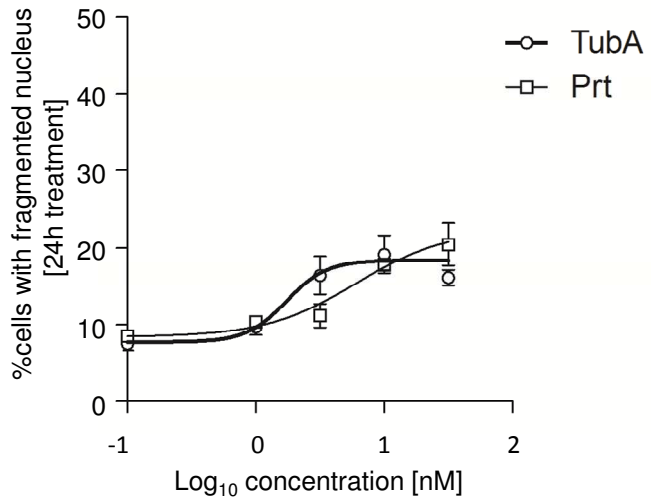

Fig. 3.7 Nuclear fragmentation in HUVEC after 24 h, treated under similar conditions as for the migration assays with TubA and Prt, is negligible. (N=3)

3.4 Tube formation on Matrigel™

The tube formation (formation of capillary like structures) on Matrigel™ is an *in vitro* assay that recapitulates many complex features of angiogenesis. By measuring number of node points and total tube length, tube formation of HMEC-1 endothelial cells was quantitatively determined after 16 h.

3.4.1 Prt inhibits EC tube formation similarly to TubA

Again, we could see a totally different inhibitory potential among the derivatives, with Prt (representative images shown in Fig 3.8 A) and TubA being similarly active and the strongest tube formation inhibitors, followed by AU816 (Fig. 3.8 B1).

TubA and Prt showed an approximate 50-70 % decrease of tube length and node number at about 30 nmolar. The resulting ranking order was concordant with all previous experiments (Fig 3.8 B2-B3).

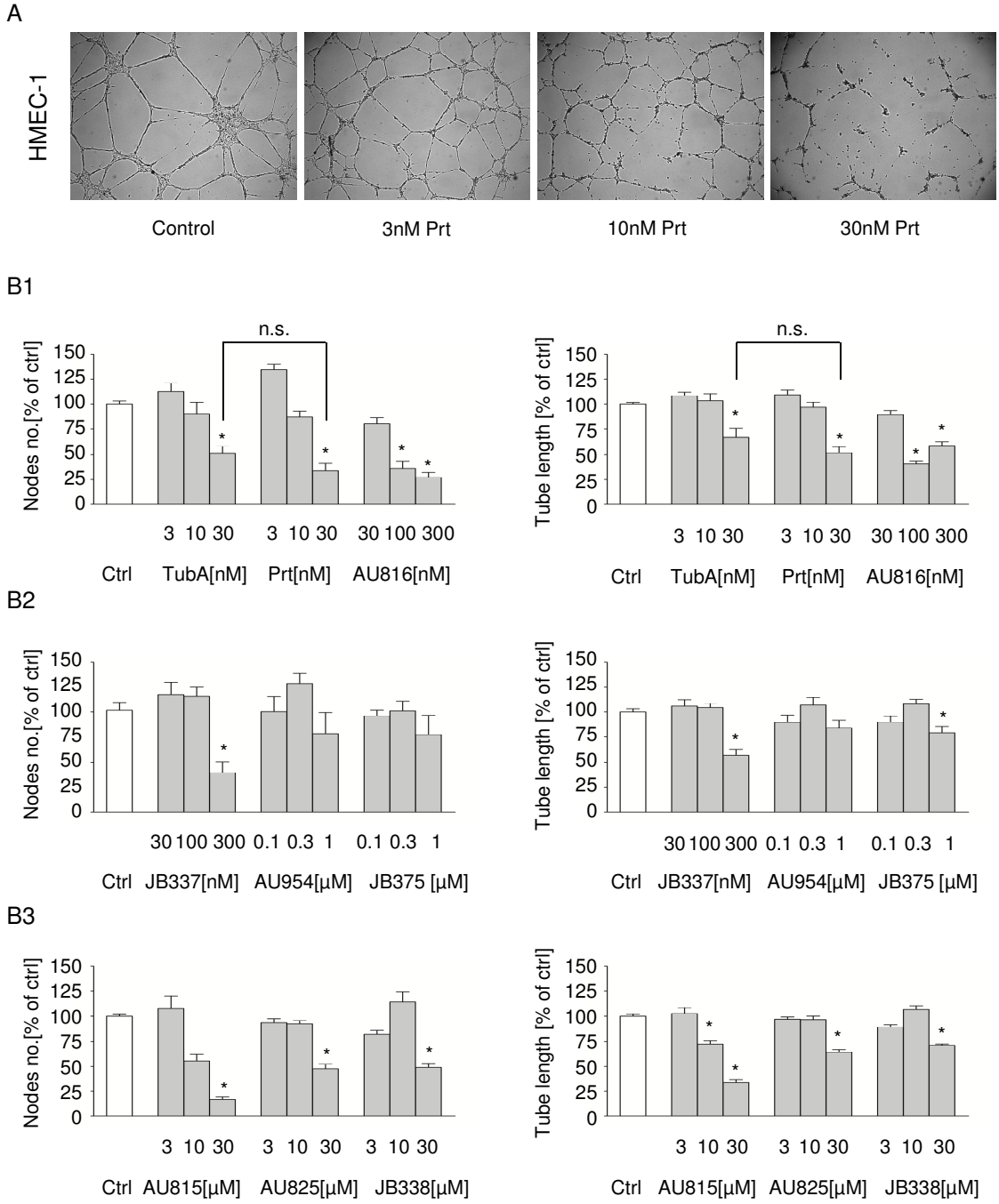

Fig. 3.8 TubA, Prt and Prt-derivatives inhibit endothelial tube formation. A) Representative images of Prt-treated HMEC-1 after 16 h of tube formation on Matrigel, 5x magnification. B) Quantitative evaluation of branching point number connecting the tubes (left panels from B1 to B3) and total tube length (right panels from B1 to B3) using WIMASIS software. Data are means ± SEM of three independent experiments. *Significantly different from controls, $p < 0.05$, n.s. not significant, 1-way ANOVA, Bonferroni t-test

3.4.2 Cytotoxic side effects of Prt in the tube formation assay

As determined by measurement of nuclear fragmentation, in sub-confluent HMEC-1 no drastic cytotoxic effects occurred within 24 h (Fig. 3.3). Furthermore, no substantial amount of dead cells was detected by fluorescence microscopy of PI uptake during tube formation *in situ* in comparison to untreated cells (Fig. 3.9).

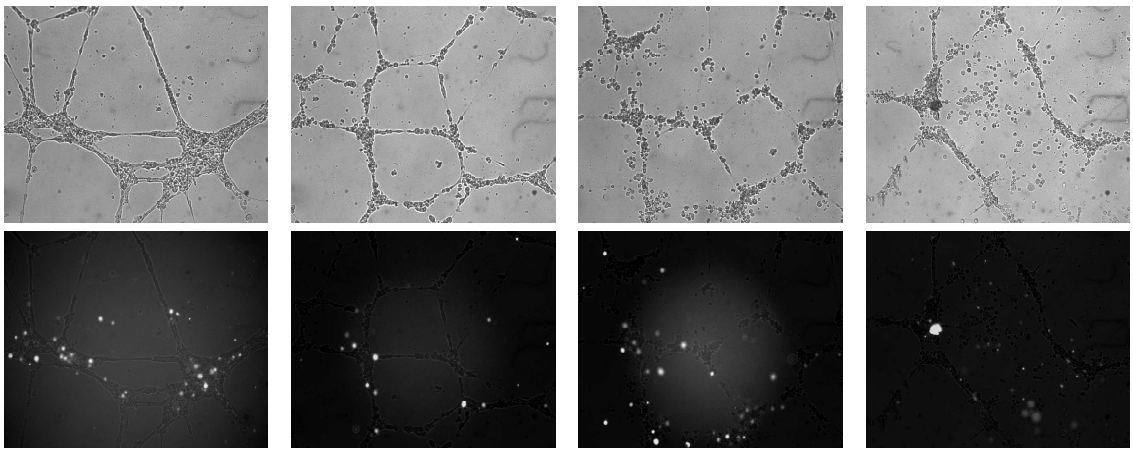

Fig. 3.9 *In situ* propidium iodide (PI) uptake in the HMEC-1 tube formation assay. 10µg/mL PI was added to the media, to test membrane integrity. No significant difference in Prt-treated cells could be detected in comparison to control cells. Representative light transmission (upper panels) and fluorescence (lower panels) images, 10x magnification, similar x,y,z settings, from three independent experiments

3.5 Inhibition of tubulin polymerization *in vitro*

To get an impression, whether the different efficacies of the compounds might have a cell based origin (e.g. by different drug membrane penetration, metabolism or export), all compounds were also tested in a cell-free tubulin polymerization assay using turbidimetry.

Among all tested compounds TubA, Prt and AU816 were the most potent (Fig. 3.10, left panel). 1 µmolar of TubA, as well as 2 µmolar of Prt or AU816 led to a comparable residual tubulin polymerization of about 50% and less. To reach similar effects, a 10-fold higher concentration had to be used for all other Prt derivatives (middle and right panel). JB 375 (18%); JB337 (35.7%) and AU954 (37.2%) had an intermediate potency (middle panel), whereas JB338 (40.3%), AU815 (57%) and AU825 (75.15%) had the weakest influence on tubulin polymerization (right panel).

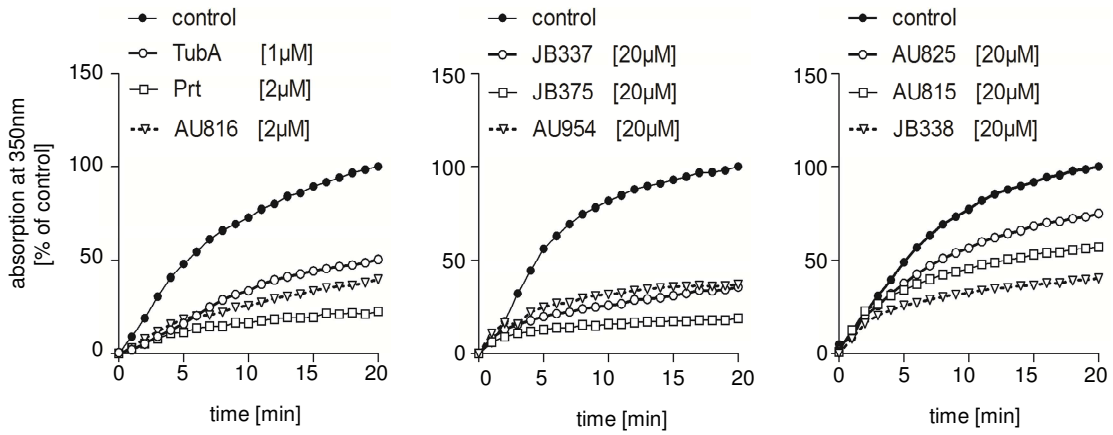

Fig. 3.10 Tubulysin A (TubA), pretubulysin (Prt) and prt-derivatives inhibit tubulin polymerization *in vitro.* Purified tubulin was allowed to polymerize *in vitro* alone or in the presence of selected concentrations of TubA, Prt and Prt-derivatives. Changes in relative absorbance correlate to tubulin polymerization. Compounds with similar potency are grouped together, (left, middle, right panel). n=1

3.6 *In vivo* HuH7 xenograft tumor model

3.6.1 Prt reduces HuH7 tumor growth and vascularization *in vivo*

In a murine xenograft tumor model with HuH7 cells (hepatocellular carcinoma), Prt treatment arrested tumor growth in contrast to saline treatment (Fig. 3.11 A), which finally led to a significant 17-fold reduction of tumor mass sixteen days after tumor cell application (Fig. 3.11 B) in comparison to control group.

Focusing on angiogenesis aspects in immune-histological analysis (Fig. 3.11 D), we detected a significantly lower microvessel density in tumor slices of Prt treated mice in comparison to the control group (Fig. 3.11 E). A further hint towards reduced tumor vascularization under treatment with Prt is the different phenotype of the tumors: while in the controls the tumors were dark red and filled with blood, the Prt treated tumors were not only smaller, but also strikingly pale (Fig. 3.11 C).

Importantly, the animal weight did not differ significantly between the Prt and the control group during the treatment period (Fig.3.11 F), which argues against acute and severe side effects in mice.

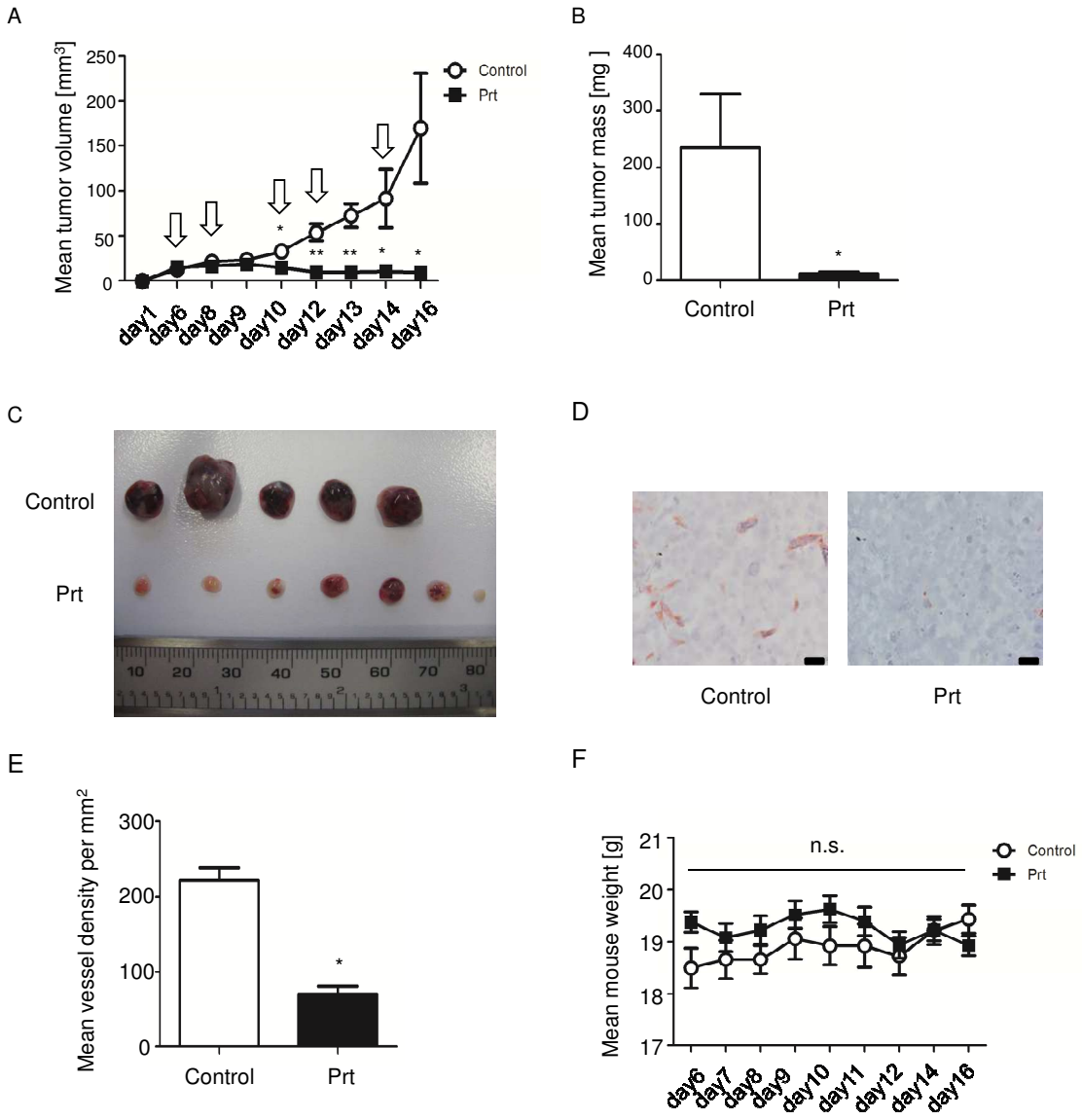

Fig. 3.11 *In vivo* xenograft tumor assay using metronomic application of pretubulysin.

A) HuH7 tumor growth curves. Starting at day six after tumor cell application, mice were treated i.v. either with 0.1 mg/kg Prt (dissolved in 200 µl PBS) or 200 µl PBS alone. Arrows indicate days of treatment. **B) Final HuH7 tumor mass**. **C) Images of explanted tumors**. Note the obvious decrease in size and color due to lesser blood perfusion in the treatment group. **D) Microvessel density images:** slices were stained for CD31 (red) and nuclei (Hematoxylin, blue). Scale bars indicate 20 µm. **E) Quantitative evaluation of vessel density**; n=80 (40x images for both Control and Prt treated groups) for microvessel counting. **F) Animal weight curves.** To exclude severe side effects, the weight of the mice was determined routinely throughout the period of treatment. n=5 mice for control and 6 mice for Prt group, respectively. Data are expressed as means ± SEM. * $p<0.05$; n.s. no significant difference between treatment and control; unpaired t-test.

3.6.2 *In vitro* growth inhibition of HuH7 cells

The influence of Prt on HuH7 proliferation was tested *in vitro* (Fig 3.12), where it effectively reduced HuH7 cell increase with an EC_{50} of 1.5 nmolar, TubA in this case had an EC_{50} of 0.2 nmolar.

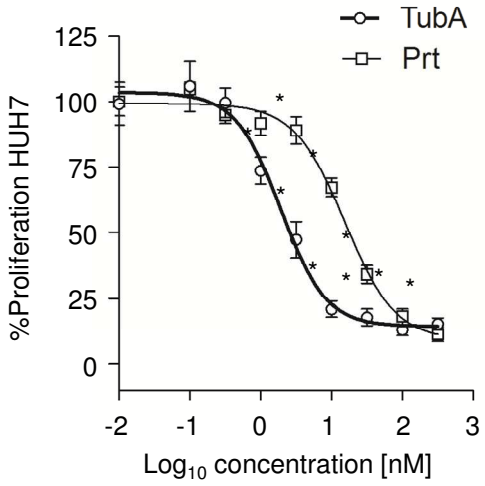

Fig. 3.12 Growth inhibition curves of HuH7 cells, treated with Prt or with TubA. Data are means ± SEM of three independent experiments. * $p<0.05$ vs. control, One way ANOVA, Dunnett's multiple comparison.

3.7 Synopsis of EC_{50} values

Tabelle 3.1 Synopsis of EC_{50} values. Where appropriate, EC_{50} values are indicated as best fit values and 95% Confidence Interval (CI).

	very potent			intermediately potent			less potent		
	TubA	**Prt**	**AU816**	**JB337**	**JB375**	**AU954**	**AU815**	**AU825**	**JB338**
Complete MT washout 16 h HMEC-1	~ 30 nM	~ 30 nM	≥ 100 nM	>0.3 µM	~ 1 µM	> 1 µM	> 30 µM	> 30 µM	≥ 30 µM
EC_{50} growth Inhibition 72 h HMEC-1	1.2 nM (1.0 -1.3 nM)	2.3 nM (1.9 -2.8 nM)	4.4nM (3.3 -5.8 nM)	14 nM (11 -16 nM)	55 nM (45 -67 nM)	60 nM (49 -73 nM)	2.2µM (0.9 -5.1 µM)	1.2µM (0.9 -1.5 µM)	1.5µM (0.9 –2.6 µM)
EC_{50} growth Inhibition 72 h HuH7	0.2 nM (0.1 - 0.3 nM)	1.5 nM (1.1 -2.0 nM)							
EC_{50} G_2M-arrest 48 h HMEC-1	1.9 nM (1.7-2.2 nM)	4.1 nM (3.5-4.6 nM)	25 nM (22-28 nM)	54 nM (48-61 nM)	0.2 µM (0.2-0.3 µM)	0.3 µM (0.3-0.4 µM)	25 µM (15-44 µM)	7.6 µM (4.4 -13 µM)	7.0 µM (0.5 -10 µM)
EC_{50} nucl. fragm. 48 h HMEC-1	2.4 nM (1.9-3.1 nM)	2.9 nM (2.3-3.8 nM)	22 nM (17-28 nM)	63 nM (58-69 nM)	0.3 µM (0.2-0.3 µM)	0.3 µM (0.3 -0.4 µM)	10 µM (8.1-13 µM)	7.0 µM (4.9-9.7 µM)	8.0 µM (5.9-11 µM)
EC_{50} wound repair 16 h HUVEC	3.4 nM (2.9-3.9 nM)	5.3 nM (4.3-6.5 nM)	11 nM (9.9-13 nM)	36 nM (19-35 nM)	0.2 µM (0.2-0.3 µM)	0.3 µM (0.2-0.3 µM)	4.2 µM (3.3-5.4 µM)	3.0 µM (2.6-3.6 µM)	5.9 µM (5.0-6.9 µM)

4 Results – part 2: Characterization of the anti-angiogenic effects of concanamycin A

4.1 Expression and sub-cellular distribution of the v-ATPase 16kDa subunit c in human endothelial cells

For the start, we tested HMEC-1 and HUVEC for the expression and distribution of a constitutive element of the v-ATPase complex, the membrane integrated 16kDa subunit c (syn.: ductin or ATP6L). By western blot analysis, the subunit c protein was detected in both endothelial cell types. (Fig. 4.1 A).

Under migratory conditions in a scratch assay, we performed an immune-fluorescent staining (Fig. 4.1 B), since the v-ATPase has been described to be expressed at the leading edge in migrating cells, particularly in microvascular endothelial cells, where it contributes to migration and invasion [22, 25].

In our setting, the vast majority of subunit c protein (green) appears diffusively distributed in vesicular patterns in both HMEC-1 (microvascular endothelial cells) and HUVEC (macrovascular endothelial cells). In HMEC-1, only a very thin line of subunit c molecules can be detected at the leading edge together with lamellipodia structures, that are clearly defined by staining for filamentous actin (Fig. 4.1 B red).

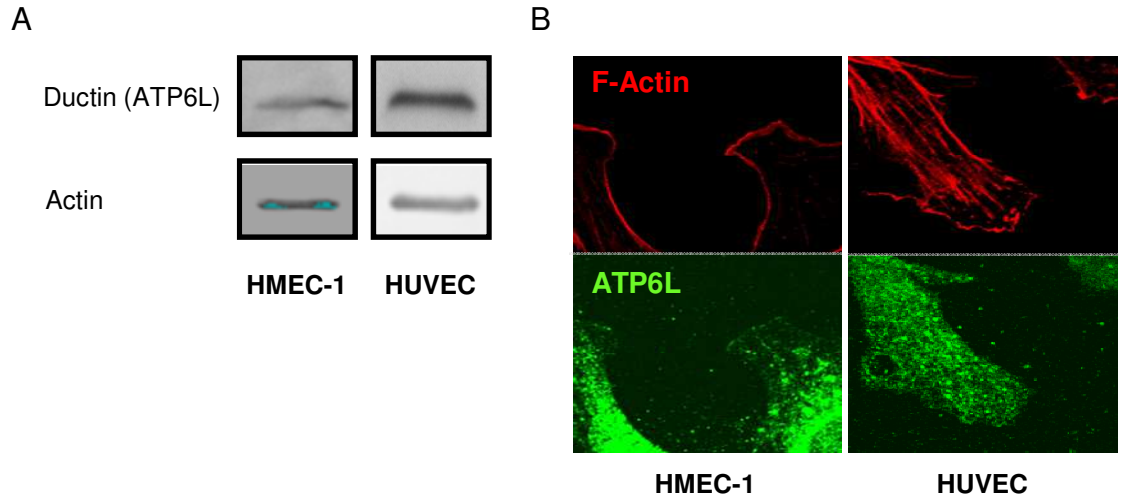

Fig. 4.1 Endothelial subunit c (ATP6L) expression. (A) Western blot detection of HMEC-1 and HUVEC subunit c protein (n=3). (B) Immune-cytochemistry images of subunit c distribution (green) under migratory conditions in HMEC-1 (left panel) and HUVEC (right panel) (n=3). F-actin is depicted in red.

4.2 Effects of concanamycin A (ConcmA) on lysosomal pH and cell morphology in human endothelial cells

4.2.1 ConcmA quickly increases lysosomal pH in HMEC-1

The inhibitory activity of Concanamycin A (ConcmA) on endothelial cell v-ATPases was confirmed by the use of the pH dependent staining reagent Lysotracker® Red that accumulates in acidic vesicles like lysosomes in live cells. Nanomolar concentrations of ConcmA clearly increase the lysosomal pH in HMEC-1 within 4 h as indicated by the loss of red staining (Fig. 4.2, middle and right panels).

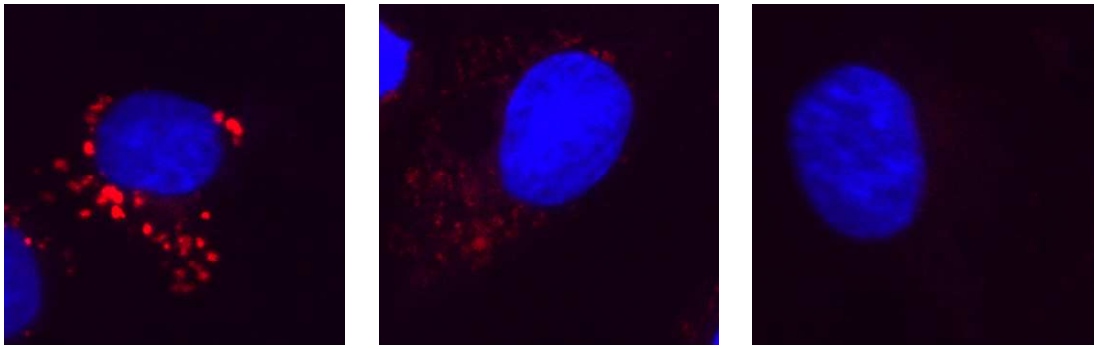

Fig. 4.2 ConcmA quickly alkalizes lysosomes in HMEC-1 at nanomolar dose. Confocal images from HMEC-1 treated with ConcmA. Lysotracker Red was added for 2 h to stain acidic lysosomes (n=3), nuclei are shown in blue.

4.2.2 Morphological changes in EC in response to ConcmA

Many publications describe morphological changes in a broad range of eukaryotic organisms in correlation to genetic or pharmacological inhibition of v-ATPases [23, 98, 99]. Having shown the primary effects of ConcmA on lysosomal pH, we next were interested in the secondary effects on cellular shape of endothelial cells after different time points of ConcmA treatment.

HUVEC, treated with low nanomolar concentrations of ConcmA, did not alter their cell shape after 2 h but after 20 h, as observed with phase contrast microscopy (Fig. 4.3 A upper and lower panels, respectively). At the latter time point, treated HUVEC clearly increased in cell size and appear less flat than untreated cells (Fig. 4.3 A lower panels). In a high magnified detail of phase contrast images (Fig. 4.3 B), clear accumulations of enlarged vesicles can be seen.

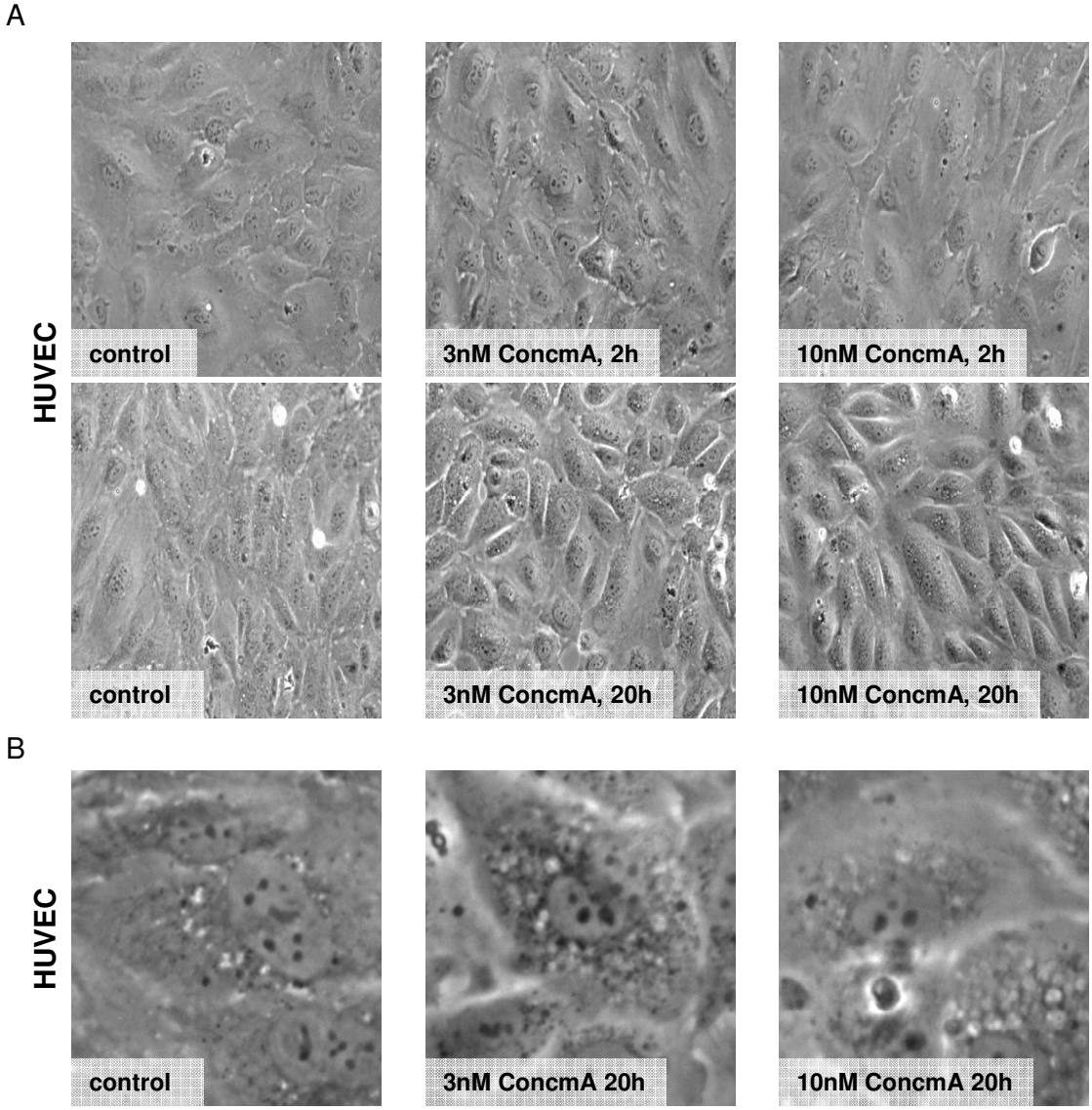

Fig. 4.3 (A) Time and dose dependent increase of cell size in HUVEC after ConcmA addition. 40 x phase contrast images (n=3). (B) Detailed image from (A) showing increase in vesicle size and number.

4.3 Influences of v-ATPase inhibition on angiogenesis related cell functions *in vitro*

4.3.1 Endothelial cell growth and survival

Co-incubation of sparse HMEC-1 with ConcmA, efficiently reduced the cell proliferation within 72 h. The EC_{50} value for this assay was calculated as 0.24 nM (Fig. 4.4.).

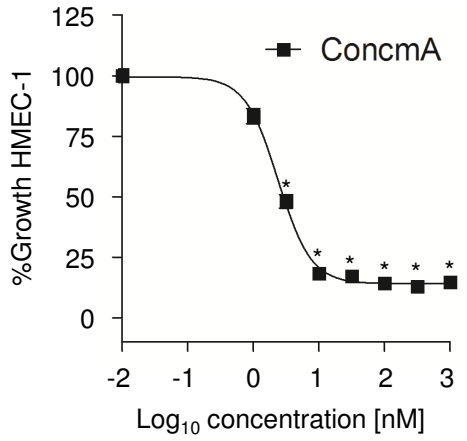

Fig. 4.4 Dose dependent growth curve of HMEC-1 treated with concanamycin A. Data are means ± SEM. of three independent experiments, * $p<0.001$ vs. control. One way ANOVA, Dunnett's multiple comparison test

Suppression of endothelial cell proliferation by ConcmA might be associated with the induction of cell cycle arrest and apoptosis similar to tubulin inhibitors [97]. In order to test this hypothesis, proliferating HMEC-1 were treated with ConcmA for 24 h and 48 h. Subsequently, the DNA content was analyzed by flow cytometry. After 24 h of ConcmA treatment, no obvious DNA fragmentation as a late sign of apoptosis occurred (Fig. 4.5 A, left side). Cell cycle distribution was not affected as well at this time point (Fig. 4.5 B, left side). After 48 h however, a clear increase of sub-diploid cells, i.e. dead cells, could be detected in HMEC-1 (Fig 4.5 A, right side). Furthermore, at this point of treatment, the cell cycle distribution was shifted from a G_0/G_1-phase majority to higher percentages in S- and G_2/M-phase, suggesting, that endothelial cell cycle progression was blocked or delayed (Fig 4.5 B, right side).

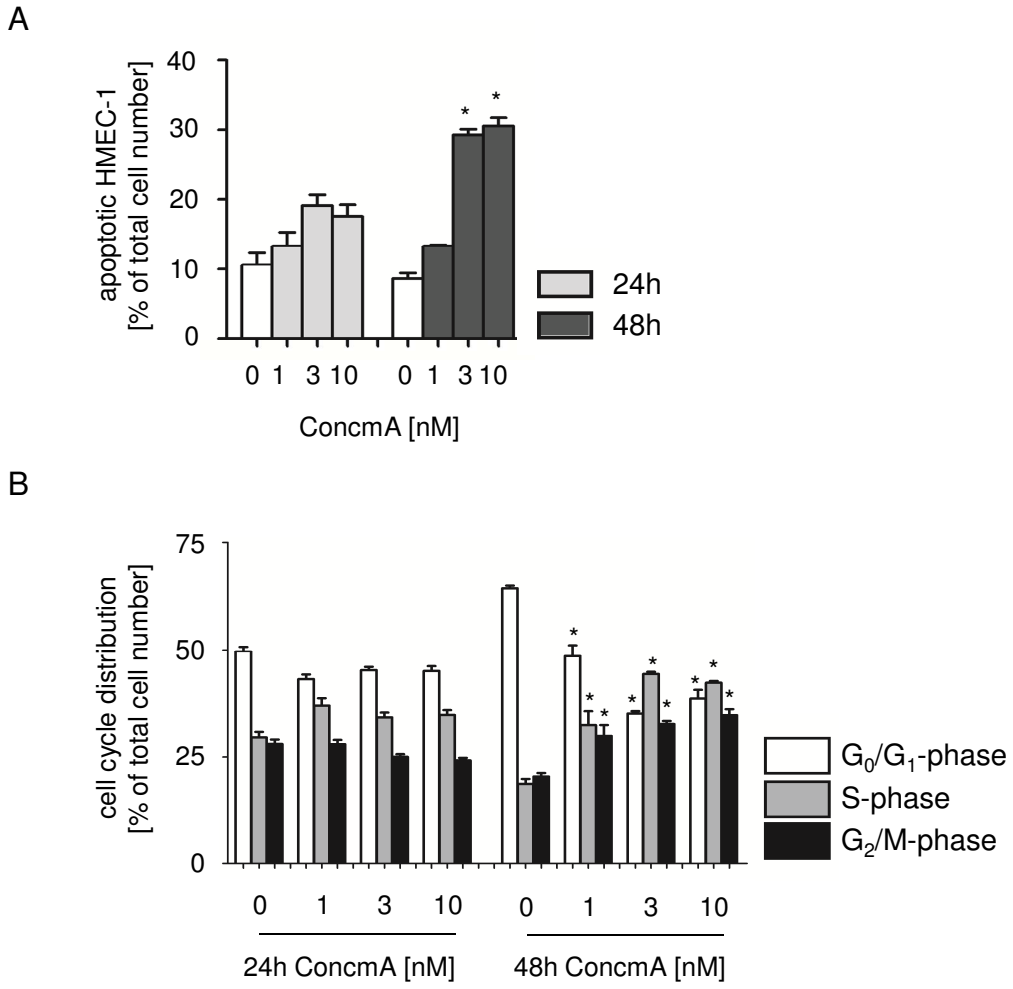

Fig. 4.5 Flow cytometry analysis of DNA content in HMEC-1 after ConcmA treatment.
(A) Quantification of cells with fragmented nucleus, i.e. apoptotic cells. B) Quantification of cell cycle distribution. N=3, Data are means ± SEM., * $p<0.05$, One Way ANOVA, Dunnett's multiple comparison

Next we tested, if the anti-proliferative and anti-survival effects observed in HMEC-1 in response to ConcmA could be connected to impaired VEGF signaling. Therefore we investigated the phosphorylation of two serine threonine kinases that among other functions translate the mitogenic and prosurvival signaling downstream of VEGF, Akt and ERK1/2 [100, 101]. While in untreated HMEC-1 the addition of VEGF resulted in a clear phosphorylation of both kinases (Fig 4.6 A-D, lane 2), pre-treatment with ConcmA reduced the VEGF induced activation at different extent and different kinetics for Akt and ERK1/2. Activation of Akt was already hampered after 6 h incubation with 10 nM ConcmA (A, lane 6) and completely abolished after 24 h incubation with 3 and 10 nM ConcmA (C, lane 5 and 6). In contrast, ERK1/2 activation was only reduced to the half after 24 h incubation with 3 nM and 10 nM ConcmA (D, lane 5 and 6) or not affected at all after 6 h incubation (Fig. 4.6 B).

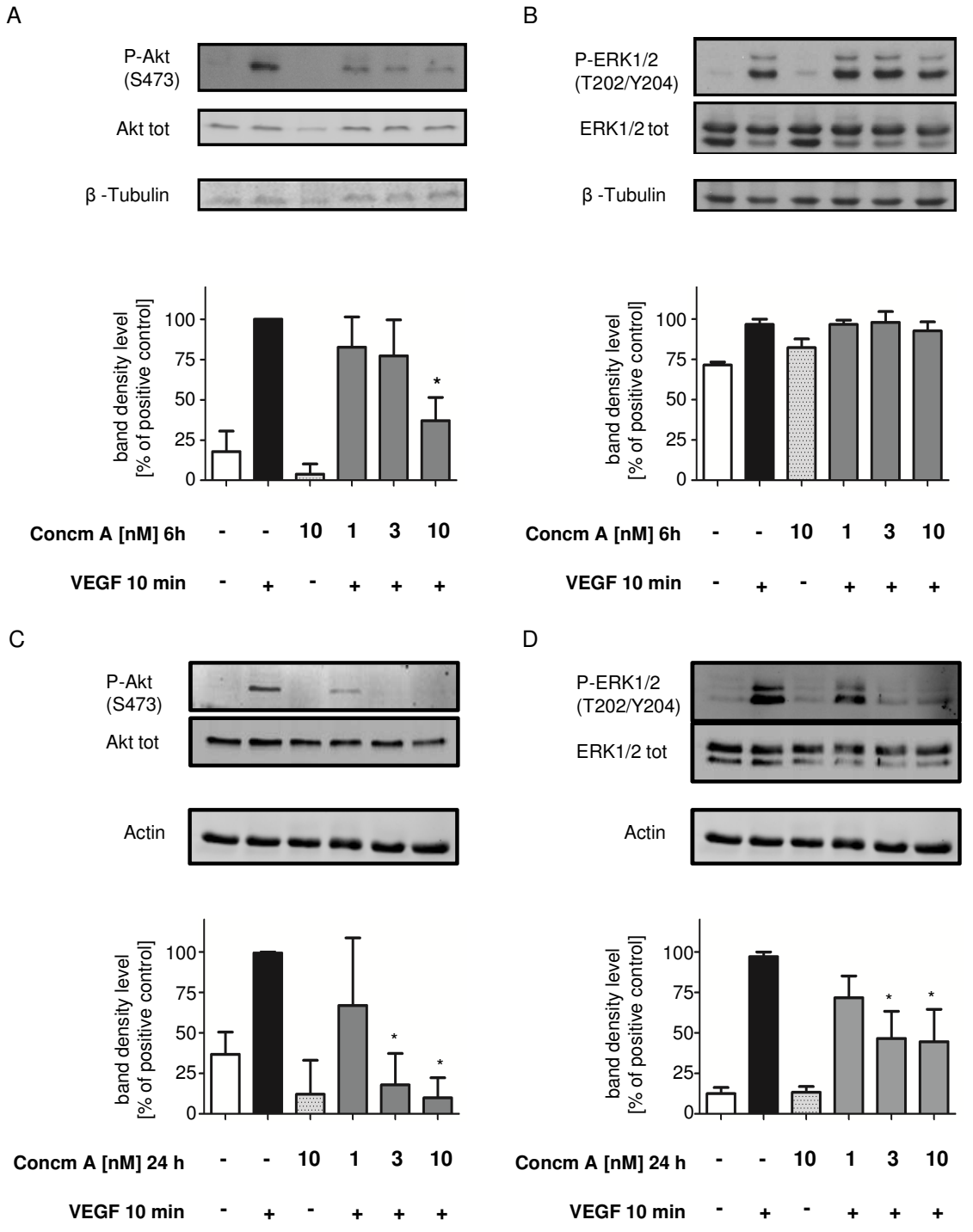

Fig. 4.6 Effects of concanamycinA on the VEGF induced phosphorylation of Akt (S473) and ERK1/2 (T202/Y204) in HMEC-1. A and C: 6 h and 24 h pre-treatment with ConcmA prior to VEGF stimulation, time and dose dependently abolished VEGF induced phosphorylation (S473) of Akt, (A n=4, C n=5). B and D: VEGF stimulated ERK1/2 phosphorylation (T202/Y204) was completely unaffected by 6 h pre-incubation with ConcmA. In contrast, after 24 h with 3 and 10 nM ConcmA, ERK1/2 activation levels were reduced by half, compared to control (lane 2) (B and D, n=3). For quantification, Western blots were densitometrically analyzed using Image J. The ratio P-Kinase/total Kinase was calculated and normalized to loading control, either β-tubulin or actin. VEGF treated control cells were set as positive control (100% phosphorylation, black columns). Data are means ± SEM. $^{*}p>0.05$, One way ANOVA, Dunnett's multiple comparison

4.3.2 Endothelial cell migration

From the results on endothelial cell growth and survival, we had the impression that relevant inhibitory effects of nanomolar ConcmA concentrations occurred after 20 to 24 h, but not immediately.

This was corroborated by experiences with archazolids, potent v-ATPase inhibitors from myxobacteria that were previously tested in migrating cancer cells [23] and in endothelial cells (personal communication, S.Zahler). Thus, we chose a 24 h pre-stimulation of confluent endothelial cells, followed by presence of v-ATPase inhibitor in the functional assay as experimental condition for cell functional assays (prolonged treatment), if not differently stated.

Knowing, that with this scheme the probability of toxic side events increases, we performed *in situ* cytotoxicity tests, where possible.

4.3.2.1 Wound healing assay (scratch assay)

Endothelial cell migration within wounded HUVEC and HMEC-1 monolayers was potently inhibited by prolonged ConcmA treatment with EC_{50} values of 1.5 nM and 3 nM respectively (Fig 4.7 B).

The *in situ* uptake of propidium iodide (PI), used as a cytotoxicity control, was very slightly increased in treated HUVEC (15% vs. 5% in control cells, Fig. 4.7 C, left diagram), as determined by flow cytometry. This value was similar to starvation induced cell death (Fig 4.7 C, st.).

In HMEC-1, such cytotoxic effects were not detectable (Fig. 4.7 C, right diagram).

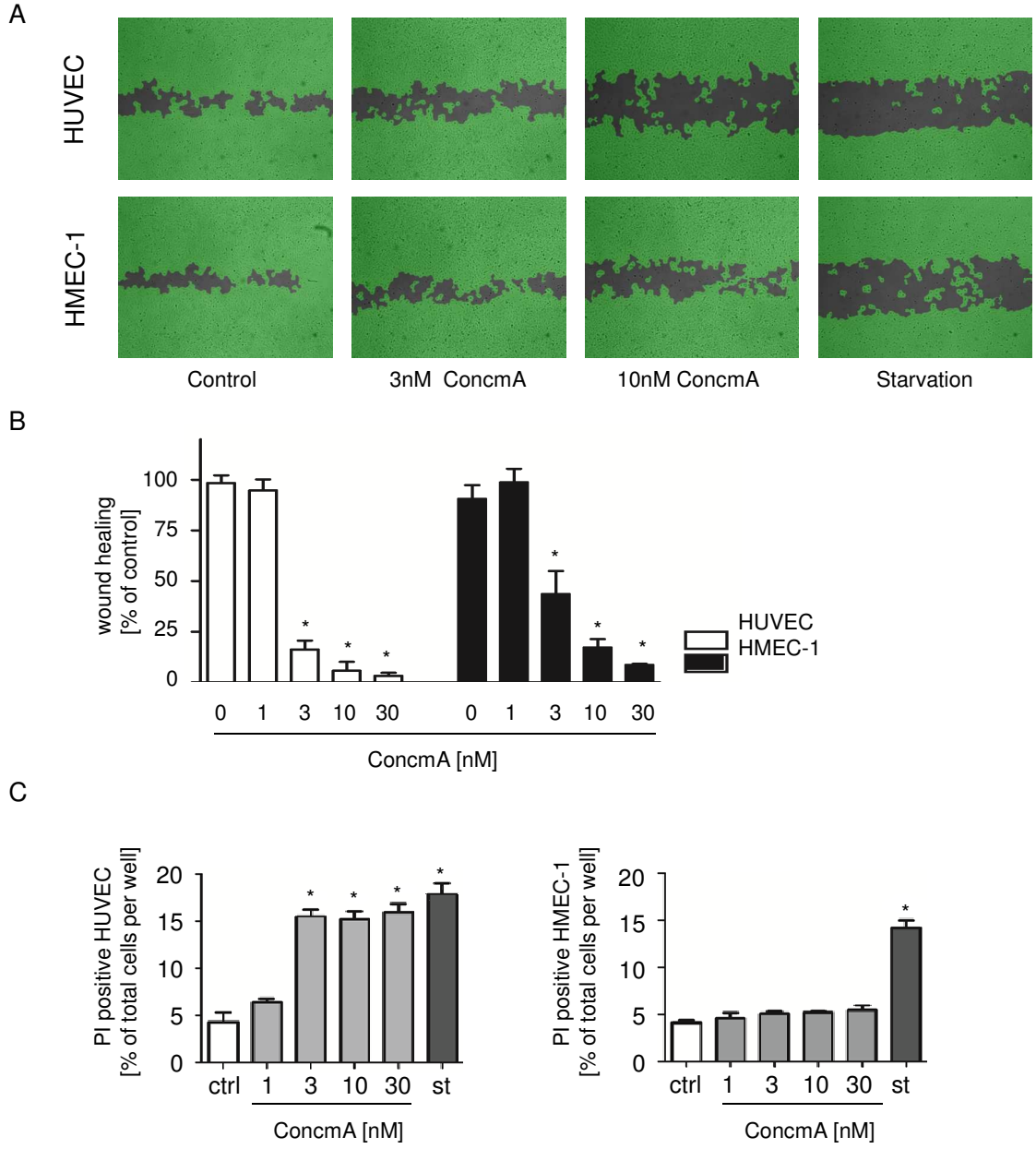

Fig. 4.7 ConcmA inhibits endothelial migration in the wound healing assay. (A) Representative images of wounded HUVEC and HMEC-1 monolayers, 16 h after wound infliction, 5 x magnification. WIMScratch quantification software (WIMASIS, Munich) colorizes cell covered area in green and cell free area in gray. (B) Quantification of relative wound healing (% of control). (C) PI- uptake, a marker for cell death, was determined by flow cytometry. Abbrevations: ctrl, untreated control cells; st, starved cells. Data are means ± SEM, n=3. * p< 0.05, One way ANOVA, Dunnett's multiple comparison

Importantly, we could show, that not only pharmacological inhibition, but also knockdown of the v-ATPase subunit c (ATP6L) by use of siRNA, significantly impaired the HUVEC migration in a scratch assay (Fig 4.8 A and B), confirming the importance of this v-ATPase element for cell migration. The knockdown efficiency was demonstrated by real time PCR analysis (Fig.4.8 C). The PI *in situ* incubation of HUVEC at the end of the wound repair confirmed no increased cytotoxity due to the knockdown (Fig 4.8 D).

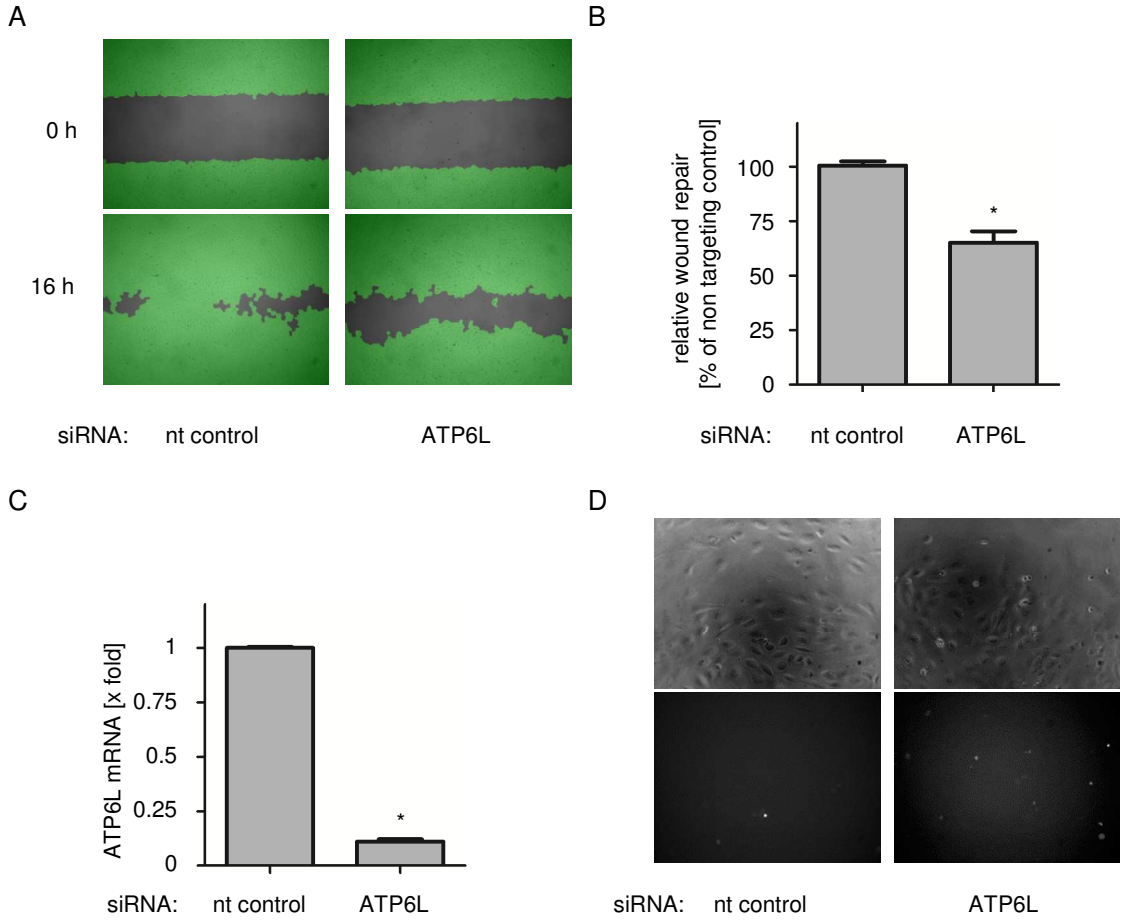

Fig. 4.8 Knockdown of ATP6L impairs endothelial cell migration in a HUVEC monolayer.
(A) Representative images from wound size in HUVEC monolayers, directly after wound infliction (0 h), and 16 h later. HUVEC had been transfected with control or with ATP6L targeting siRNA, 24 h before scratch infliction. (B) Quantification of wound repair, related to control (%). (C) x-fold ratio of ATP6L mRNA expression in ATP6L target siRNA transfected group against control group, as determined by RT-PCR analysis, 24 h after siRNA transfection. mRNA values were normalized against the GAPDH control gene. (D) *In situ* PI (propidium iodide) uptake is negligible in both, control and ATP6L siRNA transfected cells, as determined by fluorescence microscopy. Representative light transmission (upper panels) and fluorescence (lower panels) images, 10 x magnification, similar x,y,z settings. Data are means ± SEM, from three independent experiments, *p<0.05, unpaired t-test

4.3.2.2 Chemotaxis assay

Having observed significant anti-migratory effects in the scratch assay, we next tested single aspects of migration (orientation and overall motility), using the two dimensional FCS chemotaxis assay. Orientation parameters, such as the y-forward index and the Euclidean distance (Fig. 4.9 B1) were significantly decreased by prolonged treatment with 3 nM ConcmA. This was however not a pure effect on cell orientation, since the walking radius in the tracking plots (Fig. 4.9 A), and the accumulative distance and velocity (Fig. 4.9 B1) were also clearly decreased by ConcmA. Furthermore, cell viability seemed to be affected. The number of apparent viable cells was decreased by

ConcmA (Fig. 4.9 B2). This effect is not statistically significant, but has to be considered for interpretation.

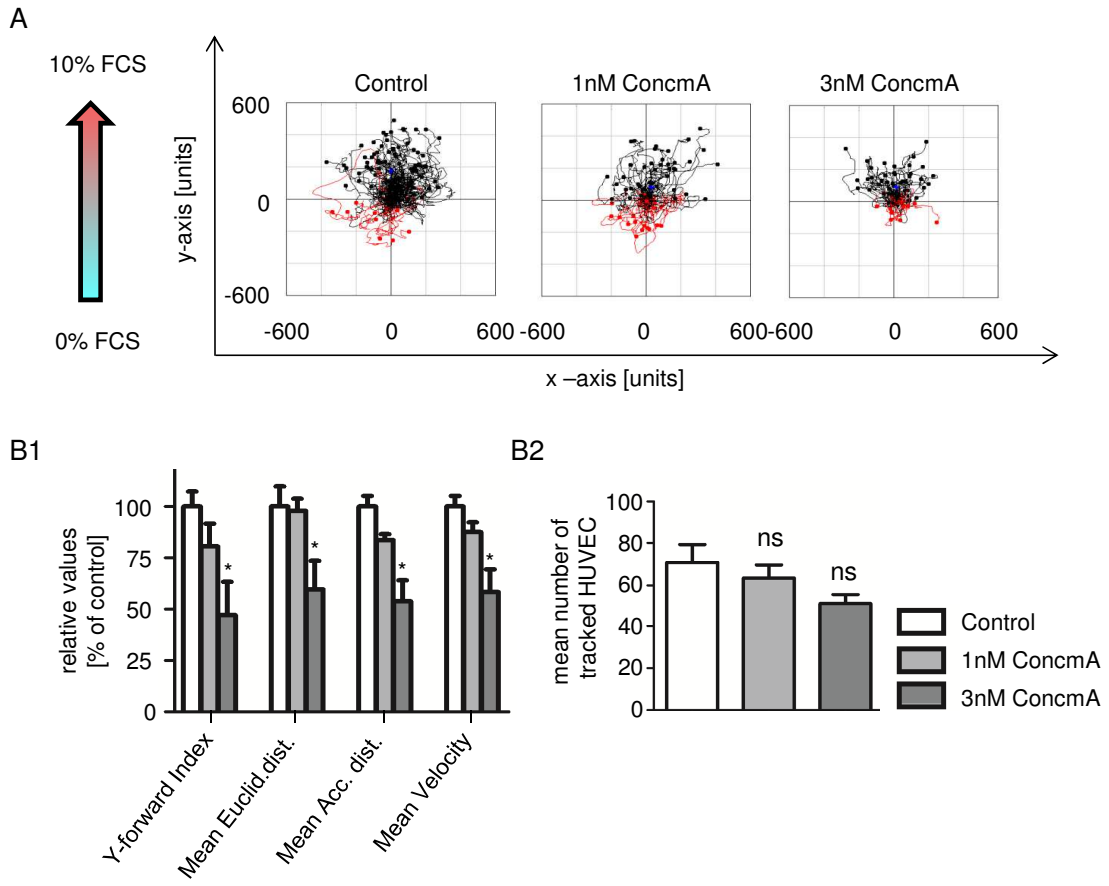

Fig. 4.9 Serum orientated chemotaxis of HUVEC is decreased by ConcmA treatment.
(A) Representative plots of HUVEC tracks, normalized to one common starting point in the middle of the plot. Along the y-axis, a 0-10% serum gradient was set up. (B1) Quantification of directional (y-forward index and Euclidean distance) and non-directional values (accumulative distance and velocity) describing the chemotactical movement. (B2) The mean number of tracked cells per experiment is decreased by ConcmA. Data are means ± SEM of four independent experiments, *P < 0.05, ns: no significant difference to control. One way ANOVA, Dunnett's multiple comparison

4.3.3 Endothelial cell – matrix interaction

A crucial pre-condition for both, endothelial cell migration and capillary formation (*in vitro* referred to as tube formation), is the ability of endothelial cells to interact with the matrix environment in order to perform matrix induced morphogenic changes [102, 103].

Thus, we next tested the influence of 24 h ConcmA treatment on cell matrix adhesion *per se* and on the degree of matrix induced formation of membrane protrusions, so called 'ruffles' (Fig. 4.10 A). By counting adhered HMEC-1 endothelial cells on various matrix protein coatings (Fig. 4.10 B), no significant

change could be detected. However, the degree of prominent ruffle formation in adhered HMEC-1 was clearly decreased (Fig. 4.10 C).

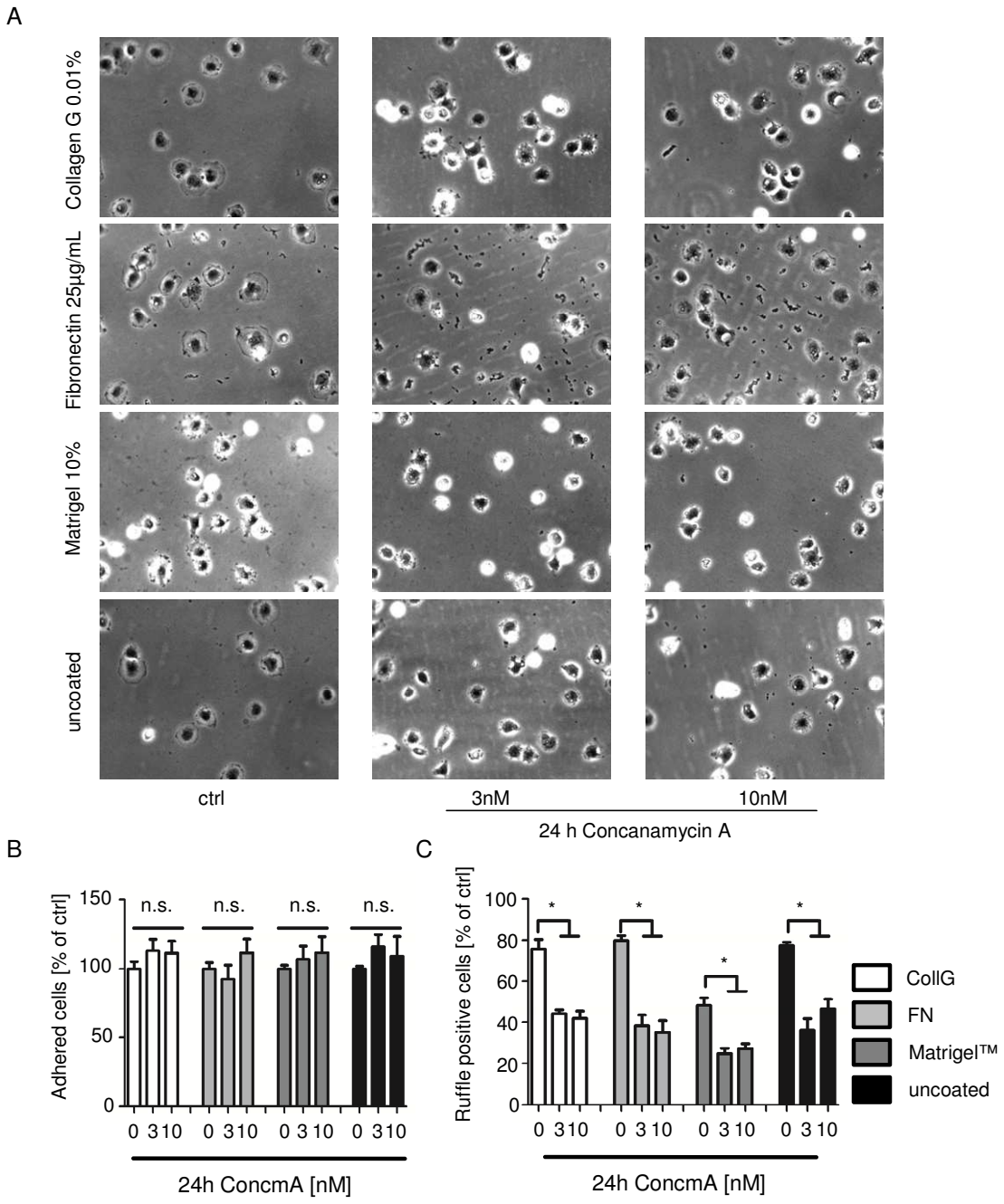

Fig. 4.10 ConcmA affects matrix induced ruffle formation in HMEC-1. (A) HMEC-1 were pre-treated for 24 h and then seeded either on collagen, fibronectin, diluted matrigel or on plastic. After 30 min, cells were fixed with formaldehyde and analyzed by microscopy. Representative images at 20x magnification. Note the loss of sharp membrane protrusions (ruffles) in treated HMEC-1. (B and C): Quantification of adhered cells (B) and of ruffle formation (C). Two central images per setting and experiment were evaluated. Data are means ± SEM, n=3, *p< 0.05, One way ANOVA, Dunnett's mulltple comparison.

In HUVEC treated with ConcmA, we could also observe a clear decrease in ruffle formation (Fig. 4.11 A). We hypothesized to find a decreased Rac-1 activation as an

explanation for this effect, since the small Rho GTPase Rac-1 is known to be highly active in lamellipodia formation and consequently membrane ruffling [104].

Indeed, by use of a pulldown assay, we could detect 50 % lower collagen adhesion induced Rac-1 activation after ConcmA pre-inubation (Fig. 4.11 B).

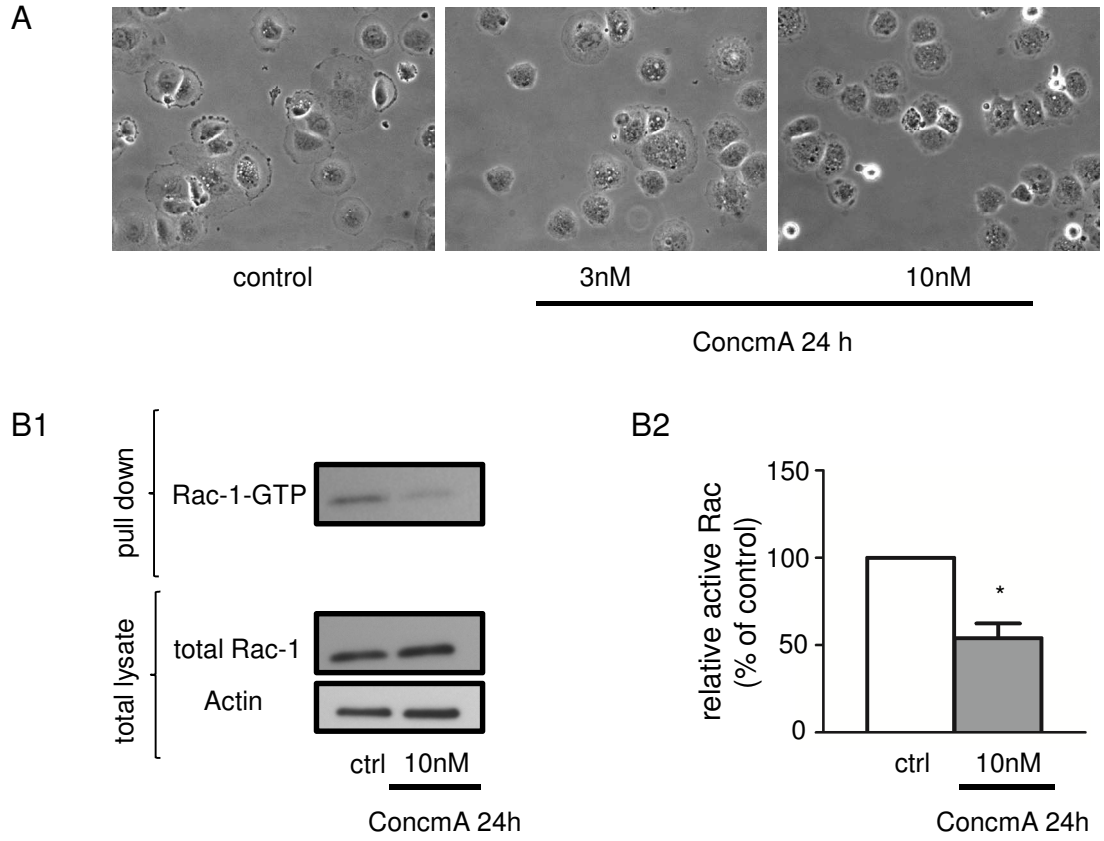

Fig. 4.11 ConcmA reduces ruffle formation in HUVEC, an effect associated with a decrease of Rac-1 activation (A) Representative images of HUVEC, 30 min after being seeded on collagen, either treated or untreated with ConcmA, 40x magnification, phase contrast microscopy, n=3. (B) Rac-GTP pull-down of HUVEC, being adhered to Collagen for 30min B1) Western Blot of active, GTP-bound Rac-1 (upper panel). Total Rac-1 and actin indicate equal loading (lower panel). B2) Quantification of five independent experiments, activated Rac-1 band intensity was normalized to the total Rac-1 amount and related to control. Data are means ± SEM, * P< 0.05, unpaired t-test.

4.3.4 Tube formation on Matrigel™

We have observed clear inhibitory effects of ConcmA on endothelial cell migration, ruffle formation and Rac-1 activation. Therefore, we next tested the effect of v-ATPase inhibition in a more complex setting, measuring the degree of capillary formation (tube formation) of pretreated HUVEC and HMEC-1 on Matrigel™.

Astonishingly, we observed completely different cell type specific effects of ConcmA in this assay. In HUVEC, tube formation was dose dependently decreased (Fig. 4.12 A, upper panels), however HMEC-1 were not affected at all by ConcmA, even when treated with 10-fold higher concentrations (Fig. 4.12 A, lower panels).

By quantification of node number and total tube length, tube formation in treated HMEC-1 appears to be increased (Fig. 4.12 B, black columns).

The same impression comes up for HUVEC treated with 1nM of ConcmA (Fig. 4.12 B white columns).

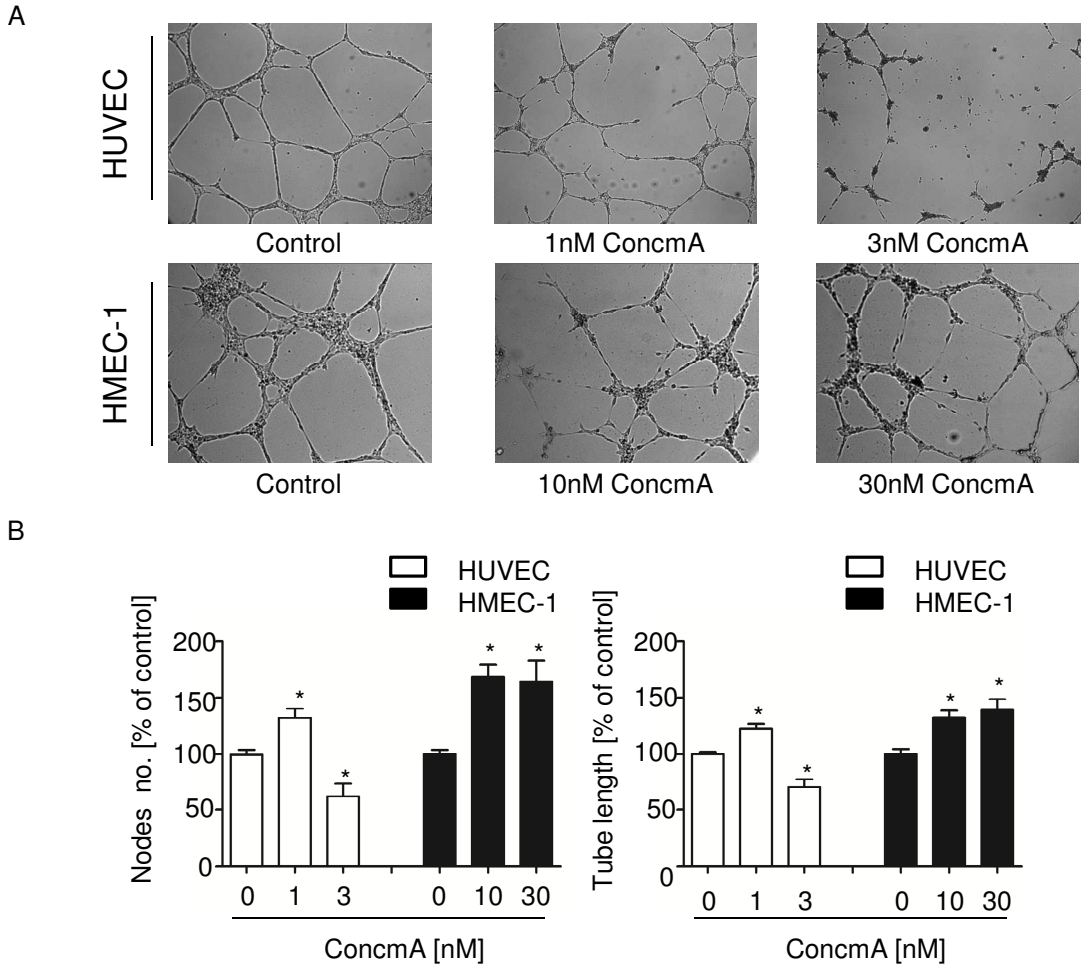

Fig. 4.12 Tube formation after prolonged treatment with ConcmA. (A) Representative images of treated HUVEC (top panel) and HMEC-1 (bottom panel), 16 h after seeding on Matrigel™, 5x magnification B) Quantitative evaluation of branching point number connecting the tubes (node no., left panel) and total tube length (right panel) using WIMTube module from WIMASIS, Munich. Data are means ± SEM, n=3, * $p<0.05$, One way ANOVA, Dunnett's multiple comparison

Since the membrane surface of the established tubes (in Fig 4.12), seemed to be roughened in both HUVEC and HMEC-1 compared to the control cells, we assumed cytotoxic effects. Indeed, *in situ* PI staining revealed a massive loss of membrane integrity in treated HUVEC as determined by fluorescence microscopy, suggesting an increase of cell death [105] (Fig. 4.13 A). However, in the HMEC-1 tube formation assay, we could not detect a relevant increase in cell death by this method (Fig 4.13 B, lower panels), which further indicates a different endothelial cell specific sensitivity.

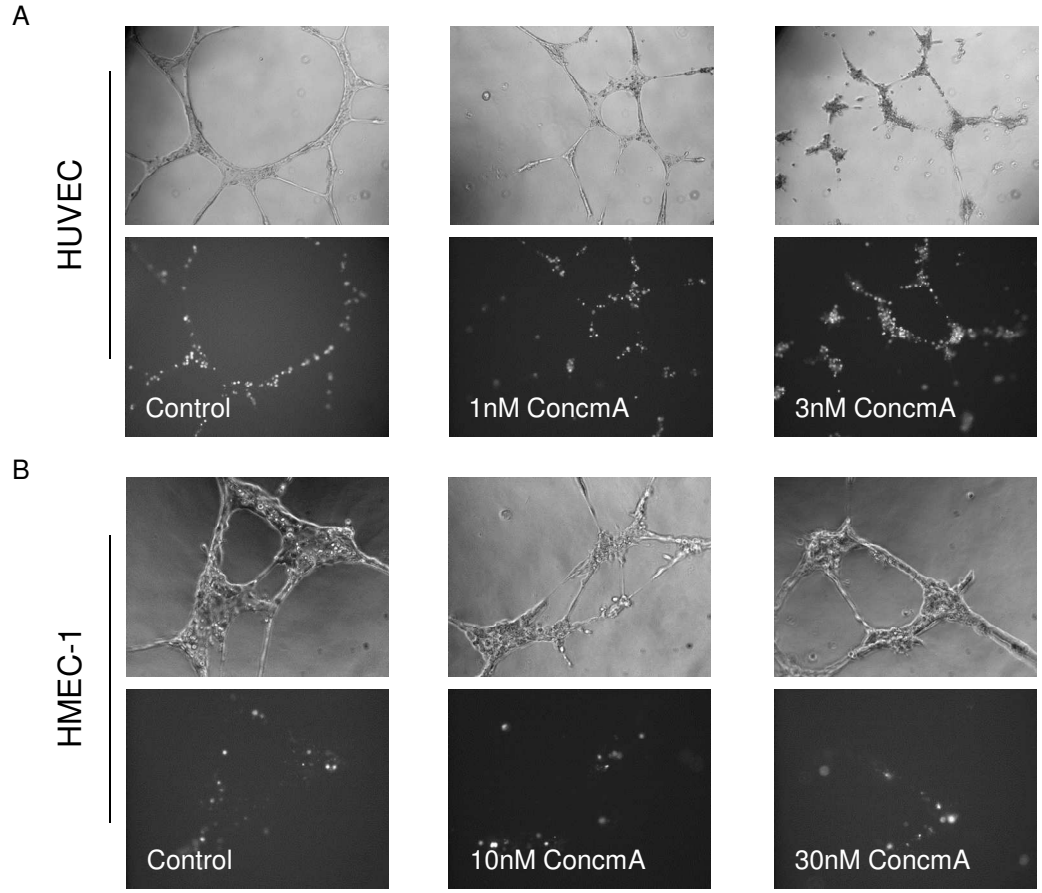

Fig. 4.13 Tube formation, *in situ* cytotoxicity test. 10µg/ml of propidium iodide (PI) was added to the tube supernatant for 30 min. PI uptake was analyzed by fluorescence microscopy. A) ConcmA treated HUVEC obviously lost membrane integrity, a late sign of cell death [105], indicated by incorporation of PI at higher levels than control cells. B) ConcmA treated HMEC-1 exhibited no increased cytotoxic phenotype vs. control, as determined by this assay. Representative light transmission images (upper panels) and fluorescence images (lower panels), 10xmagnification, similar x,y,z settings, n=3

4.4 Influences of v-ATPase inhibition on VEGFR2

VEGF is recognized as the most prominent pro-angiogenic growth factor, which signals mainly via the VEGFR2 axis [106]. We wanted to elucidate, whether ConcmA affects the function and distribution of this key receptor, which then could be taken as an explanation to anti-angiogenic effects, apart from inhibition of plasma membrane v-ATPases [25].

4.4.1 VEGFR2 function

VEGF induces the dimerization and subsequent autophosphorylation of VEGFR2 at a number of tyrosine residues e.g. tyrosine 1175, which consequently leads to the activation of downstream signaling cascades and the corresponding cellular function, e.g. survival, proliferation, migration [36, 107].

In HMEC-1, pre-treated with 10 nM of ConcmA for 24 h, VEGFR2 autophosphorylation at tyrosine 1175 was reduced by 50 % (Fig. 4.14 A, B). Moreover, it appears that the treatment with ConcmA leads to reduction of intact VEGFR2 in HMEC-1 (Fig 4.14 C), this effect was increased by addition of VEGF (Fig 4.14 A and C, lane 6).

Corroborating this impression, at the same time, VEGFR2 fragments of 130 kDa and 80 kDa (Fig. 4.14, E and F, lane 3 and 6) accumulated in HMEC-1, treated with 10 nM of ConcmA.

Thus, it seems that ConcmA impairs intrinsic VEGFR2 sensitivity on the one hand. On the other it promotes VEGF induced VEGFR2 degradation, which additionally weakens the signaling sensitivity.

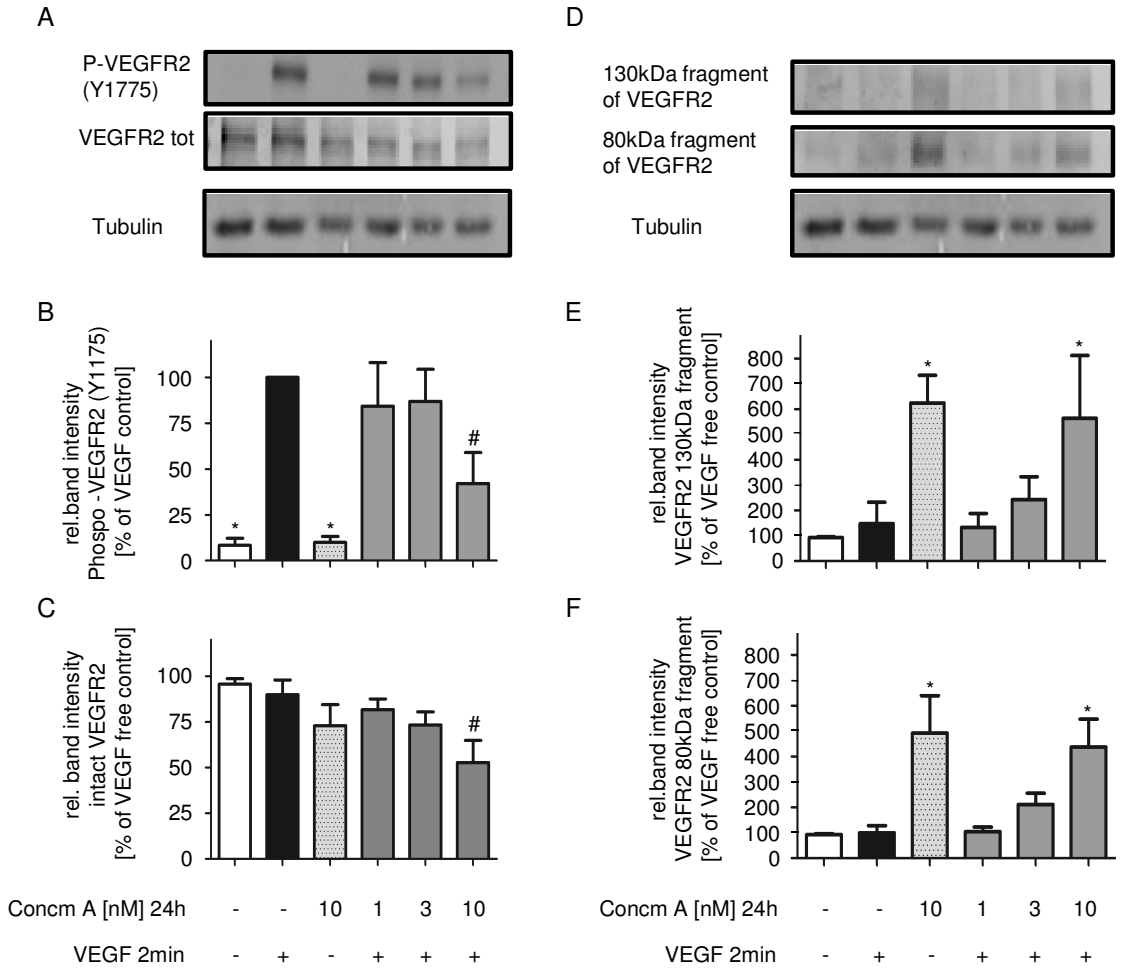

Fig. 4.14 ConcmA treatment reduces VEGF induced autophosphorylation of VEGFR2 and decreases total level of intact VEGFR2 A) Representative Western blots of phosphorylated VEGFR2 (Y1775) and total amount of VEGFR2. B) Densitometric quantification of phosphorylation level of VEGFR2 (Y1775) related to VEGF control (black column). C) Quantification of intact VEGFR2 (230 kDa), related to VEGF free control (white column). D) Representative Western blots of 130 kDa and 80 kDa fragments of VEGFR2. E and F) Quantification of 130 kDa and 80 kDa VEGFR2 fragments, respectively, related to VEGF free control (white columns). Band intensities were normalized to β-tubulin. Data are means ± SEM. from three independent experiments. # $p<0.05$, *$p<0.01$, one way ANOVA, Dunnett's multiple comparison.

4.4.2 VEGFR2 distribution

4.4.2.1 VEGFR2 at the cell surface

Endothelial cells exhibit a relatively stable steady state of VEGFR2 between the cell surface (approximately 50 % of the total VEGFR2) and intracellular compartments [28, 87]. Surface pools are stabilized e.g. by interactions with VE-cadherin [108, 109]. We wanted to know, whether surface VEGFR2 levels under serum reduced conditions would be affected by prolonged ConcmA treatment, in order to answer the question, if the reduced autophosphorylation of the receptor (Fig. 4.14 B) might be due to reduced surface levels prior to stimulation with VEGF. Therefore, after a 2 h starvation period, surface receptors were labeled, using a membrane-impermeant biotinylation reagent (Materials and Methods, 2.2.9).

By Western blot analysis, we could detect a dose dependent reduction of VEGFR2 surface pools by 20 to 30% (Fig 4.15). As confirmation for the specificity of this method, biotinylation negative controls (0/-) contained almost no VEGFR2 in the ‘surface fraction’ (Fig 4.15 A, lane 1). Furthermore, the membrane integrity was unaffected, as shown by the absence of actin in the surface fraction (Fig 4.15 A, upper panels). Altogether, these findings support the impression, that the VEGFR2 surface pool is reduced by prolonged ConcmA treatment, thus weakening the sensitivity to VEGF stimulation (Fig. 4.14 B).

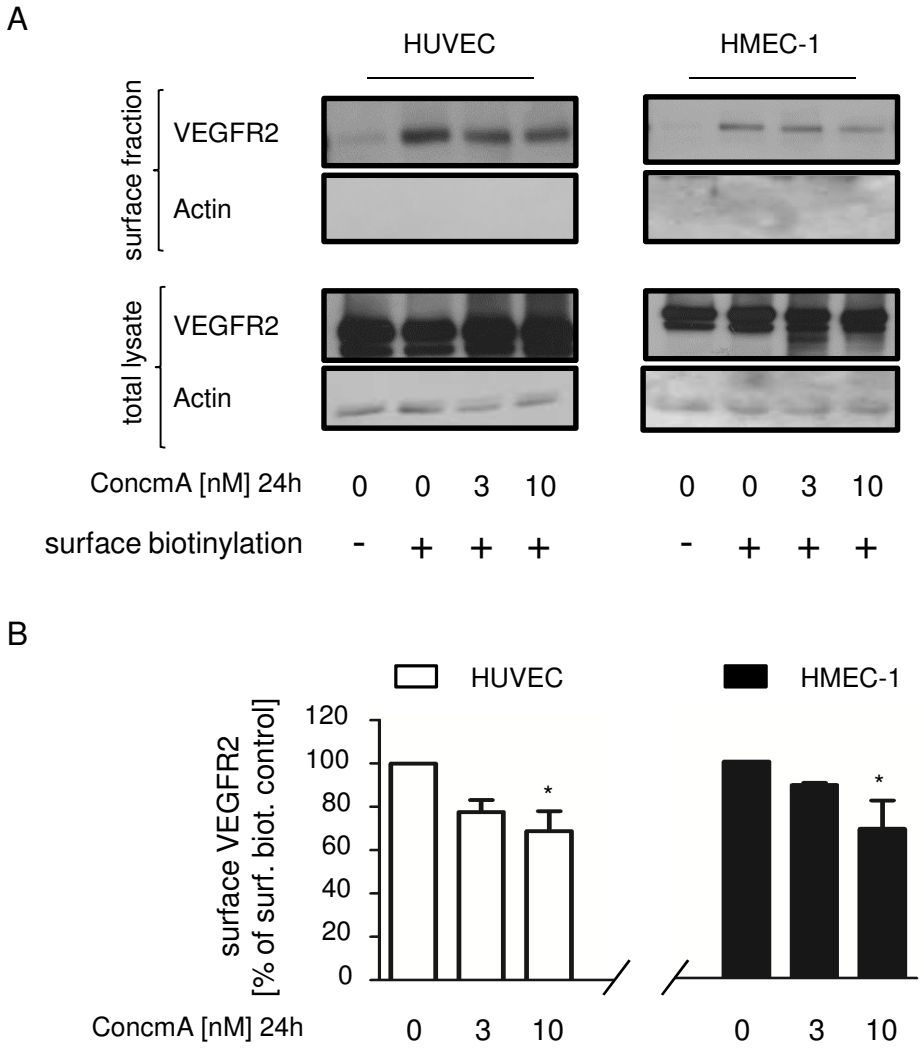

Fig. 4.15 VEGFR2 surface levels are reduced in HMEC-1 and HUVEC after ConcmA treatment. (A) Immune-blot detection of VEGFR2 in surface fractions upon surface biotinylation reaction, and total lysates of HUVEC and HMEC-1, respectively. (B) Densitometric quantification of surface VEGFR2 in relation to surface biotinylated control (0/+) in %. n=3 for both HUVEC and HMEC-1. Data are means ± SEM. *p<0.05, one way ANOVA, Dunnett's multiple comparison.

4.4.2.2 VEGFR2 in intracellular compartments

Having investigated effects on the surface distribution of VEGFR2, we next assessed the influence of ConcmA on intracellular VEGFR2 levels, using immune-cytochemistry. By confocal microscopy, we could observe a clear time and dose dependent formation of VEGFR2 containing vesicles after ConcmA addition. This process started after 2 h with relatively diffuse accumulations at 3 nM and 10 nM and was evident after 24 h, already at a concenctration of 1 nM (Fig 4.16 A). We could exclude that these accumulations were caused by higher VEGFR2 expression, as we could not detect increased but rather decreased VEGFR2 protein levels in a Western blot (Fig 4.16 B), consistent with previous findings (Fig. 4.14 C).

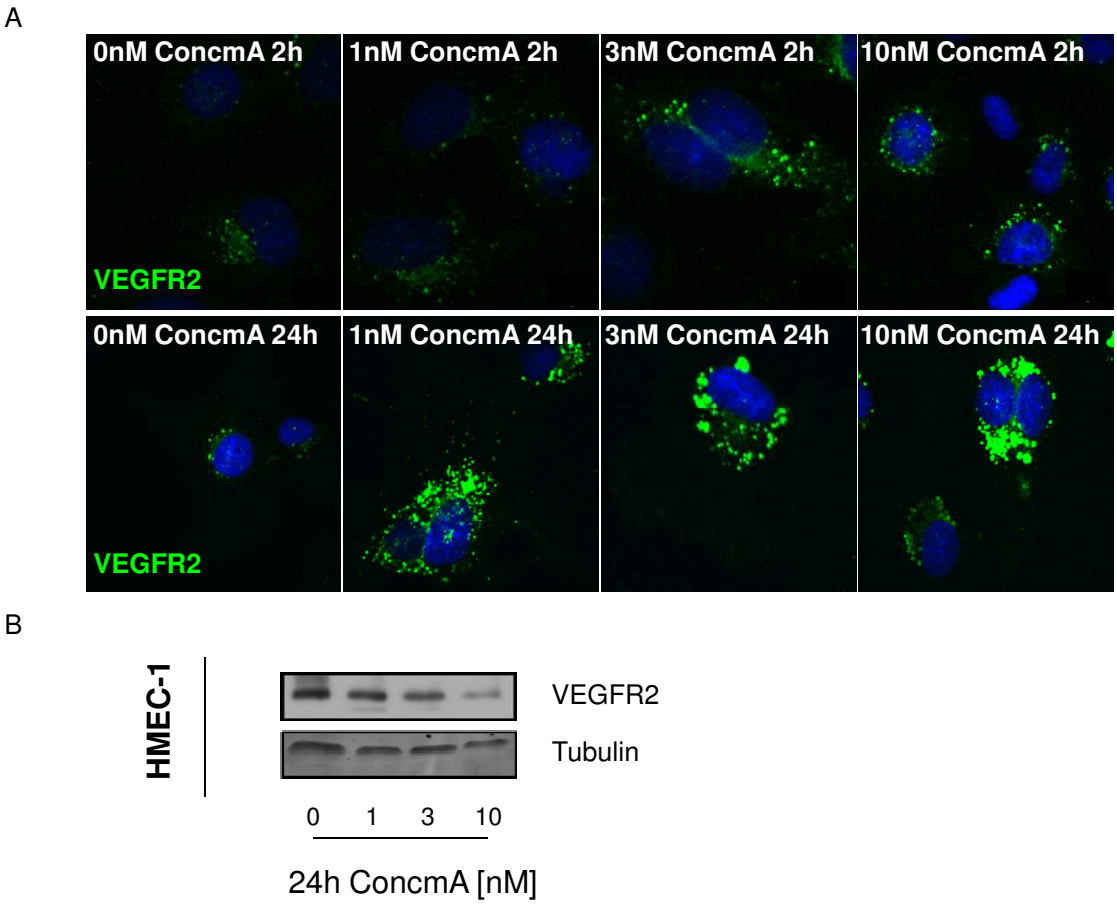

Fig. 4.16 VEGFR2 accumulates over time in enlarged vesicles in response to prolonged ConcmA treatment. (A) Representative immune-cytochemistry images of HMEC-1, after 2 h (upper panel) and 24 h (lower panel) incubation with ConcmA. VEGFR2 is depicted in green, nuclei are depicted in blue, n=2 for 2 h and n=3 for 24 h setting. (B) As confirmed by Western blot experiment, the overall amount of VEGFR2 is decreased rather than increased by ConcmA, underlining that enlarged VEGFR2 vesicles derive from altered distribution and not from increased protein synthesis, n=3.

In order to clarify, whether VEGFR2 accumulates in a specific compartment, we performed an immune-fluorescent co-labeling of selected marker proteins characteristic for the upper and lower parts of the endocytic pathway.

Since it is known, that VEGFR2 internalization is controlled in part by caveolin [110], a membrane protein, we labeled both VEGFR2 and caveolin1 (Cav1), with adequate immune-staining. By confocal microscopy, we could not detect merging areas between the VEGFR2 positive vesicles and Cav1 (Fig. 4.17, upper panels).

Yet another surface protein, clathrin, which is known to mediate receptor tyrosine kinase internalization [111, 112], was additionally tested for co-localization with VEGFR2 patterns. Here, we could also find no overlapping with VEGFR2 (Fig. 4.17, lower panels) in pattern or color, suggesting that VEGFR2 is not trapped in a semi-internalized state or surface near compartment, which is in line with the observed decrease of extracellular receptor levels (Fig 4.15).

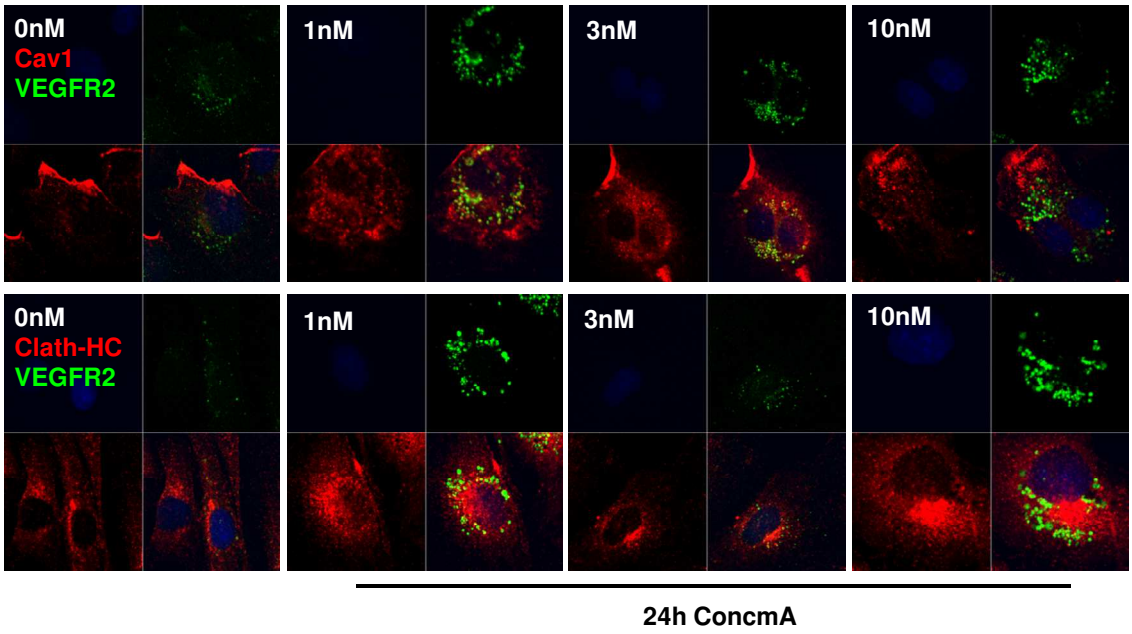

Fig. 4.17 Confocal images of co-immune stainings of VEGFR2 with RTK internalization regulating proteins upon ConcmA treatment. VEGFR2 accumulating vesicles (depicted in green) don't merge with Caveolin (upper panel in red, Cav1: caveolin 1) or with Clathrin-immune-staining pattern (lower panel in red, Clath-HC: clathrin heavy chain). Nuclei are shown in blue. N=3

As further possibility for the identity of the VEGFR2 accumulating vesicles, we used immune-staining for a marker of early endosomes, Rab5. However, we could not detect merging structures between Rab5 and VEGFR2 patterns (Fig. 4.18, upper panel), since shape and color of both were clearly different.

Next, we tested if the lysosomal compartment, known as the place for receptor degradation [111], might be identical with VEGFR2 containing vesicles. Therefore we applied co-immune-staining for a lysosomal marker, lysosomal associated marker protein1, Lamp1. Here, we could find clear merging patterns between VEGFR2 and Lamp1 staining (Fig. 4.18, lower panels), which were increasing in intensity in response to higher concentrations of ConcmA. This suggests that prolonged v-ATPase inhibition leads to entrapment of VEGFR2 in lysosomes.

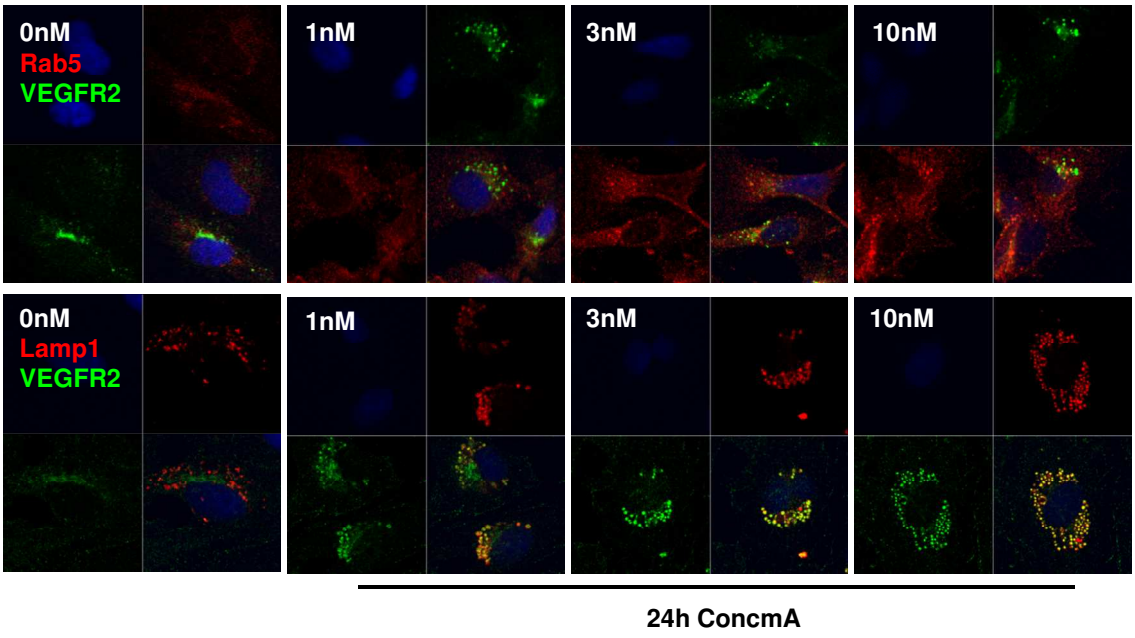

Fig. 4.18 Prolonged ConcmA treatment leads to the accumulation of VEGFR2 in lysosomes. Upper panel: The immune-staining pattern for a marker of early endosomes, Rab5, does not merge with the VEGFR2 pattern. Lower panel: By application of co-immunestaining for a lysosome marker (Lamp1), clear merging with VEGFR2 pattern can be detected, depending on the ConcmA concentration. Representative images are shown for each marker, n=3. VEGFR2 is depicted in green, respective markers are depicted in red, merging structures are depicted in yellow, nuclei are shown in blue.

5 Discussion and Outlook

5.1 Natural anti-cancer drugs with anti-angiogenic profile

One highly causal strategy in the battle on cancer is the inhibition of tumor angiogenesis, since this process is a common feature to solid tumors, which continuously fuels cancer growth and moreover is a pre-requisite to metastases [2, 31, 113].

Many selective anti-angiogenic drugs, that are used in tumor therapy, inhibit only one or few angiogenesis signaling pathways, predominantly the VEGF/VEGFR2 axis (e.g. bevacizumab, sorafenib). This specific approach turned out to be clinically less efficient than expected [3, 114], due to compensation by other signaling networks, such as for example the Notch complex [4, 5, 114].

Conventional cytotoxic chemotherapeutics, such as DNA or microtubule binding drugs, were recently considered for their anti-angiogenic potential in a therapeutic regimen of frequently low dosed application ('metronomic chemotherapy'), with the aim to decrease adverse side effects [8, 9, 42, 43, 115]. Hence, the tumor endothelium displays a further important target for cytotoxic drugs. In contrast to cancer cells, the genetically more stable endothelial cells possess the advantages of lower tendency to become drug-resistant and of being directly addressable via the blood stream [8, 116].

In the present work, we have evaluated two pharmacologically distinct groups of cytotoxic natural compounds or derivatives thereof concerning their potential to inhibit angiogenesis. These compounds target either tubulin, an 'established' cellular structure for the anti-angiogenic approach [46, 55, 117], or the vacuolar H^+ - ATPase (v-ATPase), which is yet 'unestablished' in the sense of only few preclinical studies in the field of angiogenesis inhibition [24, 25].

For a better overview, the results of both parts will be first discussed one by one, and then combined in a final outlook discussion.

5.2 Anti-angiogenic effects of pretubulysin and analogues

For decades, natural tubulin binding agents (nTBAs) or TBAs based on natural leads are established in the therapy of cancer [45]. The number of compounds in this field is growing as a result of screenings in marine, botanical and myxobacterial sources [45, 49, 118-120]. Among the features that novel agents have to possess in order to improve tumor therapy are insensitivity to chemoresistance [45, 121], less neurotoxicity, increased tumor specificity[45] and, last but not least, the ability to exert anti-angiogenic activity, even at low, non-toxic concentrations [46, 67, 69, 117, 122].

In the first part of this work, we assessed pretubulysin (Prt), a chemically accessible precursor [18] of the microtubule-depolymerizing tubulysins [11], and pretubulysin analogues for their anti-angiogenic effects. Tubulysin A (TubA) itself already has been evaluated as a very potent anti-angiogenic drug [13], and the application of polymeric tubulysin peptide nanoparticles has been reported to reduce tumor growth in colorectal and non-small cell lung carcinoma [51]. However, due to tedious and inefficient natural supply [11, 19] and chemically challenging synthesis of TubA, clinical progress was hampered to date [17]. In contrast, the chemistry of the biosynthetic precursor Prt is less complex and suitable for efficient total synthesis as well as numerous chemical modification [15, 16, 18, 60].

5.2.1 Pretubulysin exhibits similar activity as tubulysin A in cellular angiogenesis assays

Comparison of Prt and TubA revealed a similar efficacy in all *in vitro* angiogenesis assays. This makes pretubulysin an attractive and simplified alternative, in terms of use as an anti-angiogenic compound and for structure activity studies. This is in line with findings of Herrmann and colleagues who found nearly similar activity of Prt and tubulysins in multiple cancer cell functional tests and in tubulin studies [19].

5.2.2 Pretubulysin derivatives display a continuous structure activity relationship throughout all assays

The tested Prt analogues were chemically altered at different sites of the tetra-peptidic skeleton, either at the C- or N- terminus [15] or in the centre of the molecule [16]. Importantly, these alterations had a consistent influence on the pharmacological potential in all test systems, which finally led to the classification of compounds into three groups of either high (tubulysin A, pretubulysin and AU816), intermediate (JB337, JB375, AU954) or low potency (AU825, JB338, AU815). This ranking order matched with the results of the *in vitro* tubulin polymerization assay and the assay on microtubule depolymerization, suggesting that a different binding affinity to tubulin is the most likely explanation for different bioactivity among these compared agents.

With respect to the structure, it can be said, that an intact piperidin ring at the N-terminus and an intact (2-desmethyl or 2,3 didehydro)-tubuphenylalanine at the C-terminus seem to be prerequisite for high pharmacological efficacy, since small alterations at these positions caused dramatic loss of activity (Fig. 2.1 B, left panel). Replacement of the central C-desacetoxy-tubuvaline block in pretubulysin by alternative spacers leads in cases of phenyl- and phenoxypretubulysin (JB337 and JB375, respectively) to moderate loss of activity, while the introduction of a triazole containing spacer (in JB338) is deleterious (Fig. 2.1 A and B right panel).

5.2.3 Anti-angiogenic effects of pretubulysin and tubulysinA can be discriminated into 'mitotic' and 'non-mitotic'

Many investigations reveal that tubulin binding agents (TBAs) modulate the microtubule cytoskeleton in endothelial cells in a fairly subtle fashion, without necessarily being cytotoxic [46, 117]. By these modulations, angiogenesis relevant transport processes of both, non-membranous cargo [56] and of vesicles carrying important signaling complexes [63, 64, 67, 123], are disturbed. Moreover, the re-orientation of the microtubule organizing centre (MTOC) is impaired by non-mitotic TBA concentrations, inhibiting cell polarization and thus oriented migration [69, 124].

Indeed, in our study we can distinguish between mitotic and non-mitotic effects of the test compounds, since prominent cell cycle arrest and consequently cell death occurs at late time points (48 h), while inhibition of migration and tube formation is significant at earlier time points, when cell death is not yet prominent both in HMEC-1 and in HUVEC. Furthermore, it is shown in the chemotaxis assay, that predominantly the tendency of serum orientated migration is impaired, while overall motility is not significantly affected (Fig. 3.6). Hence, loss of orientation may truly be the primary cause of these early anti-angiogenic effects as described by Hotchkiss et al. [69].

5.2.4 Pretubulysin blocks hepatocellular carcinoma (HCC) growth and vascularization in an *in vivo* murine model

As final assessment, we applied Prt in a subcutaneous murine xenograft model, with hepatocellular carcinoma cells (HuH7), since these tumors are known to be very well vascularized [125]. TubA itself has already been tested in colorectal and non-small cell lung carcinoma murine xenograft models [51]. Interestingly, in the report by Schluep et al. [51], TubA did not show pronounced reduction of tumor growth, limited to its toxicity. Only linking of this compound to cyclodextrin-polyethylenepolymer nanoparticles, which allowed a sustained release of the drug, resulted in a safe and effective tumor size reduction and prolonged survival [51]. In our study, Prt showed no obvious toxicity at a metronomic schedule of 0.1mg/kg given i.v. every second day, as indicated by the absence of weight loss (Fig 3.11).

Still it caused a dramatic reduction of tumor growth. This might be partly due to direct affection of HuH7 proliferation, since we saw a prominent reduction of growth of this cell line *in vitro* at similar concentrations as for HMEC-1 (table 3.1).

Most importantly, Prt had an obvious inhibiting effect on tumor angiogenesis, with respect to the significant reduction of mean vascular density and the clearly visible absence of blood perfusion (Fig 3.11 C, D, E).

5.2.5 Conclusion – part 1

All together, we proofed that Prt, a chemically accessible tubulysin precursor, exhibits very potent anti-angiogenic effects despite considerable simplification in comparison to its more complex relative TubA (Fig. 1.3) *in vitro.* Most importantly, Prt diminishes cancer growth and perfusion *in vivo* at frequent application without the occurrence of severe side effects. Some of the analogues based on Prt still retain high anti-angiogenic efficacy, giving important insights in structure activity relationship.

5.3 Anti-angiogenic effects of v-ATPase inhibition – Role of VEGFR2 function

V-ATPases are evidently involved in numerous physiological, but similarly in pathological processes, making them an attractive target for the development of therapeutics [70, 74], with high expectations in the fields of cancer and osteoporosis [23, 52, 126].

In cancer research, particular interest was so far concentrated on the participation of v-ATPases in multi-drug resistance [127-130] and cancer metastasis [22, 23, 34, 131]. To our knowledge, only two publications exist, that describe the role of v-ATPases in a tumor angiogenesis relevant context. Rojas et al. found, that high v-ATPase levels at the plasma membrane (pm v-ATPases) increase endothelial cell migration [25], whereas non-migrating endothelial cells from a diabetic model show a clearly reduced pm v-ATPase expression [24].

However complex morphogenic events during angiogenesis such as capillary formation were not yet analyzed under influence of v-ATPase inhibition. Furthermore and most important, the impact of v-ATPase inhibition on angiogenesis signaling appears rather unelucidated. Therefore, we have used a specific v-ATPase inhibitor, concanamycin A (ConcmA) to test its anti-angiogenic effects on the cellular and the receptor level, focusing on the function and sub-cellular distribution of the most important pro-angiogenic receptor: VEGFR2.

5.3.1 Kinetics of morphological changes in endothelial cells in response to v-ATPase inhibition

One primary consequence of v-ATPase inhibition is the collapse of finely regulated pH gradients [74] in vesicular compartments along the secretory and endocytic pathway in eukaryotic cells [85]. This is often accompanied by morphological changes of the referred organelles [98, 99, 132]. We found that 3 nmolar of ConcmA were sufficient to increase lysosomal pH in HMEC-1 (Fig. 4.2) within four hours. Clear morphological changes, like the accumulation of enlarged vacuoles and increase of cell size, occur in

HUVEC at similarly low concentrations, however with a delay of approximately fifteen hours after lysosmoal alkalization (Fig. 4.3). HMEC-1 also change their morphology within this time frame, but to a less prominent extent, probably due to their smaller size (data not shown). The interval between effects on pH and vacuolar swelling was also demonstrated in a previous study [23], and seems to be shorter at 10 to 100 fold higher drug concentrations, inferred from studies that used a similarly active v-ATPase inhibitor, bafilomycin [52, 85, 99]. With the intention to use the lowest effective concentrations, we continued experiments with 1-10 nmolar ConcmA.

5.3.2 Influences of v-ATPase inhibition on endothelial cell proliferation and survival

Enhanced endothelial cell proliferation and survival are key hallmarks during the angiogenesis process [101, 133]. Thus we assessed the impact of v-ATPase blockade on these parameters. We found that ConcmA efficiently inhibits HMEC-1 endothelial cell proliferation at subnanomolar concentrations (Fig. 4.4), which does not come as a surprise, since v-ATPase inhibitors are known to be strong anti-proliferative agents [134]. The analysis of DNA content reveals an impaired cell cycle progression in HMEC-1 after 48 h (Fig. 4.5 B) in response to ConcmA. In parallel, increased nuclear fragmentation can be detected, indicating that cell death is additionally occurring[105]. Concerning kinetics, tubulin antagonists like TubA and Prt already show the onset of impaired cell cycle progression in endothelial cells after 24 h (Fig. 3.3 A). At this time point, no such effects can be seen with ConcmA (Fig 4.5 B), corroborating the impression of certain latency until cellular functions are inhibited by low nanomolar concentrations of v-ATPase inhibitors.

VEGF generates pleiotropic pro-angiogenic signaling via VEGFR2 [6, 36]. The serine and threonine kinases Akt and ERK1/2 are two main switch-points, that translate VEGFR2 activation into increased endothelial cell proliferation [135, 136] and survival [100, 101, 137] among other cell functions [36]. The VEGF induced activation of Akt in HMEC-1 starts to be impaired after 6 h incubation with ConcmA (Fig. 4.6 A), whereas ERK1/2 activation is unaffected at this time point (Fig 4.6 B). A pretreatment of 24 h with the inhibitor completely abolishes the effect of VEGF on Akt (Fig 4.6 C) and reduces ERK1/2 activation to the half level compared to control (Fig. 4.6 D). This is astonishing, as it demonstrates a different sensitivity of both kinase networks to the v-ATPase inhibitor. With respect to the high importance of v-ATPases in membrane trafficking [27], a different dependence on spatial distribution might be the cause for this disparity. Interestingly, in migrating SKBR3 breast cancer cells it was indeed shown, that Akt distribution and function both are impaired by v-ATPase inhibition, while EGF induced ERK1/2 activation was even increased (Romina M.Wiedmann, Dissertation LMU München, 2011).

5.3.3 Effects of v-ATPase inhibition on endothelial cell migration and differentiation functions

The role of v-ATPases in endothelial cell migration and invasion has been previously analyzed in two studies from the Martinez-Zaguilan group. Therein it was demonstrated, that enhanced expression of v-ATPases at the plasma membrane of the cellular leading edge (pm v-ATPases) increases endothelial cell migration and invasion, respectively [24, 25]. Similarly, it was reported, that microvascular endothelial cells are particularly sensitive to v-ATPase inhibition. This was constituted with increased expression of pm v-ATPases [25] in contrast to macrovascular cells.

Our model of microvascular cells, HMEC-1, expresses only marginally higher pm v-ATPase levels under migrating condition in comparison to the macrovascular HUVEC. In both cell lines, the vast majority of v-ATPases is distributed in intracellular vesicles (Fig. 4.1).

In a wound healing assay, we could not observe any inhibition of migration upon direct addition of v-ATPase antagonists, both in HMEC-1 and in HUVEC (S.Zahler, personal communication). This is in line with findings of Wiedmann and colleagues, who analyzed cancer cell migration under influence of low dosed archazolid B [23], a novel and very potent v-ATPase inhibitor from myxobacteria [78, 138].

However with 24 h pre-incubation and sustained treatment with ConcmA during the assay (16 h), efficient inhibition of wound healing can be obtained similarly in HMEC-1 and HUVEC (Fig. 4.7 A and B). With respect to cytotoxic events, it must be considered, that in the wound healing assay all cells, except for those adjacent to the wound, are in close intercellular contact. Hence, increased activity of the cell to cell connecting VE-cadherin [139] may decrease cytotoxic effects in response to ConcmA, as observed in HMEC-1 (Fig. 4.7 C). Astonishingly, HUVEC show a slight increase in cell death, indicating an endothelial cell specific sensitivity to ConcmA (Fig. 4.7 C). In order to estimate eventual off-target effects, we applied knockdown of the specific target of ConcmA [52], the v-ATPase subunit c (ATP6L), in HUVEC. Then, we performed a similar wound healing assay. Thereby we could confirm the importance of this v-ATPase element in endothelial cell migration. Importantly, in this setting no significant cytotoxic events occurred (Fig 4.8).

For the assessment of chemotactic endothelial cell migration, we tested HUVEC movement in a two dimensional FCS gradient [67, 91]. Here, ConcmA does not only inhibit cell orientation, but the general cellular motility (Fig. 4.9 B1), which stands in strong contrast to the fine disturbance of direction parameters by pretubulysin and tubulysin A (Fig. 3.6 B1). Furthermore, due to the prolonged presence of ConcmA (total of 40 h) and to the isolated cellular state in this assay, cytotoxity may substantially contribute to the overall effect (Fig. 4.9 B2).

From a mechanistic point of view, we were interested in important signaling molecules controlling the migration process. The essential role of the small Rho-GTPases Rac-1, Cdc42 and RhoA in cell migration and polarization is well defined [66, 140-142]. Rac-1 for instance contributes to cell motility by induction of protrusive sheet-like actin polymers (lamellipodia), which are clearly visible as 'ruffles' at the cell front. This activity can be either induced by cell-matrix interaction or growth factor stimulation[142]. We showed, that ConcmA pre-treatment in HMEC-1 and HUVEC significantly impairs the formation of ruffles upon cell-matrix adhesion (Fig. 4.10 C and 4.11 A), without prominent effects on adhesion *per se* (Fig 4.10 B). According to reduced lamellipodia formation, we could demonstrate an impaired Rac-1 activation under similar conditions (Fig. 4.11 B).

Besides adhesion and migration, Rac1 is required for even more complex morphogenic events like lumen formation [102, 140, 141]. Hence, we expected an inhibitory effect of prolonged v-ATPase inhibition on endothelial cell capillary formation. Interestingly, we found a cell line specific effect on this functional aspect. HUVEC show massive reduction of tube length and number of connection points (nodes) at 3 nmolar ConmA, while capillary formation of HMEC-1 appears to be even increased, though treated with tenfold higher concentration (Fig. 4.12). We further found, that the membrane surface in both cell lines looks remarkably 'blebby', when treated with ConcmA, which we interpreted as a sign of cell death [105]. Indeed, after prolonged ConcmA incubation (24h + 16h) HUVEC lose membrane integrity, as indicated by the uptake of a normally membrane impermeant fluorescent dye, propidium iodide. In comparison, HMEC-1 still possess membrane integrity (Fig. 4.13). Thus, inhibition of tube formation appears to be rather a secondary consequence of cell death than a subtle inhibition of differentiation as observed with low dosed tubulin antagonists.

5.3.4 Function and distribution of VEGFR2 in response to prolonged v-ATPase inhibition

V-ATPases are functionally integrated in the process of membrane trafficking [27, 72]. Thus, v-ATPase inhibition may alter trafficking of important signaling molecules, similarly to the inhibition of microtubule trafficking function[56, 64].

We hence hypothesized, that v-ATPase inhibition could alter VEGFR2 trafficking and signaling function as explanation for the observed cell functional effects.

As a primary result to support this idea, VEGF induced auto-activation of the receptor is decreased by 24 h treatment with low dosed ConcmA in HMEC-1 (Fig. 4.14 B). This suggests less sensitivity to the ligand, possibly due to reduced surface expression. Indeed under similar conditions, we could detect a decrease of surface receptor levels by 20-30%, both in HUVEC and HMEC-1 (Fig. 4.15).

In addition, the overall amount of intact VEGFR2 was clearly diminished (Fig. 4.14 C). At the same time, receptor fragments accumulated (Fig. 4.14 D-F). Recently, Bruns

and others [143] have described such VEGFR2 fragments as a result of VEGF induced limited proteolysis within endosomes. They had observed similar VEGFR2 fragment accumulations upon concomitant use of bafilomycin and VEGF stimulation[143], and have proposed a blockade in endosome to lysosome trafficking, and inactivation of lysosomal enzymes [143, 144].

In our experimental setup, we could detect intracellular vacuolar accumulations of VEGFR2 in HMEC-1 (Fig. 4.16). These vacuoles were identified as lysosomes (Fig. 4.18). Thus, we suggest that the endosomal lysosomal trafficking might not be blocked [144] but delayed by low nmolar concentrations of ConcmA.

Furthermore, we could exclude, that VEGFR2 accumulations are located in endocytic compartments characterized by markers for membranes (Caveolin) [110], internalization proteins (Clathrin) [145], or endosomes (Rab5) [146]. All together, this leads to the impression, that prolonged treatment with a v-ATPase inhibitor predominantly induces a one way route towards lysosomes with impaired recycling to the membrane. By alkalization, lysosomal enzymes are inactivated, which leads to a dose dependent accumulation of VEGFR2 fragments.

Our findings (impaired endothelial cell proliferation, survival and migration, combined with a decrease of VEGFR2 function and signaling, less surface expression and increased receptor degradation), are in close similarity to those of Mannell and coworkers[147]. They recently reported, that VEGFR2 trafficking and angiogenesis related cell functions can be effectively disturbed by application of an inhibitor of ARNO, which itself, together with Arf6, is an important interaction partner of v-ATPases. Hurtado-Lorenzo and others found, that the connection between Arf6, ARNO and v-ATPases is subtly controlled by pH [148, 149]. This strikingly suggests, that v-ATPase inhibition impairs the fine regulated interaction of v-ATPases with ARNO and Arf6, and thus disorganizes the membrane trafficking function.

5.3.5 Conclusion – part 2

Rojas and colleagues correlated over-expression of plasma membrane v-ATPases with highly active endothelial cell migration and invasion [24, 25], hence important angiogenesis related functions. They further demonstrated that microvascular endothelial cells, which express high levels of pm v-ATPases react particularly sensitive to v-ATPase inhibition, in contrast to macrovascular endothelial cells[25].

In our work we could show, that both macro- and microvascular endothelial cells (HUVEC and HMEC-1, respectively) exhibit impaired angiogenesis related cell functions, in connection with decreased VEGFR2 function and distribution, putatively as a consequence of disorganized membrane trafficking in response to v-ATPase inhibition.

To our knowledge, this connection is presented for the first time and displays a novel explanation for anti-angiogenic effects in response to v-ATPase inhibition.

5.4 Outlook

The high anti-cancer [19] and anti-angiogenic [20] potential of pretubulysin *in vitro* and *in vivo,* together with its reliable supply, should lead to further investigations in pre-clinical and potentially clinical studies. Furthermore, its less complex structure in comparison to tubulysins makes it suitable for chemical modification in the sense of developing new analogues [16], which can serve in improving the understanding of 'drug target biology' [60], and of signaling influences. A further possible application could be the design of smart delivery systems, as demonstrated for tubulysin A [51].

V-ATPase research is still quite young, with respect to the discovery of the first specific antagonist, i.e. pharmacological tool, bafilomycin in 1984[75]. If one thinks of the multiple functions of v-ATPases that have been elucidated until today [72, 148, 150, 151], it appears that effects of v-ATPase inhibition could be pleiotropic or even completely chaotic. But this impression can also arise for the approach of tubulin antagonism [56, 64, 67, 152-154], which is clinically established since decades[45]. Thus, understanding of signaling will be one important key to further development and potentially to the clinical application of v-ATPase antagonists.

In the field of tumor angiogenesis only few publications about the role v-ATPase antagonism exist [24, 25]. We could show an important role of v-ATPase activity for the distribution and function of VEGFR2. To discriminate, whether differential effects occur upon v-ATPase inhibition, one should investigate further receptors with importance in angiogenesis. Notch activation for instance is known to depend on v-ATPase function [155, 156]. In contrast, the relationship between v-ATPases and other important pro-angiogenic signaling systems, like for example Ang1 and Ang2/Tie2 and FGF/FGFRs, appears rather unelucidated.

Besides promising *in vitro* results, it could be recently demonstrated, that v-ATPase inhibitors exhibit also considerable anti-tumor effects *in vivo* [23, 157]. Archazolid B was shown to reduce the tumor metastasis in a syngeneic breast cancer model [23]. Further tests with archazolid in a xenograft model of herceptin resistant breast cancer cells, referred to as JIMT-1 [158], resulted in clearly reduced tumor growth (personal communication, K. v. Schwarzenberg). But the level of tumor vascularization, in terms of vascular structure and density, still needs to be histologically analyzed, to determine whether anti-angiogenic effects might have contributed to the anti-tumor effect.

Thus, many findings about v-ATPases as target for anti-angiogenic approaches are promising, but the potential and the involved signaling mechanisms, such as inhibition of VEGFR2, still need to be further investigated.

6 Summary

6.1 Part 1: Anti-angiogenic potential of the tubulysin precursor pretubulysin and its analogues

Tubulysins are highly potent tubulin binding agents of myxobacterial origin. Tubulysin A was recently evaluated as a very potent anti-angiogenic agent. Its supply however is inefficient due to low biosynthesis rate and challenging chemical synthesis, respectively. A structurally simplified tubulysin precursor, pretubulysin, is efficiently available and modifiable via total chemical synthesis.

We tested the anti-angiogenic effects of this compound and seven of its analogues *in vitro* and could demonstrate that pretubulysin shows nearly similar efficacy (EC_{50} in the low nmolar range in cellular angiogenesis assays) as tubulysin A. The seven pretubulysin analogues possess various structural modifications, and showed moderate (EC_{50} about 100nmolar) or dramatic loss of activity (EC_{50} about 10µmolar), giving important insights in structure activity relationships.

In vivo, pretubulysin blocked tumor growth of hepatocellular carcinoma xenografts in SCID mice and reduced tumor vessel density by 70%. Pretubulysin has the advantage towards tubulysin A to be efficiently available via chemical synthesis and is thus a highly attractive anti-angiogenic alternative with very high potency *in vitro* and *in vivo*.

6.2 Part 2: Characterization of anti-angiogenic effects of the v-ATPase inhibitor concanamycin A, with emphasis on VEGFR2 function

In the second part of the present work, we analyzed inhibitory effects of prolonged (24h – 40 h) and low dosed (1-10nmolar) application of a specific v-ATPase inhibitor (concanamycin A) on angiogenesis related cellular functions in HUVEC and HMEC-1 endothelial cells. We found, that the treatment predominantly affected endothelial cell proliferation, survival and migration. Astonishingly, *in vitro* capillary formation appears only to be indirectly inhibited in HUVEC, but not in HMEC-1, as a consequence of cytotoxicity. We analyzed the signaling function of the most important pro-angiogenic growth factor and its receptor (VEGF A/VEGFR2) in endothelial cells upon v-ATPase inhibition, and found a decreased activation of key signaling markers (Akt, ERK1/2 and VEGFR2). In addition, VEGFR2 sub-cellular localization was significantly changed, with decreased levels at the cell surface and increased levels in large intracellular compartments that were identified as lysosomes. Furthermore, v-ATPase inhibition was found to increase VEGF induced receptor degradation.

Thus, we propose decreased VEGFR2 function and maintenance, putatively caused by disturbed receptor trafficking, as a novel explanation for anti-angiogenic effects, observed after v-ATPase inhibition.

7 References

1. Folkman, J. Tumor angiogenesis: therapeutic implications. *The New England journal of medicine* **285**, 1182-6 (1971).
2. Ferrara, N. & Kerbel, R.S. Angiogenesis as a therapeutic target. *Nature* **438**, 967-74 (2005).
3. Kerbel, R.S. Tumor angiogenesis. *The New England journal of medicine* **358**, 2039-49 (2008).
4. Eikesdal, H.P. & Kalluri, R. Drug resistance associated with antiangiogenesis therapy. *Semin Cancer Biol* **19**, 310-7 (2009).
5. Li, J.L. et al. DLL4-Notch signaling mediates tumor resistance to anti-VEGF therapy in vivo. *Cancer Res* **71**, 6073-83 (2011).
6. Shibuya, M. Vascular endothelial growth factor-dependent and -independent regulation of angiogenesis. *BMB Rep* **41**, 278-86 (2008).
7. Gossage, L. & Eisen, T. Targeting multiple kinase pathways: a change in paradigm. *Clinical cancer research : an official journal of the American Association for Cancer Research* **16**, 1973-8 (2010).
8. Kerbel, R.S. & Kamen, B.A. The anti-angiogenic basis of metronomic chemotherapy. *Nat Rev Cancer* **4**, 423-36 (2004).
9. Hanahan, D., Bergers, G. & Bergsland, E. Less is more, regularly: metronomic dosing of cytotoxic drugs can target tumor angiogenesis in mice. *J Clin Invest* **105**, 1045-7 (2000).
10. Pasquier, E. et al. Moving forward with metronomic chemotherapy: meeting report of the 2nd International Workshop on Metronomic and Anti-Angiogenic Chemotherapy in Paediatric Oncology. *Transl Oncol* **4**, 203-11 (2011).
11. Sasse, F., Steinmetz, H., Heil, J., Hofle, G. & Reichenbach, H. Tubulysins, new cytostatic peptides from myxobacteria acting on microtubuli. Production, isolation, physico-chemical and biological properties. *J Antibiot (Tokyo)* **53**, 879-85 (2000).
12. Khalil, M.W., Sasse, F., Lunsdorf, H., Elnakady, Y.A. & Reichenbach, H. Mechanism of action of tubulysin, an antimitotic peptide from myxobacteria. *Chembiochem* **7**, 678-83 (2006).
13. Kaur, G. et al. Biological evaluation of tubulysin A: a potential anticancer and antiangiogenic natural product. *Biochem J* **396**, 235-42 (2006).
14. Wenzel, S.C. et al. Heterologous expression of a myxobacterial natural products assembly line in pseudomonads via red/ET recombineering. *Chem Biol* **12**, 349-56 (2005).
15. Ullrich, A., Herrmann, J., Müller, R. & Kazmaier, U. Synthesis and Biological Evaluation of Pretubulysin and Derivatives. *European Journal of Organic Chemistry* **2009**, 6367-6378 (2009).
16. Burkhart, J.L., Müller, R. & Kazmaier, U. Syntheses and Evaluation of Simplified Pretubulysin Analogues. *European Journal of Organic Chemistry* **2011**, 3050-3059 (2011).
17. Raghavan, B., Balasubramanian, R., Steele, J.C., Sackett, D.L. & Fecik, R.A. Cytotoxic simplified tubulysin analogues. *Journal of medicinal chemistry* **51**, 1530-3 (2008).

18. Ullrich, A. et al. Pretubulysin, a potent and chemically accessible tubulysin precursor from Angiococcus disciformis. *Angew Chem Int Ed Engl* **48**, 4422-5 (2009).
19. Herrmann, J. et al. Pretubulysin: from hypothetical biosynthetic intermediate to potential lead in tumor therapy. *PloS one* **7**, e37416 (2012).
20. Rath, S. et al. Anti-angiogenic effects of the tubulysin precursor pretubulysin and of simplified pretubulysinerivatives. *Br J Pharmacol* (2012).
21. Perez-Sayans, M., Somoza-Martin, J.M., Barros-Angueira, F., Rey, J.M. & Garcia-Garcia, A. V-ATPase inhibitors and implication in cancer treatment. *Cancer Treat Rev* **35**, 707-13 (2009).
22. Sennoune, S.R., Luo, D. & Martinez-Zaguilan, R. Plasmalemmal vacuolar-type H+-ATPase in cancer biology. *Cell Biochem Biophys* **40**, 185-206 (2004).
23. Wiedmann, R.M. et al. The V-ATPase-inhibitor Archazolid abrogates tumor metastasis via inhibition of endocytic activation of the Rho-GTPase Rac1. *Cancer Res* (2012).
24. Rojas, J.D. et al. Plasmalemmal vacuolar H+-ATPase is decreased in microvascular endothelial cells from a diabetic model. *J Cell Physiol* **201**, 190-200 (2004).
25. Rojas, J.D. et al. Vacuolar-type H+-ATPases at the plasma membrane regulate pH and cell migration in microvascular endothelial cells. *Am J Physiol Heart Circ Physiol* **291**, H1147-57 (2006).
26. Mellman, I. The importance of being acid: the role of acidification in intracellular membrane traffic. *J Exp Biol* **172**, 39-45 (1992).
27. Marshansky, V. & Futai, M. The V-type H+-ATPase in vesicular trafficking: targeting, regulation and function. *Curr Opin Cell Biol* **20**, 415-26 (2008).
28. Scott, A. & Mellor, H. VEGF receptor trafficking in angiogenesis. *Biochem Soc Trans* **37**, 1184-8 (2009).
29. Chung, A.S., Lee, J. & Ferrara, N. Targeting the tumour vasculature: insights from physiological angiogenesis. *Nat Rev Cancer* **10**, 505-14 (2010).
30. Jain, R.K. & Carmeliet, P. SnapShot: Tumor angiogenesis. *Cell* **149**, 1408-1408 e1 (2012).
31. Hanahan, D. & Weinberg, R.A. Hallmarks of cancer: the next generation. *Cell* **144**, 646-74 (2011).
32. Potente, M., Gerhardt, H. & Carmeliet, P. Basic and therapeutic aspects of angiogenesis. *Cell* **146**, 873-87 (2011).
33. Bergers, G. et al. Matrix metalloproteinase-9 triggers the angiogenic switch during carcinogenesis. *Nat Cell Biol* **2**, 737-44 (2000).
34. Chung, C. et al. The vacuolar-ATPase modulates matrix metalloproteinase isoforms in human pancreatic cancer. *Lab Invest* **91**, 732-43 (2011).
35. Shibuya, M. & Claesson-Welsh, L. Signal transduction by VEGF receptors in regulation of angiogenesis and lymphangiogenesis. *Experimental cell research* **312**, 549-60 (2006).

36. Olsson, A.K., Dimberg, A., Kreuger, J. & Claesson-Welsh, L. VEGF receptor signalling - in control of vascular function. *Nat Rev Mol Cell Biol* **7**, 359-71 (2006).
37. Shibuya, M., Ito, N. & Claesson-Welsh, L. Structure and function of vascular endothelial growth factor receptor-1 and -2. *Current topics in microbiology and immunology* **237**, 59-83 (1999).
38. Ferrara, N., Hillan, K.J., Gerber, H.P. & Novotny, W. Discovery and development of bevacizumab, an anti-VEGF antibody for treating cancer. *Nat Rev Drug Discov* **3**, 391-400 (2004).
39. Hurwitz, H. et al. Bevacizumab plus irinotecan, fluorouracil, and leucovorin for metastatic colorectal cancer. *The New England journal of medicine* **350**, 2335-42 (2004).
40. Sandler, A. et al. Paclitaxel-carboplatin alone or with bevacizumab for non-small-cell lung cancer. *The New England journal of medicine* **355**, 2542-50 (2006).
41. Sakurai, T. & Kudo, M. Signaling pathways governing tumor angiogenesis. *Oncology* **81 Suppl 1**, 24-9 (2011).
42. Klement, G. et al. Continuous low-dose therapy with vinblastine and VEGF receptor-2 antibody induces sustained tumor regression without overt toxicity. *J Clin Invest* **105**, R15-24 (2000).
43. Browder, T. et al. Antiangiogenic scheduling of chemotherapy improves efficacy against experimental drug-resistant cancer. *Cancer Res* **60**, 1878-86 (2000).
44. Noguera-Troise, I. et al. Blockade of Dll4 inhibits tumour growth by promoting non-productive angiogenesis. *Nature* **444**, 1032-7 (2006).
45. Dumontet, C. & Jordan, M.A. Microtubule-binding agents: a dynamic field of cancer therapeutics. *Nat Rev Drug Discov* **9**, 790-803 (2010).
46. Schwartz, E.L. Antivascular actions of microtubule-binding drugs. *Clinical cancer research : an official journal of the American Association for Cancer Research* **15**, 2594-601 (2009).
47. Newman, D.J. & Cragg, G.M. Microbial antitumor drugs: natural products of microbial origin as anticancer agents. *Curr Opin Investig Drugs* **10**, 1280-96 (2009).
48. Reichenbach, H. & Hofle, G. Biologically active secondary metabolites from myxobacteria. *Biotechnol Adv* **11**, 219-77 (1993).
49. Weissman, K.J. & Muller, R. Myxobacterial secondary metabolites: bioactivities and modes-of-action. *Nat Prod Rep* **27**, 1276-95 (2010).
50. Steinmetz, H. et al. Isolation, crystal and solution structure determination, and biosynthesis of tubulysins--powerful inhibitors of tubulin polymerization from myxobacteria. *Angew Chem Int Ed Engl* **43**, 4888-92 (2004).
51. Schluep, T. et al. Polymeric tubulysin-peptide nanoparticles with potent antitumor activity. *Clinical cancer research : an official journal of the American Association for Cancer Research* **15**, 181-9 (2009).
52. Huss, M. et al. Concanamycin A, the specific inhibitor of V-ATPases, binds to the V(o) subunit c. *The Journal of biological chemistry* **277**, 40544-8 (2002).

53. Drose, S. et al. Inhibitory effect of modified bafilomycins and concanamycins on P- and V-type adenosinetriphosphatases. *Biochemistry* **32**, 3902-6 (1993).
54. Kinashi, H., Someno, K. & Sakaguchi, K. Isolation and characterization of concanamycins A, B and C. *J Antibiot (Tokyo)* **37**, 1333-43 (1984).
55. Bayless, K.J. & Johnson, G.A. Role of the cytoskeleton in formation and maintenance of angiogenic sprouts. *Journal of Vascular Research* **48**, 369-85 (2011).
56. Lomakin, A.Y. & Nadezhdina, E.S. Dynamics of nonmembranous cell components: role of active transport along microtubules. *Biochemistry (Mosc)* **75**, 7-18 (2010).
57. Inoue, S. Cell division and the mitotic spindle. *The Journal of cell biology* **91**, 131s-147s (1981).
58. Staton, C.A. et al. Current methods for assaying angiogenesis in vitro and in vivo. *Int J Exp Pathol* **85**, 233-48 (2004).
59. Kubicek, K., Grimm, S.K., Orts, J., Sasse, F. & Carlomagno, T. The tubulin-bound structure of the antimitotic drug tubulysin. *Angew Chem Int Ed Engl* **49**, 4809-12 (2010).
60. Eirich, J. et al. Pretubulysinerived probes as novel tools for monitoring the microtubule network via activity-based protein profiling and fluorescence microscopy. *Mol Biosyst* **8**, 2067-75 (2012).
61. Egerton, N. Ixabepilone (ixempra), a therapeutic option for locally advanced or metastatic breast cancer. *P T* **33**, 523-31 (2008).
62. Jordan, M.A. & Wilson, L. Microtubules as a target for anticancer drugs. *Nat Rev Cancer* **4**, 253-65 (2004).
63. Pasquier, E. et al. Antiangiogenic concentrations of paclitaxel induce an increase in microtubule dynamics in endothelial cells but not in cancer cells. *Cancer Res* **65**, 2433-40 (2005).
64. Watanabe, T., Noritake, J. & Kaibuchi, K. Regulation of microtubules in cell migration. *Trends in cell biology* **15**, 76-83 (2005).
65. Bayless, K.J. & Davis, G.E. Microtubule depolymerization rapidly collapses capillary tube networks in vitro and angiogenic vessels in vivo through the small GTPase Rho. *The Journal of biological chemistry* **279**, 11686-95 (2004).
66. Fryer, B.H. & Field, J. Rho, Rac, Pak and angiogenesis: old roles and newly identified responsibilities in endothelial cells. *Cancer Lett* **229**, 13-23 (2005).
67. Rothmeier, A.S. et al. Investigation of the marine compound spongistatin 1 links the inhibition of PKCalpha translocation to nonmitotic effects of tubulin antagonism in angiogenesis. *FASEB J* **23**, 1127-37 (2009).
68. Vacca, A. et al. Antiangiogenesis is produced by nontoxic doses of vinblastine. *Blood* **94**, 4143-55 (1999).
69. Hotchkiss, K.A. et al. Inhibition of endothelial cell function in vitro and angiogenesis in vivo by docetaxel (Taxotere): association with impaired repositioning of the microtubule organizing centre. *Mol Cancer Ther* **1**, 1191-200 (2002).
70. Hinton, A., Bond, S. & Forgac, M. V-ATPase functions in normal and disease processes. *Pflugers Arch* **457**, 589-98 (2009).

71. Wada, Y., Sun-Wada, G.H., Tabata, H. & Kawamura, N. Vacuolar-type proton ATPase as regulator of membrane dynamics in multicellular organisms. *J Bioenerg Biomembr* **40**, 53-7 (2008).
72. Forgac, M. Vacuolar ATPases: rotary proton pumps in physiology and pathophysiology. *Nat Rev Mol Cell Biol* **8**, 917-29 (2007).
73. Li, Y.P., Chen, W., Liang, Y., Li, E. & Stashenko, P. Atp6i-deficient mice exhibit severe osteopetrosis due to loss of osteoclast-mediated extracellular acidification. *Nat Genet* **23**, 447-51 (1999).
74. Huss, M. & Wieczorek, H. Inhibitors of V-ATPases: old and new players. *J Exp Biol* **212**, 341-6 (2009).
75. Werner, G., Hagenmaier, H., Drautz, H., Baumgartner, A. & Zahner, H. Metabolic products of microorganisms. 224. Bafilomycins, a new group of macrolide antibiotics. Production, isolation, chemical structure and biological activity. *J Antibiot (Tokyo)* **37**, 110-7 (1984).
76. Erickson, K.L., Beutler, J.A., Cardellina, I.J. & Boyd, M.R. Salicylihalamides A and B, Novel Cytotoxic Macrolides from the Marine Sponge Haliclona sp. *J Org Chem* **62**, 8188-8192 (1997).
77. Kunze, B., Jansen, R., Sasse, F., Hofle, G. & Reichenbach, H. Apicularens A and B, new cytostatic macrolides from Chondromyces species (myxobacteria): production, physico-chemical and biological properties. *J Antibiot (Tokyo)* **51**, 1075-80 (1998).
78. Sasse, F., Steinmetz, H., Hofle, G. & Reichenbach, H. Archazolids, new cytotoxic macrolactones from Archangium gephyra (Myxobacteria). Production, isolation, physico-chemical and biological properties. *J Antibiot (Tokyo)* **56**, 520-5 (2003).
79. Gagliardi, S. et al. Synthesis and structure-activity relationships of bafilomycin A1 derivatives as inhibitors of vacuolar H+-ATPase. *Journal of medicinal chemistry* **41**, 1883-93 (1998).
80. Bockelmann, S. et al. Archazolid A binds to the equatorial region of the c-ring of the vacuolar H+-ATPase. *The Journal of biological chemistry* **285**, 38304-14 (2010).
81. Osteresch, C. et al. The binding site of the V-ATPase inhibitor apicularen is in the vicinity to those of bafilomycin and archazolid. *The Journal of biological chemistry* (2012).
82. Bowman, E.J., Graham, L.A., Stevens, T.H. & Bowman, B.J. The bafilomycin/concanamycin binding site in subunit c of the V-ATPases from Neurospora crassa and Saccharomyces cerevisiae. *The Journal of biological chemistry* **279**, 33131-8 (2004).
83. Wang, Y., Inoue, T. & Forgac, M. Subunit a of the yeast V-ATPase participates in binding of bafilomycin. *The Journal of biological chemistry* **280**, 40481-8 (2005).
84. Neri, D. & Supuran, C.T. Interfering with pH regulation in tumours as a therapeutic strategy. *Nat Rev Drug Discov* **10**, 767-77 (2011).
85. Schoonderwoert, V.T., Holthuis, J.C., Tanaka, S., Tooze, S.A. & Martens, G.J. Inhibition of the vacuolar H+-ATPase perturbs the transport, sorting, processing and release of regulated secretory proteins. *Eur J Biochem* **267**, 5646-54 (2000).

86. Palamidessi, A. et al. Endocytic trafficking of Rac is required for the spatial restriction of signaling in cell migration. *Cell* **134**, 135-47 (2008).
87. Gampel, A. et al. VEGF regulates the mobilization of VEGFR2/KDR from an intracellular endothelial storage compartment. *Blood* **108**, 2624-31 (2006).
88. Jopling, H.M., Howell, G.J., Gamper, N. & Ponnambalam, S. The VEGFR2 receptor tyrosine kinase undergoes constitutive endosome-to-plasma membrane recycling. *Biochem Biophys Res Commun* **410**, 170-6 (2011).
89. Sorkin, A. & Goh, L.K. Endocytosis and intracellular trafficking of ErbBs. *Experimental cell research* **315**, 683-96 (2009).
90. Ades, E.W. et al. HMEC-1: establishment of an immortalized human microvascular endothelial cell line. *J Invest Dermatol* **99**, 683-90 (1992).
91. Liebl, J. et al. Cyclin-dependent kinase 5 regulates endothelial cell migration and angiogenesis. *The Journal of biological chemistry* **285**, 35932-43 (2010).
92. Gaskin, F., Cantor, C.R. & Shelanski, M.L. Turbidimetric studies of the in vitro assembly and disassembly of porcine neurotubules. *Journal of molecular biology* **89**, 737-55 (1974).
93. Nicoletti, I., Migliorati, G., Pagliacci, M.C., Grignani, F. & Riccardi, C. A rapid and simple method for measuring thymocyte apoptosis by propidium iodide staining and flow cytometry. *J Immunol Methods* **139**, 271-9 (1991).
94. Bradford, M.M. A rapid and sensitive method for the quantitation of microgram quantities of protein utilizing the principle of protein-dye binding. *Anal Biochem* **72**, 248-54 (1976).
95. Laemmli, U.K. Cleavage of structural proteins during the assembly of the head of bacteriophage T4. *Nature* **227**, 680-5 (1970).
96. Pfaffl, M.W. A new mathematical model for relative quantification in real-time RT-PCR. *Nucleic Acids Res* **29**, e45 (2001).
97. Jordan, M.A. Mechanism of action of antitumor drugs that interact with microtubules and tubulin. *Curr Med Chem Anticancer Agents* **2**, 1-17 (2002).
98. Bowman, E.J., Kendle, R. & Bowman, B.J. Disruption of vma-1, the gene encoding the catalytic subunit of the vacuolar H(+)-ATPase, causes severe morphological changes in Neurospora crassa. *The Journal of biological chemistry* **275**, 167-76 (2000).
99. Robinson, D.G., Albrecht, S. & Moriysu, Y. The V-ATPase inhibitors concanamycin A and bafilomycin A lead to Golgi swelling in tobacco BY-2 cells. *Protoplasma* **224**, 255-60 (2004).
100. Gupta, K. et al. VEGF prevents apoptosis of human microvascular endothelial cells via opposing effects on MAPK/ERK and SAPK/JNK signaling. *Experimental cell research* **247**, 495-504 (1999).
101. Liu, W. et al. Endothelial cell survival and apoptosis in the tumor vasculature. *Apoptosis* **5**, 323-8 (2000).
102. Davis, G.E., Koh, W. & Stratman, A.N. Mechanisms controlling human endothelial lumen formation and tube assembly in three-dimensional

extracellular matrices. *Birth Defects Res C Embryo Today* **81**, 270-85 (2007).
103. Bayless, K.J. & Davis, G.E. The Cdc42 and Rac1 GTPases are required for capillary lumen formation in three-dimensional extracellular matrices. *Journal of cell science* **115**, 1123-36 (2002).
104. Machesky, L.M. & Hall, A. Role of actin polymerization and adhesion to extracellular matrix in Rac- and Rho-induced cytoskeletal reorganization. *The Journal of cell biology* **138**, 913-26 (1997).
105. Vermes, I., Haanen, C. & Reutelingsperger, C. Flow cytometry of apoptotic cell death. *J Immunol Methods* **243**, 167-90 (2000).
106. Tammela, T., Enholm, B., Alitalo, K. & Paavonen, K. The biology of vascular endothelial growth factors. *Cardiovascular research* **65**, 550-63 (2005).
107. Zachary, I. VEGF signalling: integration and multi-tasking in endothelial cell biology. *Biochem Soc Trans* **31**, 1171-7 (2003).
108. Calera, M.R., Venkatakrishnan, A. & Kazlauskas, A. VE-cadherin increases the half-life of VEGF receptor 2. *Experimental cell research* **300**, 248-56 (2004).
109. Lampugnani, M.G., Orsenigo, F., Gagliani, M.C., Tacchetti, C. & Dejana, E. Vascular endothelial cadherin controls VEGFR-2 internalization and signaling from intracellular compartments. *The Journal of cell biology* **174**, 593-604 (2006).
110. Labrecque, L. et al. Regulation of vascular endothelial growth factor receptor-2 activity by caveolin-1 and plasma membrane cholesterol. *Molecular biology of the cell* **14**, 334-47 (2003).
111. Clague, M.J. & Urbe, S. The interface of receptor trafficking and signalling. *Journal of cell science* **114**, 3075-81 (2001).
112. Vieira, A.V., Lamaze, C. & Schmid, S.L. Control of EGF receptor signaling by clathrin-mediated endocytosis. *Science* **274**, 2086-9 (1996).
113. Folkman, J. Angiogenesis: an organizing principle for drug discovery? *Nat Rev Drug Discov* **6**, 273-86 (2007).
114. Bergers, G. & Hanahan, D. Modes of resistance to anti-angiogenic therapy. *Nat Rev Cancer* **8**, 592-603 (2008).
115. Kamat, A.A. et al. Metronomic chemotherapy enhances the efficacy of antivascular therapy in ovarian cancer. *Cancer Res* **67**, 281-8 (2007).
116. Dutour, A. & Rigaud, M. Tumor endothelial cells are targets for selective therapies: in vitro and in vivo models to evaluate antiangiogenic strategies. *Anticancer research* **25**, 3799-807 (2005).
117. Bijman, M.N., van Nieuw Amerongen, G.P., Laurens, N., van Hinsbergh, V.W. & Boven, E. Microtubule-targeting agents inhibit angiogenesis at subtoxic concentrations, a process associated with inhibition of Rac1 and Cdc42 activity and changes in the endothelial cytoskeleton. *Mol Cancer Ther* **5**, 2348-57 (2006).
118. Morris, P.G. & Fornier, M.N. Microtubule active agents: beyond the taxane frontier. *Clinical cancer research : an official journal of the American Association for Cancer Research* **14**, 7167-72 (2008).
119. Kingston, D.G. Tubulin-interactive natural products as anticancer agents. *J Nat Prod* **72**, 507-15 (2009).

120. Skropeta, D. Deep-sea natural products. *Nat Prod Rep* **25**, 1131-66 (2008).
121. Kavallaris, M. Microtubules and resistance to tubulin-binding agents. *Nat Rev Cancer* **10**, 194-204 (2010).
122. Wang, J., Lou, P., Lesniewski, R. & Henkin, J. Paclitaxel at ultra low concentrations inhibits angiogenesis without affecting cellular microtubule assembly. *Anticancer Drugs* **14**, 13-9 (2003).
123. Pourroy, B. et al. Antiangiogenic concentrations of vinflunine increase the interphase microtubule dynamics and decrease the motility of endothelial cells. *Cancer Res* **66**, 3256-63 (2006).
124. Ueda, M., Graf, R., MacWilliams, H.K., Schliwa, M. & Euteneuer, U. Centrosome positioning and directionality of cell movements. *Proc Natl Acad Sci U S A* **94**, 9674-8 (1997).
125. Tanaka, S. & Arii, S. Molecular targeted therapies in hepatocellular carcinoma. *Semin Oncol* **39**, 486-92 (2012).
126. Niikura, K., Takano, M. & Sawada, M. A novel inhibitor of vacuolar ATPase, FR167356, which can discriminate between osteoclast vacuolar ATPase and lysosomal vacuolar ATPase. *Br J Pharmacol* **142**, 558-66 (2004).
127. Perez-Sayans, M. et al. Multidrug resistance in oral squamous cell carcinoma: The role of vacuolar ATPases. *Cancer Lett* **295**, 135-43 (2010).
128. Torigoe, T. et al. Enhanced expression of the human vacuolar H+-ATPase c subunit gene (ATP6L) in response to anticancer agents. *The Journal of biological chemistry* **277**, 36534-43 (2002).
129. Murakami, T. et al. Elevated expression of vacuolar proton pump genes and cellular PH in cisplatin resistance. *International journal of cancer Journal international du cancer* **93**, 869-74 (2001).
130. De Milito, A. & Fais, S. Proton pump inhibitors may reduce tumour resistance. *Expert Opin Pharmacother* **6**, 1049-54 (2005).
131. Lu, X. et al. The growth and metastasis of human hepatocellular carcinoma xenografts are inhibited by small interfering RNA targeting to the subunit ATP6L of proton pump. *Cancer Res* **65**, 6843-9 (2005).
132. Sun-Wada, G.H., Wada, Y. & Futai, M. Vacuolar H+ pumping ATPases in luminal acidic organelles and extracellular compartments: common rotational mechanism and diverse physiological roles. *J Bioenerg Biomembr* **35**, 347-58 (2003).
133. Carmeliet, P. & Jain, R.K. Molecular mechanisms and clinical applications of angiogenesis. *Nature* **473**, 298-307 (2011).
134. Manabe, T., Yoshimori, T., Henomatsu, N. & Tashiro, Y. Inhibitors of vacuolar-type H(+)-ATPase suppresses proliferation of cultured cells. *J Cell Physiol* **157**, 445-52 (1993).
135. Shiojima, I. & Walsh, K. Role of Akt signaling in vascular homeostasis and angiogenesis. *Circ Res* **90**, 1243-50 (2002).
136. Wu, L.W. et al. Utilization of distinct signaling pathways by receptors for vascular endothelial cell growth factor and other mitogens in the induction of endothelial cell proliferation. *The Journal of biological chemistry* **275**, 5096-103 (2000).

137. Gerber, H.P. et al. Vascular endothelial growth factor regulates endothelial cell survival through the phosphatidylinositol 3'-kinase/Akt signal transduction pathway. Requirement for Flk-1/KDR activation. *The Journal of biological chemistry* **273**, 30336-43 (1998).
138. Roethle, P.A., Chen, I.T. & Trauner, D. Total synthesis of (-)-archazolid B. *J Am Chem Soc* **129**, 8960-1 (2007).
139. Carmeliet, P. & Collen, D. Molecular basis of angiogenesis. Role of VEGF and VE-cadherin. *Ann N Y Acad Sci* **902**, 249-62; discussion 262-4 (2000).
140. Connolly, J.O., Simpson, N., Hewlett, L. & Hall, A. Rac regulates endothelial morphogenesis and capillary assembly. *Molecular biology of the cell* **13**, 2474-85 (2002).
141. Liu, K.D. et al. Rac1 is required for reorientation of polarity and lumen formation through a PI 3-kinase-dependent pathway. *Am J Physiol Renal Physiol* **293**, F1633-40 (2007).
142. Ridley, A.J. Rho family proteins: coordinating cell responses. *Trends in cell biology* **11**, 471-7 (2001).
143. Bruns, A.F., Bao, L., Walker, J.H. & Ponnambalam, S. VEGF-A-stimulated signalling in endothelial cells via a dual receptor tyrosine kinase system is dependent on co-ordinated trafficking and proteolysis. *Biochem Soc Trans* **37**, 1193-7 (2009).
144. van Weert, A.W., Dunn, K.W., Geuze, H.J., Maxfield, F.R. & Stoorvogel, W. Transport from late endosomes to lysosomes, but not sorting of integral membrane proteins in endosomes, depends on the vacuolar proton pump. *The Journal of cell biology* **130**, 821-34 (1995).
145. Mukherjee, S., Tessema, M. & Wandinger-Ness, A. Vesicular trafficking of tyrosine kinase receptors and associated proteins in the regulation of signaling and vascular function. *Circ Res* **98**, 743-56 (2006).
146. Jopling, H.M. et al. Rab GTPase regulation of VEGFR2 trafficking and signaling in endothelial cells. *Arterioscler Thromb Vasc Biol* **29**, 1119-24 (2009).
147. Mannell, H.K. et al. ARNO regulates VEGF-dependent tissue responses by stabilizing endothelial VEGFR-2 surface expression. *Cardiovascular research* **93**, 111-9 (2012).
148. Hurtado-Lorenzo, A. et al. V-ATPase interacts with ARNO and Arf6 in early endosomes and regulates the protein degradative pathway. *Nat Cell Biol* **8**, 124-36 (2006).
149. Maranda, B. et al. Intra-endosomal pH-sensitive recruitment of the Arf-nucleotide exchange factor ARNO and Arf6 from cytoplasm to proximal tubule endosomes. *The Journal of biological chemistry* **276**, 18540-50 (2001).
150. Strasser, B., Iwaszkiewicz, J., Michielin, O. & Mayer, A. The V-ATPase proteolipid cylinder promotes the lipid-mixing stage of SNARE-dependent fusion of yeast vacuoles. *The EMBO journal* **30**, 4126-41 (2011).
151. Nishi, T. & Forgac, M. The vacuolar (H+)-ATPases--nature's most versatile proton pumps. *Nat Rev Mol Cell Biol* **3**, 94-103 (2002).

152. Carbonaro, M., O'Brate, A. & Giannakakou, P. Microtubule disruption targets HIF-1alpha mRNA to cytoplasmic P-bodies for translational repression. *The Journal of cell biology* **192**, 83-99 (2011).
153. Meissner, M. et al. Microtubule-targeted drugs inhibit VEGF receptor-2 expression by both transcriptional and post-transcriptional mechanisms. *J Invest Dermatol* **128**, 2084-91 (2008).
154. Pasquier, E. & Kavallaris, M. Microtubules: a dynamic target in cancer therapy. *IUBMB Life* **60**, 165-70 (2008).
155. Vaccari, T., Duchi, S., Cortese, K., Tacchetti, C. & Bilder, D. The vacuolar ATPase is required for physiological as well as pathological activation of the Notch receptor. *Development* **137**, 1825-32 (2010).
156. Yan, Y., Denef, N. & Schupbach, T. The vacuolar proton pump, V-ATPase, is required for notch signaling and endosomal trafficking in Drosophila. *Dev Cell* **17**, 387-402 (2009).
157. Kim, J.S. et al. Apicularen A induces cell death through Fas ligand up-regulation and microtubule disruption by tubulin down-regulation in HM7 human colon cancer cells. *Clinical cancer research : an official journal of the American Association for Cancer Research* **13**, 6509-17 (2007).
158. Tanner, M. et al. Characterization of a novel cell line established from a patient with Herceptin-resistant breast cancer. *Mol Cancer Ther* **3**, 1585-92 (2004).

8 Appendix

8.1 Abbreviations

Table 8.1 List of Abbreviations

µg, µl, µM	microgram,microliter,micromolar
ANOVA	analysis of variance
approx.	approximate(ly)
APS	ammoniumpersulfate
Arf6	ADP ribosylation factor 6
ARNO	Arf nucleotide binding site opener
ATP	adenosine triphosphate
BSA	bovine serum albumine
cDNA	complementary desoxyribonucleic acid
ConcmA	concanamycin A
DMEM	Dulbecco's modified eagle medium
DMSO	dimethylsulfoxid
DTT	dithiothreitol
EC	endothelial cell(s)
EC_{50}	half maximal effective concentration
ECGM	endothelial cell growth medium
ECL	enhanced chemiluminescence
ECM	extracellular matrix
EDTA	ethylene diamine tetraacetic acid
EGF	epidermal growth factor
EGFR	epidermal growth factor receptor
EGTA	ethylene glycol tetraacetic acid
ERK1/2	extracellular signal regulated kinases
FACS	fluorescence activated cell sorting
FCS	fetal calf serum
Fig.	figure
GTP	guanosine triphosphate
h	hour
HCC	hepatocellular carcinoma
HFS	hypotonic fluorescent solution

HRP	horse raddish peroxidase
kDa	kilo Dalton
l	liter
LSM	laser scanning microscope
MAP	microtubule associated proteins
MAPK	mitogen activated protein kinase(s)
mg, ml, mM	milligram, milliliter, millimolar
min	minute(s)
MMP	matrix metalloprotease
mRNA	messenger ribonucleic acid
nM	nanomolar
nt siRNA	non targeting small interfering ribonucleic acid
PAA	polyacrylamide
PAGE	polyacrylamide gel electrophoresis
PBS	phosphate buffered saline
PBS-T	phosphate buffered saline with 0.1 % Tween 20
pc	pericyte(s)
PlGF	placental growth factor
PIPES	1,4-piperazinebis(ethanesulfonic acid)
pm	plasma membrane or plasma membranous
ppm	parts per million
PMSF	phenylmethanesulfonylfluoride
PNRC	perinuclear recycling compartment
Prt	pretubulysin
rcf	relative centrifugal force
RT	room temperature
RT PCR	reverse transcriptase polymerase chain reaction
RTK	receptor tyrosine kinase
RTKI	receptor tyrosine kinase inhibitor
S, T, Y, #	serine, threonine, tyrosine, kinase phosphorylation residues
SDS	sodium dodecylsulfate
sec	second(s)
siRNA	small interfering ribonucleic acid

TBA	tubulin binding agent(s)
TEMED	tetramethylethylenediamine
Tris	tris(hydroxymethyl)aminomethane
TubA	tubulysin A
VE-cadherin	vascular endothelium cadherin
VEGF	vascular endothelial growth factor
VEGFR2	vascular endothelial growth factor receptor 2

8.2 Publications

8.2.1 Original publications

Rath S, Liebl J, Fürst R, Ullrich A, Burkhart JL, Kazmaier U, Herrmann J, Müller R, Günther M, Schreiner L, Wagner E, Vollmar AM, Zahler S. Anti-angiogenic effects of the tubulysin precursor pretubulysin and of simplified pretubulysinerivatives. Br J Pharmacol. 2012, Epub ahead of print

8.2.2 Poster presentations

Rath S, Fürst R, Ullrich A, Burkhart JL, Vollmar AM, Kazmaier U, Zahler, S. Anti-angiogenic potential of pretubulysin and its derivatives *in vitro*. 77th Annual Meeting of the Deutsche Gesellschaft für experimentelle und klinische Pharmakologie und Toxikologie, March 30 – April 1, 2011, Frankfurt a.M., Germany. Naunyn-Schiedeberg‘s Archives of Pharmacology, 2011; 383 Suppl.1, Abstract P066.

Rath S, Fürst R, Ullrich A, Burkhart JL, Herrmann J, Liebl J, Günther M, Vollmar AM, Kazmaier U, Zahler S. Anti-angiogenic potential of Pretubulysin and ist derivatives. Joint Meeting European Society of Microcirculation (ESM) and Society of Microcirculation and Vascular Biology (GfMVB), October 13-16 2011, Munich, Germany. Journal of Vascular Research, 2011; 48 Suppl. 1, Abstract P120.

8.2.3 Oral presentations

Rath S, Liebl J, Fürst R, Ullrich A, Burkhart JL, Kazmaier U, Herrmann J, Müller R, Günther M, Schreiner L, Wagner E, Vollmar AM, Zahler S. Inhibition of angiogenesis by pretubulysin and its derivatives. International Congress Natural Anticancer Drugs, June 30 - July 4, 2012, Olomouc, Czech Republic. Biomedical Papers, 2012, Vol 156, Supplement 1, June 2012, Abstract O-26.

8.3 Acknowledgement

I would like to deeply thank Prof. Dr. Angelika M. Vollmar and Prof. Dr. Stefan Zahler.

Ms. Vollmar, thank you for giving me the chance to perform my PhD thesis in your lab, for trusting in me and for motivating me throughout the work. I really enjoyed the opportunity to exchange with the scientific community in numerous interesting meetings, which pushed me forward, both scientifically and personally. It was a true pleasure and honor for me to be part of your research team. Thank you as well for being my second examiner and for offering your time and effort to appraise this work.

Mr. Zahler, you helped me a lot with scientific advice and technical expertise. You were always open for input from my side and very patient and interested when things turned out different than expected, which I appreciate a lot. I am glad, how we managed two fantastic projects together. Thank you.

Moreover, I would like to thank Dr. Johanna Liebl, Dr. Bettina Mayer, Dr. Romina Wiedmann, Dr. Karin von Schwarzenberg, Dr. Simone Braig and PD Dr. Robert Fürst for much very useful advice and for fruitful discussions during meetings and presentations.

I want to sincerely acknowledge the time and interest of the members of my thesis committee: Prof. Dr. Ernst Wagner, Prof. Dr. Gerhard Winter, Prof. Dr. Franz Bracher and Prof. Dr. Wolfgang Friess.

Very special thanks go to the cooperation partners, who contributed to this work: Dr. Angelika Ullrich, Dr. Jens Burkhart and Prof. Dr. Uli Kazmaier from the Institute for Organic Chemistry, University of Saarland for providing pretubulysin and its analogues, Jennifer Herrmann from the Helmholtz Centre for Pharmaceutical Research, University of Saarland for performing the *in vitro* tubulin polymerization assay, and Laura Schreiner, Dr. Michael Günther and Dr. Johanna Liebl from the Department of Pharmacy, Ludwig Maximilians University Munich for planning and performing the *in vivo* tumor xenograft assay.

I would like to express my thanks to the wonderful people, who create the pleasant working atmosphere, starting with the invaluable technical support from Jana, Bianca, Rita, Kerstin, Bernadette and Frau Schnegg, you keep the business running.

Siwei, che che very much for being such a wonderful bench neighbor and friend. Sabine, thank you for – you know – so many things. Liesl and Karin, thank you for jamming together. Michi, Tini, Sandra, Verena, Simone, Flo, Julia and Lena, thank you so much for the great time together inside and outside the lab and for cheering me up during the writing period. Susanne and Martha, thank you for your busy contribution to this project. Thank you, Tini and Karin, for proofreading the manuscript.

Friends in Munich: Anne, Dave, Christian, Jo, Claudia and many others, thank you for welcoming me in this wonderful city and for feeling like home.

My family: particularly my Mum, my Dad and my brothers Krischi and Jörni, thank you for your continuous support and belief.